

**Fatty acid-modified poly(glycerol adipate) as a versatile matrix for
parenteral depot formulations**

Dissertation

zur Erlangung des

Doktorgrades der Naturwissenschaften (Dr. rer. nat.)

der

Naturwissenschaftlichen Fakultät I

Biowissenschaften

der Martin-Luther-Universität

Halle-Wittenberg

vorgelegt

von Herrn Jonas Steiner

geb. am 06.03.1991 in Würzburg

Gutachter:

1. Prof. Karsten Mäder

2. Prof. Jörg Kreßler

3. Prof. Michaela Schulz-Siegmund

Datum der öffentlichen Verteidigung: Halle (Saale), 07.07.2022

*Die Wissenschaft, richtig verstanden, heilt den Menschen von seinem Stolz;
denn sie zeigt ihm seine Grenzen.*

Albert Schweitzer (1875-1965)

Abbreviations and Symbols	V
1 Introduction	1
1.1 Parenteral Controlled Drug Delivery	1
1.2 Biodegradable Polymers	4
1.2.1 Poly(lactic-co-glycolic acid)	5
1.2.2 Poly(glycerol adipate)	6
1.3 Lipophilic Thiamine Derivatives	8
1.4 Aims and Objectives	9
2 Materials	11
2.1 Fatty Acid-modified Poly(glycerol adipate)	11
2.2 Thiamine Derivatives	12
2.3 Fluorescent Dyes	13
2.4 Miscellaneous	14
3 Methods	16
3.1 Characterization of Bulk Polymers	16
3.1.1 Differential Scanning Calorimetry (DSC)	16
3.1.2 Gel Permeation Chromatography (GPC)	16
3.1.3 Stability Testing	16
3.1.4 Static Contact Angle	16
3.1.5 Oscillatory Rheology	17
3.1.6 Electron Paramagnetic Resonance (EPR)	18
3.2 Preparation and Characterization of Microparticles	19
3.2.1 Preparation of Microparticles	19
3.2.2 Laser Diffraction Analysis	20
3.2.3 Scanning Electron Microscopy (SEM)	21

3.2.4	Determination of Drug Loading and Encapsulation Efficiency by High-Performance Liquid Chromatography (HPLC).....	21
3.2.5	X-Ray Powder Diffraction (XRD)	23
3.2.6	<i>In Vitro</i> Release of Dibenzoyl Thiamine	23
3.2.7	Cytotoxicity	24
3.2.8	Electron Beam Sterilization.....	26
3.2.9	<i>In Vitro</i> Release of DiR.....	26
3.2.10	Fluorescence Imaging.....	27
3.2.11	Fluorescence Spectroscopy.....	27
3.2.12	<i>In Vivo</i> Characterization	27
3.2.12.1	Animal Care.....	27
3.2.12.2	Sample Preparation.....	28
3.2.12.3	Injections And Anesthesia	28
3.2.12.4	Multispectral Fluorescence Imaging.....	29
3.3	Preparation and Characterization of Preformed Implants.....	29
3.3.1	Preparation of Preformed Implants.....	29
3.3.2	Light Microscopy	30
3.3.3	Texture Analysis	30
3.3.4	Determination of Drug Loading and Drug Distribution by High Performance Liquid Chromatography (HPLC)	31
3.3.5	<i>In Vitro</i> Release of Dibenzoyl Thiamine	31
4	Results and Discussion	32
4.1	Characterization of Bulk Polymers	32
4.1.1	Differential Scanning Calorimetry (DSC)	32
4.1.2	Stability Testing	34
4.1.3	Static Contact Angle	35

4.1.4	Macroviscosity	37
4.1.5	Water Penetration and Microviscosity	42
4.2	Preparation and Characterization of Microparticles.....	47
4.2.1	Preparation of Microparticles	47
4.2.2	Size Distribution	48
4.2.2.1	Influence of Stirring Speed and Polymer Concentration	48
4.2.2.2	Influence of Drug Loading	52
4.2.3	Particle Morphology	54
4.2.4	Encapsulation Efficiency	57
4.2.5	X-Ray Powder Diffraction (XRD)	59
4.2.6	<i>In Vitro</i> Release Experiments	62
4.2.6.1	Selection of Release Medium.....	62
4.2.6.2	Selection of Sampling Technique and Duration of Release Experiments	64
4.2.6.3	<i>In Vitro</i> Release of Dibenzoyl Thiamine.....	65
4.2.7	Comparison to PLGA	70
4.2.8	Cytotoxicity	73
4.2.9	Impact of Electron Beam Sterilization.....	78
4.2.10	<i>In Vitro</i> Release of DiR.....	81
4.2.11	<i>In vivo</i> Fluorescence Imaging.....	83
4.3	Preparation and Characterization of Preformed Implants.....	88
4.3.1	Preparation of Preformed Implants and Texture analysis.....	88
4.3.2	Determination of Drug Distribution	90
4.3.3	<i>In Vitro</i> Release of Dibenzoyl Thiamine	91
5	Summary and Perspectives.....	94
	References.....	VIII

Supplementary Data.....	XXIX
Deutsche Zusammenfassung.....	XXXI
Acknowledgements	XXXVI
Curriculum Vitae	XXXVIII
Publications	XXXIX
Selbstständigkeitserklärung.....	XLI

ABBREVIATIONS AND SYMBOLS

% (mol)	Percentage by molecular weight
% (v/v)	Percentage by volume
% (w/v)	Percentage by weight per volume
% (w/w)	Percentage by weight
% RH	Relative humidity
°C	Degree Celcius
3T3	Mouse embryonic fibroblasts
A	Ampere
ACN	Acetronitrile
API	Active pharmaceutical ingredient
c	Concentration
c _s	Saturation concentration
CAL-B	<i>Candida antarctica</i> lipase B
CL/P	Cleft lip and palate
CPP	Central precocious puberty
d	Day
D/C ratio	Disperse phase/continuous phase ratio
Da	Dalton
DAB	Deutsches Arzneibuch (German Pharmacopoeia)
DBT	Dibenzoyl Thiamine
DCM	Methylene chloride
DDS	Drug delivery system
DMAP	4-Dimethylaminopyridine
DMEM	Dulbecco's Modified Eagle's Medium
DMSO	Dimethyl sulfoxide
DSC	Differential scanning calorimetry
EDC-HCl	1-Ethyl-3-(3-dimethyl aminopropyl)carbodiimide hydrochloride
EE	Encapsulation efficiency
Em.	Emission
EPR	Electron paramagnetic resonance

Ex.	Excitation
FA-PGA	Fatty acid-modified poly(glycerol adipate)
g	Gram
G'	Storage modulus
G''	Loss modulus
GPC	Gel Permeation Chromatography
Gy	Gray
h	Hour
HPLC	High-performance liquid chromatography
Hz	Hertz
IC ₅₀	Half maximal inhibitory concentration
IDMC	Indomethacin
ISFI	<i>In situ</i> forming implants
K	Kelvin
L	Liter
logP	Octanol-water partition coefficient
LVER	Linear viscoelastic region
m	Meter
M	Molar
MeOH	Methanol
min	Minute
M _n	Number average molecular weight
mol	Mole
M _w	Weight average molecular weight
N	Newton
NHDF	Normal human dermal fibroblasts
NIR	Near-infrared
NMP	N-Methyl-2-pyrrolidone
NP	Nanoparticle
O/W	Oil in water
OH	Hydroxyl group

PBS	Sørensen's phosphate-buffered saline
PCL	Polycaprolactone
PDI	Polydispersity index
PEG	Polyethylene glycol
PET	Polyethyleneterephthalate
PGA	Poly(glycerol adipate)
pH	<i>Potentia hydrogenii</i>
Ph. Eur.	European Pharmacopoeia
PLA	Poly(lactic acid)
PLGA	Poly(lactic-co-glycolic acid)
PVA	Polyvinyl alcohol
RCM	Rate-controlling membrane
rpm	Rounds per minute
s	Second
SBT	Sulbutiamine
SDS	Sodium dodecyl sulfate
SEM	Scanning electron microscopy
SAS	Sample and separate
T	Tesla
TFA	Trifluoroacetic acid
T _g	Glass transition temperature
THF	Tetrahydrofuran
T _m	Melting temperature
TPP	Thiamine diphosphate
V	Volt
XRD	X-Ray diffraction
δ	Loss angle
η*	Complex viscosity
μ	Micro
θ	Static contact angle
λ	Wavelength

1 INTRODUCTION

1.1 PARENTERAL CONTROLLED DRUG DELIVERY

Controlled drug delivery aims at a steady and sustained drug release within a therapeutically relevant concentration. The concept of controlled release was introduced in the 1960s by Judah Folkman who proposed the implantation of silicon rubber capsules as carriers for prolonged drug release [1]. Controlled drug delivery systems (DDS) offer many advantages compared to conventional immediate-release dosage forms [2–4]. Through the maintenance of therapeutic drug levels, adverse side effects are prevented and therefore therapy efficiency is improved. Furthermore, sustained depot formulations may improve patient compliance due to less frequent administrations and simpler dosing regimens [5]. Depot formulations with release kinetics from days to years have been developed and approved worldwide.

Since the majority of new drug candidates are poorly water-soluble and therefore oral bioavailability is low, the parenteral route of administration is often the only choice [6]. Another advantage of the parenteral administration, i.e. circumvention of the gastrointestinal tract, is the avoidance of the first pass effect. Therefore, the bioavailability of drugs with high first-pass metabolisms by the liver is enhanced. Parenteral depot formulations for controlled drug delivery are most commonly injected intramuscularly or subcutaneously.

The first commercially available parenteral controlled DDSs was the intrauterine device Progestasert® in the early 1970s [7,8]. Both medicinal products were based on poly(ethylene-co-vinyl acetate) (polyEVA) as a rate-controlling membrane (RCM) system. Subsequently, other RCM products were developed ranging from polymer-based implants (e.g. Norplant®, Implanon®) to hydrogel-based implants (e.g. Supprelin® LA, Vantas®) and osmotic pump systems (e.g. DUROS®) [9–13]. These products provided a long-term delivery of a drug with relatively constant release rates. Their major disadvantage is that they contain non-biodegradable materials and therefore have to be removed from the body usually via a surgical procedure after the treatment. The synthesis of the degradable structures poly(glycolic acid) and subsequently poly(lactic-co-glycolic acid) (PLGA) in the

1960s laid the foundation of the development of biodegradable polymer DDS for sustained release [14]. After continuous research conducted in the late 1960s and 1970s, the first biodegradable depot system (Decapeptyl[®]) was approved in 1986. Decapeptyl[®] is a microparticulate PLGA formulation for the delivery of triptorelin and still on the market today [3]. Over the last decades, various microparticle- (e.g. Lupron[®] Depot, Trenantone[®]) and implant-formulations (e.g. Zoladex[®]) made of biodegradable polymers were approved as injectable DDSs for prolonged controlled drug release [15]. Besides preformed implants, *in situ* forming implants like Eligard[®] were introduced onto the market [16,17]. *In situ* forming implants are injectable fluids that solidify after administration at the site of injection. While recent research works on the development of novel DDSs made from biodegradable polymers such as nano-fiber matrices and scaffolds, only microparticles, preformed implants and *in situ* forming implants reached market maturity until now [18–22]. An overview of approved biodegradable parenteral depot systems made of biodegradable polymers is displayed in Table 1. Alongside polymeric depot systems, also oil-based formulations and micro- or nanosized drug suspensions are commercially available for sustained release. Exemplary are Haldol[®] Depot as an oily solution and Invega Trinza[®] as a parenteral suspension [23]. In addition, there are a few products based on the multivesicular liposome concentrate DepoFoam[™] (e.g. DepoCyte[®]) which are used for controlled drug release [24]. Other liposomal products or polymeric nanoparticles are no characteristic depot formulations due to their limited sustained-release capacities. As apparent from this short review, the range of systems for controlled drug release is wide. However, polymeric systems (microparticles, preformed and *in situ* implants) account for the majority of commercially available and clinically established biodegradable depot formulations [23].

Table 1: Exemplary overview of approved parenteral depot systems made from biodegradable polymers (table continues on the next pages).

	Trade Name	Polymer/API	Dosing Interval	Indication
Microparticles	Vivitol®	PLGA/Naltrexone	1 month	Opioid and alcohol dependence
	RISPERDAL® Consta	PLGA/Risperidone	2 weeks	Schizophrenia
	Parlodel® LAR	PLGA-glucose/ Bromocriptine	1 month	Macroprolactinomas
	Signifor® LAR	PLGA/Pasireotide	1 month	Acromegaly/ Cushings disease
	Sandostatin® LAR	PLGA/Octreotide	1 month	Acromegaly
	TRELSTAR®	PLGA/Triptorelin	1, 3 and 6 months	Prostate cancer
	Lupron Depot®	Poly(lactic acid) (PLA)/Leuprolide	1, 3, 4 and 6 months	Endometriosis/ Fibrosis/ Central precocious puberty (CPP)/Prostate cancer
	Triptodur™	PLGA/Triptorelin	6 months	CPP
	Zilretta®	PLGA/ Triamcinolone	3 months	Osteoarthritis
	Bydureon Bcise®	PLGA/Exenatide	1 week	Diabetes type 2
	Enantone®	PLGA/ Leuproreline	1 month	Prostate cancer/ Endometriosis/CPP
	Trenantone®/ Sixantone®	PLA/Leuproreline	3 months/ 6 months	Prostate cancer/ Endometriosis/CPP
	Decapeptyl® Depot	PLGA/Triptorelin	1 month	Prostate cancer/ Endometriosis/CPP
	Salvacyl®	PLGA/Triptorelin	3 months	Men paraphilia

	Trade Name	Polymer/API	Dosing Interval	Indication
Preformed Implants	Zoladex®	PLGA/Goserelin	1 and 3 months	Prostate cancer/ Endometriosis/ Breast cancer
	Gliadel®	Poly[(carboxy phenoxy) propane-sebaic acid]/Carmustine	One-time	Cerebral tumor
	Suprefact®	PLGA/Buserelin	2 and 3 months	Prostate cancer
	OZURDEX®	PLGA/ Dexamethasone	6 months	Macular edema
	Profact®	PLGA/Buserelin	2 and 3 months	Prostate cancer
	Leuprone®	PLGA or PLA/ Leuprorelin	1 and 3 months	Prostate cancer
In situ Implants	Atridox®	PLA in N-Methyl-2-pyrrolidon (NMP)/ Doxycycline	4 months	Periodontitis
	Perseris®	PLGA in NMP/ Risperidone	1 month	Schizophrenia
	Eligard™	PLGA in NMP/ Leuprorelin	1,3 and 6 months	Prostate cancer
	Sublocade	PLGA in NMP/ Buprenorphine	1 month	Opioid dependence

1.2 BIODEGRADABLE POLYMERS

The intensive research on controlled release systems involved the development and improvement of various carrier materials. Today, a variety of biodegradable polymers is available [25]. Nevertheless, due to the complex requirements imposed on the different depot formulations in a physiological environment, the demand for new innovative materials is still high.

Biodegradable polymers possess chemical functionalities which are unstable in a physiological environment. As a result, enzymatic and/or non-enzymatic biodegradation into biocompatible oligomer or monomer units occurs [26]. Some examples of biodegradable polymer classes include synthetic polyesters (e.g. PLGA, polycaprolactone (PCL)), polyanhydrides (e.g. Poly[(carboxyphenoxy) propane–sebacic acid]), polyphosphazenes, polyurethanes and polyalkylcyanoacrylates. Furthermore, natural biodegradable polymer classes such as polysaccharides (e.g. chitosan, starch) and protein-based materials (e.g. collagen, gelatin) are used for drug delivery [25–28].

1.2.1 POLY(LACTIC-CO-GLYCOLIC ACID)

Poly(lactic-co-glycolic acid) (PLGA) is the most widely used biodegradable polymer in drug delivery and therefore represents the gold standard of degradable polymers (Figure 1). 46% of the presently marketed parenteral depot formulations are based on PLGA [23]. Its widespread use can be attributed to its biodegradability and good biocompatibility [29]. Furthermore, PLGA is commercially available in various molecular weights and with different lactide/glycolide ratios, hence, variable physicochemical properties. These different PLGAs feature variable degradation behaviours and drug release profiles [30–32]. The polymer backbone is degraded by ester cleavage through hydrolysis upon contact with water [33,34]. The corresponding alpha-hydroxy acids, lactic and glycolic acid, are incorporated into the tricarboxylic acid cycle *in vivo* and subsequently excreted [35]. They are therefore physiological well-tolerated and account for the biocompatibility of the copolymer. Despite these advantages and its extensive use, there is a major drawback to PLGA. PLGA undergoes bulk erosion, hence, the diffusion of water into the polymer is more rapid than the ester hydrolysis [36]. Accordingly, polymer degradation occurs throughout the whole polymer matrix. However, the diffusion of the acidic degradation products out of the system can be rather slow depending on the diffusion distance and mobility of the acids. Consequently, the corresponding acids accumulate and the micro-pH within the polymer matrix drops. Since ester hydrolysis is pH-dependent, the low micro-pH inside the polymer has an autocatalytic effect on the degradation of PLGA [37–42]. Changes in the microclimate were demonstrated by different methods and micro-pH drops from pH 7 to values around pH 2 were detected *in vitro* and *in vivo* [43–47]. Acidic micro-environments can cause instability of proteins, peptides and nucleic acids inside the

DDS including the covalent bonding of the monomers with amino groups [48–53]. Furthermore, due to the autocatalytic effect, heterogeneous degradation occurs which may result in complex drug release profiles [33,41,54–57]. Thus, the development of alternative biodegradable polymers with fewer acidic monomers is required. Poly(glycerol adipate) (PGA) has the potential to meet the demand and criteria of a versatile polymer matrix as an alternative to PLGA.

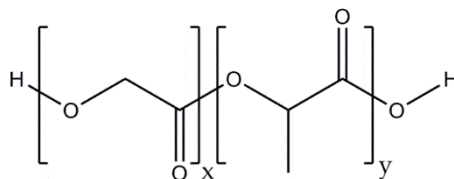


Figure 1: Chemical structure of poly(lactic-co-glycolic acid).

1.2.2 POLY(GLYCEROL ADIPATE)

Poly(glycerol adipate) is a linear polyester synthesized by enzymatic polycondensation [58]. The regioselectivity of the used lipase (*Candida antarctica* lipase B) to primary hydroxyl groups at low temperatures attributes for the formation of linear polymers with pendant hydroxyl groups [59,60]. In view of environmental sustainability, enzymatic polyester synthesis is favourable compared to conventional chemical processes. Enzymes are nontoxic, renewable biocatalysts that are recyclable and allow the avoidance of toxic metal catalysts. Moreover, mild reaction conditions, e.g. low temperatures, can be achieved for enzyme-catalyzed reactions [61–63]. Furthermore, it is often possible to use renewable bio-based monomers as starting raw materials for polyester synthesis. In the case of PGA, glycerol is used as a starting material. Bio-based glycerol is a by-product of biofuel production and therefore cheap and widely available [64]. In conclusion, the synthesis of PGA by an enzymatic-catalyzed reaction is highly selective and in line with the pursuit of sustainable environment-friendly chemistry.

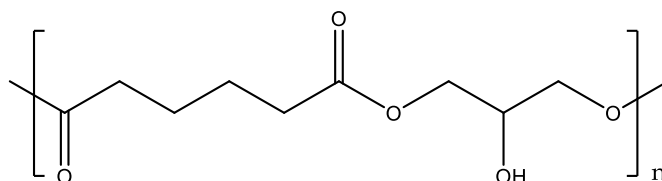


Figure 2: Chemical structure of the poly(glycerol adipate) backbone.

PGA itself is a hydrophilic but not a water-soluble biocompatible and biodegradable polyester (Figure 2) [65]. Compared to PLGA, the absence of alpha-hydroxy acids in the backbone avoids the formation of highly acidic micro-environments. Another substantial advantage over most other linear polyesters such as PGLA is the free hydroxyl group (OH) per repeating unit. This pendant hydroxyl moiety allows a variety of further modifications via simple and accessible conjugation chemistry. Due to multiple grafting opportunities resulting from the free OH-groups, the PGA backbone serves as a starting point for the synthesis of a class of biocompatible and biodegradable polymers with various physicochemical properties [66–69].

Functionalized PGA polyesters as a new biodegradable polymer matrix for drug delivery were first reported by Kallinteri et al. in 2005 [65]. They coupled acyl moieties to the PGA backbone and obtained an amphiphilic comb-like polymer able to self-assemble into nanoparticles (NP) in water. Moreover, they were able to incorporate and release hydrophilic drugs from the NPs and to demonstrate the biocompatibility of these systems [65,70]. In the early 2010s, the physicochemical properties of fatty-acid modified PGAs (FA-PGA) and their formation into nanoparticles were intensively studied by a cooperation between the workgroups around Karsten Mäder and Jörg Kressler from the Martin Luther University of Halle-Wittenberg [67,71–74]. In the course of this research, Weiss et al. reported the size dependency of the NPs to the substituted fatty acid and gave insights into the shapes (from spheres to cubes) as well as the internal structure of NPs made from comb-like polymers. First investigations of the *in vivo* distribution of the DDS in mice were conducted as well and good *in vivo* tolerability of the NPs was demonstrated [75]. As reported by Animasawun et al. and Wahab et al., the ability to alter the hydrophobicity of the PGA graft polymers introduces the possibility to increase the encapsulation efficiency of hydrophobic drugs in NPs [76,77]. Aside from fatty acids, the coupling of other moieties to the free hydroxyl groups of the PGA backbone was investigated. Jbeily et al. coupled polycaprolactone to the PGA yielding a PCL-grafted PGA [78]. Subsequently, the additional grafting of poly(ethylene oxide) to the PCL side-chain led to the formation of polymersomes and worm-like aggregates [79,80]. Moreover, the functionalization of PGA with amino acids, cholesterol and polyethylene glycol (PEG) was conducted to investigate drug-polymer interactions and their influence on NP properties

[77]. Also, the variation of the PGA backbone was performed to alter the hydrophobic/hydrophilic balance. Therefore, pentadecalactone, PEG and other functional diols were inserted into the PGA backbone to introduce additional chemical moieties [81-84]. Another approach was the synthesis of PGA-drug conjugates firstly reported by Wersig et al [85,86]. They esterified the free OH-groups of the PGA backbone with indomethacin (IDMC) and subsequently investigated the drug release from PGA-IDMC NPs. Later, the workgroup around Garnett successfully prepared nanosized DDSs from PGA-drug conjugates with methotrexate and mefenamic acid [87,88]. Recently, the formation of biodegradable PGA networks after the modification of pendant hydroxyl groups with amine-terminated side groups was published by Alaneed et al. [89]. The wide range of possibilities to alter the physicochemical properties of functionalized PGAs offers the opportunity to adjust the polymer to the requirements of the drug and the DDS. While modified PGA NPs have been studied extensively within the last decade, the potential of these materials as polymer matrices for depot formulations such as microparticles and implants has only scarcely been explored so far. The formulation of solid dosage forms such as microparticles and implants requires solid carrier materials. Due to the viscous nature of PGAs modified with short acyl chains or unsaturated oleic acid, PGAs substituted with longer saturated acyl chains (C₁₈ and C₂₂) were investigated throughout this research [71,90].

1.3 LIPOPHILIC THIAMINE DERIVATIVES

Thiamine (vitamin B₁) is a water-soluble vitamin essential for oxidative energy metabolism [91]. Its pyrophosphate ester thiamine diphosphate (TPP) is the effective form and a cofactor for enzymatic reactions. Three enzymatic systems, which are essential for cerebral glucose metabolism, depend on TPP: The mitochondrial pyruvate dehydrogenase, the alpha-ketoglutarate dehydrogenase and the cytosolic transketolase [92]. Additionally, non-coenzymatic functions of thiamine in the nervous system have been reported, e.g. its interference with structure and function of membranes [93,94].

The thiamine deficiency syndrome is categorized into beriberi and Wernicke-Korsakoff syndrome [95]. Beriberi affects the cardiovascular system and/or the nervous system and is primarily caused by malnutrition. The Wernicke-Korsakoff syndrome is associated with neurological symptoms and is more common in chronic alcoholics and HIV-infected

patients [96,97]. A thiamine deficiency requires rapid supplementation. If the correction of the vitamin B₁ levels to physiological values is achieved before the development of severe brain damage, the neurological manifestations may be reversible.

Since thiamine absorption is limited by the low turnover of high-affinity thiamine carriers, a variety of lipophilic thiamine derivatives was synthesized [91,98]. The majority of these substances has been developed in the 1950s and 1960s in Japan which suffered from many beriberi cases in the past. Some of these derivatives are allithiamine, fursultiamine, sulbutiamine (SBT), benfotiamine and dibenzoyl thiamine (DBT) [91,99]. Compared to the hydrophilic thiamine, the lipophilic derivatives have a much higher bioavailability [100–102]. For benfotiamine, for instance, the oral bioavailability was reported to be 360% related to that of thiamin hydrochloride [103]. In addition to their application as a supplement for the thiamine deficiency syndrome, other promising pharmacological effects have been reported for the lipophilic thiamine precursors. Benfotiamine has received attention as a preventive measure against complications of diabetes [104,105]. Furthermore, neuroprotective and anti-inflammatory effects have been investigated for DBT and other thiamine derivatives [99,106–108]. Recently even chemotherapeutic effects have been suggested in the literature [109]. Moreover, the correlation between low thiamine levels and the appearance of cleft lip and palate (CL/P) has been investigated [110,111]. K. Scheller et al. of the University Hospital in Halle reported a prophylactic effect of thiamine supplementation on teratogenically induced cleft appearance [112].

1.4 AIMS AND OBJECTIVES

The demand for new biodegradable polymers for drug delivery is translating into research as depicted in Figure 3. Within the last 40 years, the number of publications on biodegradable polymers has been increasing continuously. The interest in the novel biodegradable polyester poly(glycerol adipate) emerged during the last 15 years, reflected in the growing research effort regarding that subject.

This thesis focuses at the exploration of fatty acid-modified PGA as a versatile drug delivery matrix for sustained and controlled drug release. The lipophilic thiamine derivatives DBT and SBT were selected as promising APIs for the prophylactic treatment of CL/P in cooperation with Konstanze Scheller from the Department of Oral and Maxillofacial and

Facial Plastic Surgery of the University Hospital in Halle. The present work aims at the following:

- **Characterization of various FA-PGA polymers** regarding their suitability for drug delivery. With respect to this, a particular focus should be on the ability to form solid depot systems. Based on the bulk polymer characterization, possible approaches for the **formulation of DDS for controlled release of DBT** will be explored.
- Preparation and characterization of various **FA-PGA microparticles**. Including the investigation of the preparation process, drug-polymer interactions and the *in vitro* release behaviour of DBT.
- Formulation and investigation of **FA-PGA implants**. In this regard, especially the *in vitro* release from a larger geometry compared to the microparticles is of interest.
- **Comparison to PLGA** as a gold standard of biodegradable polymers for drug delivery.
- Preparation and implementation of ***in vivo* experiments** with the most promising formulation. The biocompatibility of the formulation should be addressed prior to the experiment. A suitable study design for the *in vivo* test via fluorescence imaging should be developed and executed.

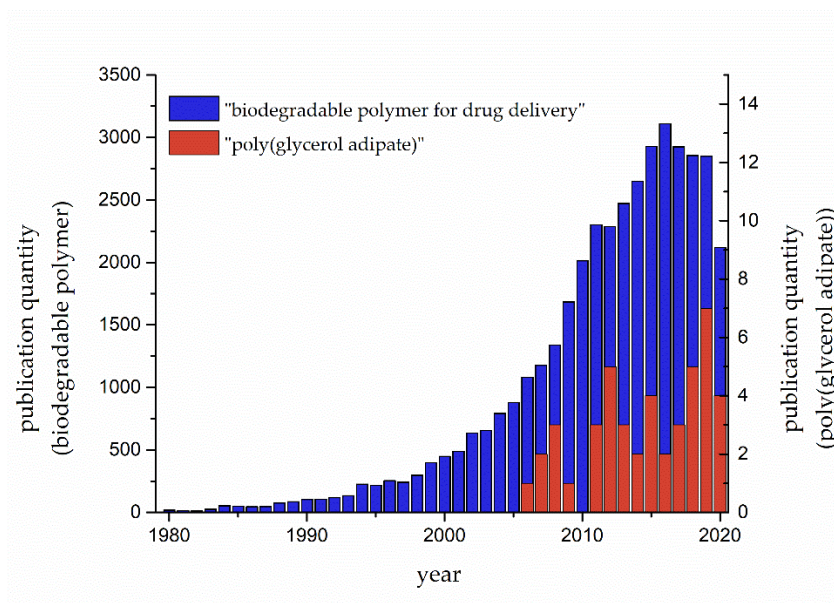


Figure 3: Literature research for the search terms „biodegradable polymers for drug delivery“ (blue) and „poly(glycerol adipate)“ (red) on PubMed.gov from 1980 to 2020.

2 MATERIALS

2.1 FATTY ACID-MODIFIED POLY(GLYCEROL ADIPATE)

The synthesis of the different FA-PGAs, as well as the measurements and calculations of the acylation degree and of the molar masses, were conducted by Prof. Krefßler's research group at the Institute of Chemistry, Department of Physical Chemistry, Martin Luther University of Halle-Wittenberg as described in [66]. A simplified reaction scheme is displayed in Figure 4. During the first reaction step, the polymer backbone was formed by polycondensation of divinyl adipate and glycerol. This polycondensation reaction was catalyzed by the regioselective *Candida antarctica* lipase B (CAL-B), an enzyme that prefers the condensation process of primary hydroxyl groups [58]. Subsequently, the resulting linear polyester was modified to various degrees with fatty acid side chains. Therefore, the pendant free hydroxyl groups of the PGA backbone were grafted with fatty acids, such as stearic acid (C18:0) and behenic acid (C22:0), via Steglich esterification. Table 2 shows the PGA-based polyesters investigated in this thesis. The various acylation degrees indicate the converted OH-groups of the PGA backbone in mol%.

Table 2: PGA and FA-PGAs investigated in this thesis. The ranges for the number average molecular weight (M_n), the weight average molecular weight (M_w), the polydispersity index (M_w/M_n) and the respective acylation degrees, and the grafted side chains are given.

Polymer	Side Chain	Acylation Degree [%] ^a	M_n [kDa] ^b	M_w [kDa] ^b	M_w/M_n (PDI) ^b
PGA	-	-	4.3 - 4.8	7.3 - 10.6	1.7 - 2.2
PGA-S65	C18:0	63 - 65	10.2 - 12.3	21.2 - 26.5	1.9 - 2.6
PGA-S90	C18:0	90 - 93	10.2 - 12.5	22.1 - 22.7	1.8 - 2.2
PGA-B45	C22:0	44 - 46	7.6 - 8.7	13.9 - 17.8	1.7 - 2.1
PGA-B75	C22:0	72 - 78	8.5 - 11.6	13.8 - 23.0	1.6 - 2.0
PGA-B45-S35	C22:0, C18:0	44 - 46, 32 - 36	9.5 - 10.9	16.8 - 18.3	1.5 - 1.9

^a Calculated from $^1\text{H-NMR}$ spectra.

^b Obtained from GPC measurements.

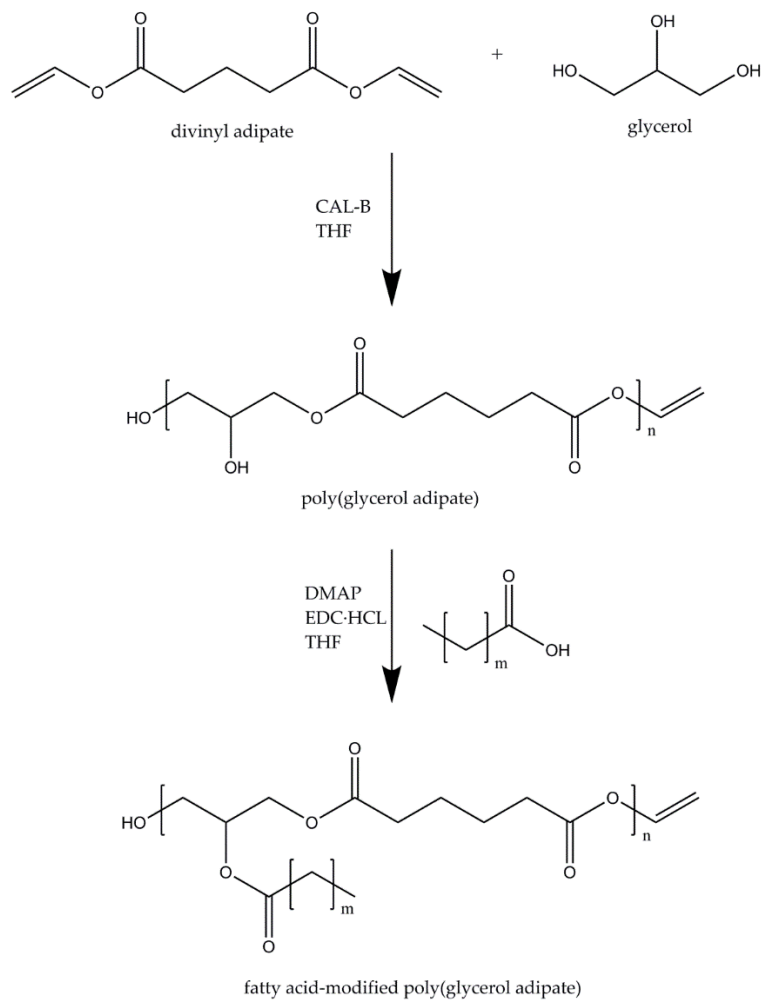


Figure 4: Simplified reaction process of the synthesis of fatty acid-modified poly(glycerol adipate).

2.2 THIAMINE DERIVATIVES

Dibenzoyl thiamine (DBT) and sulbutiamine (SBT) are lipophilic thiamine derivatives. The chemical structures of these molecules are depicted in Figure 5.

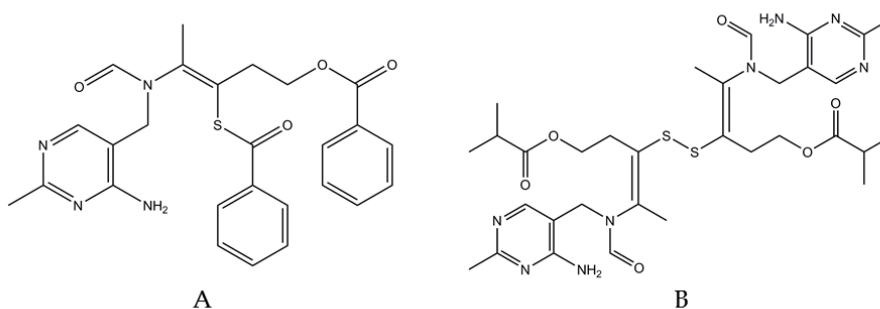


Figure 5: Chemical structures of Dibenzoyl Thiamine (A) and Sulbutiamine (B).

Both substances are white to almost white crystalline powders, which are solid at room temperature. The sources of supply, as well as some physicochemical properties, are listed in Table 3. In order to provide more reliable data, the calculation of the octanol-water partition coefficient was done by three different calculation software.

Table 3: Molecular weights (M_w), melting temperatures (T_m), octanol-water partition coefficients ($\log P$), and some additional information of the thiamine derivatives used in this work.

Substance	M_w [g/mol]	T_m [°C]	$\log P$	Purity	Source
Dibenzoyl	490.57	173	3.67 ¹	>98%	TCI Deutschland
Thiamine			3.42 – 4.99 ² 4.39 ³		GmbH (Eschborn, Germany)
Sulbutiamine	702.89	137	2.44 ¹	>98%	TCI Deutschland
			3.14 – 4.18 ² 3.83 ³		GmbH (Eschborn, Germany)

¹ Calculated by Molinspiration Cheminformatics [113]

² Calculated by VCCLAB [114]

³ Calculated by XLOGP3 [115]

2.3 FLUORESCENT DYES

Table 4: Fluorescent dyes selected for *in vivo* characterization. Molecular weights (M_w), maximum excitation (Ex.) and emission (Em.) wavelengths in methanol and sources of supply are given.

Dye	M_w [g/mol]	Ex. [nm]	Em. [nm]	Source
DY-782 (Carboxylic acid)	879.00	783	800	Dyomics GmbH (Jena, Germany)
DiR	1013.41	750	780	Thermo Fisher Scientific Inc. (Waltham, MA, USA)

2.4 MISCELLANEOUS

Table 5: Further excipients and materials and their suppliers.

Substance	Source	Remark
3T3 cells	Institute of Pharmacy, Luther University Wittenberg, Germany	Martin Halle- Provided by the Biomedical Materials Group
Acetonitrile	VWR International GmbH (Darmstadt, Germany)	HPLC Grade
<i>Aqua demin.</i>	Institute of Pharmacy, Luther University Wittenberg, Germany	Martin Halle- Produced by ion exchange and reverse osmosis
Dimethylsulfoxid	Carl Roth GmbH & Co. KG (Karlsruhe, Germany)	Purity \geq 99.5%
Disodium hydrogen phosphate	Grüssing GmbH (Filsum, Germany)	Purity 99%
Dulbecco's Modified Eagle's medium D5796	Sigma-Aldrich Chemie GmbH (Taufkirchen, Germany)	For cell culture
Dulbecco's Modified Eagle's medium D6429	Sigma-Aldrich Chemie GmbH (Taufkirchen, Germany)	For cell culture
EXPANSORB® DLG 50-2A	Merck KGaA (Darmstadt, Germany)	Lactide:glycolide 50:50, M _w : 5-20 kDa
EXPANSORB® DLG 50-3A	Merck KGaA (Darmstadt, Germany)	Lactide:glycolide 50:50, M _w : 15-40 kDa
EXPANSORB® DLG 50-5A	Merck KGaA (Darmstadt, Germany)	Lactide:glycolide 50:50, M _w : 42-65 kDa
Fetal bovine serum	Sigma-Aldrich Chemie GmbH (Taufkirchen, Germany)	For cell culture
Glycofurol	Merck KGaA (Darmstadt, Germany)	Purity \geq 98.0%
Isoflurane 100% (Forene®)	Abbvie Deutschland GmbH & Co. KG (Wiesbaden, Germany)	For veterinary use
Kolliphor® HS 15	BASF SE (Ludwigshafen am Rhein, Germany)	Ph. Eur. quality
Methanol	VWR International GmbH (Darmstadt, Germany)	HPLC Grade
Methylene chloride	Carl Roth GmbH & Co. KG (Karlsruhe, Germany)	Purity 99.5%
NHDF cells	Institute of Pharmacy, Luther University Wittenberg, Germany	Martin Halle- Provided by the Biomedical Materials Group
N-Methyl-2-pyrrolidone	Carl Roth GmbH & Co. KG (Karlsruhe, Germany)	Purity \geq 99.8%

Substance	Source	Remark
Penicillin-Streptomycin solution (10000 U/mL and 10 mg/mL)	Sigma-Aldrich Chemie GmbH (Taufkirchen, Germany)	For cell culture
Polyethylene glycol 400	Sigma-Aldrich Chemie GmbH (Taufkirchen, Germany)	Purity \geq 99.0%
Polyvinyl alcohol 5-88	Merck KGaA (Darmstadt, Germany)	Ph. Eur. quality
Potassium dihydrogen phosphate	Grüssing GmbH (Filsum, Germany)	Purity 99%
Resazurin sodium salt	Sigma-Aldrich Chemie GmbH (Taufkirchen, Germany)	Purity 80%
Sodium azide	Carl Roth GmbH & Co. KG (Karlsruhe, Germany)	Purity \geq 99%
Sodium dodecyl sulfate	Sigma-Aldrich Chemie GmbH (Taufkirchen, Germany)	Purity \geq 98.5%
Sodium pyruvate solution (100 mM)	Sigma-Aldrich Chemie GmbH (Taufkirchen, Germany)	For cell culture
Sucrose	Grüssing GmbH (Filsum, Germany)	DAB quality
Tempol-d17 (4-Hydroxy-TEMPO-d17)	Sigma-Aldrich Chemie GmbH (Taufkirchen, Germany)	Purity 95%, spin probe
Tetrahydrofuran	Carl Roth GmbH & Co. KG (Karlsruhe, Germany)	Purity \geq 99.9%
Triton® X 100	Carl Roth GmbH & Co. KG (Karlsruhe, Germany)	For cell culture
Tween® 20	Carl Roth GmbH & Co. KG (Karlsruhe, Germany)	Ph. Eur. quality
Tween® 80	Carl Roth GmbH & Co. KG (Karlsruhe, Germany)	Ph. Eur. quality

3 METHODS

3.1 CHARACTERIZATION OF BULK POLYMERS

3.1.1 DIFFERENTIAL SCANNING CALORIMETRY (DSC)

DSC measurements were performed with a PerkinElmer DSC 8000 (PerkinElmer Inc., Rodgau, Germany) in standard aluminum pans. A constant nitrogen flow at a rate of 20 mL/min was maintained during the measurements. As a reference, an empty aluminum pan was used. All samples were heated from -65 °C up to 100 °C at a heating rate of 20 K/min. After holding the temperature at 100 °C for two minutes before cooling down to -65 °C, the cooling/heating cycle was repeated. Glass transition and melting temperatures were analyzed with Pyris™ software (Version 13.3.1.0014, PerkinElmer). The given data are taken from the second heating curve, if not stated otherwise.

3.1.2 GEL PERMEATION CHROMATOGRAPHY (GPC)

The molecular weights of the PGA backbone and the FA-PGAs were determined by GPC on a Viscotek GPCmax VE 2002 using HHRH Guard-17360 and GMHH-N-18055 columns and VE 3580 refractive index detector (Malvern Panalytical GmbH, Nuremberg, Germany). All samples were measured at a concentration of 3 mg/mL with tetrahydrofuran (THF) as a mobile phase. The flow rate was 1 mL/min and the measurement temperature 25 °C. As a calibration standard polystyrene was used for all measurements.

3.1.3 STABILITY TESTING

Storage stability tests of the bulk polymers were executed over a period of 3 months under different storage conditions based on the ICH guidelines [116]. To assess long-term chemical effects accelerated storage conditions were implemented into the study. Therefore, 6 mg of polymer per timepoint were weighed out into 4 mL screw-cap glass vials and stored in the fridge at 4 °C and in a Heraeus B 6760 climate chamber (Thermo Fisher Scientific Inc., Waltham, MA, USA) at 40 °C/ 75% RH. After 1, 3, 7, 28, 56 and 84 days samples were withdrawn from both storage conditions and analyzed with GPC (see 3.1.2).

3.1.4 STATIC CONTACT ANGLE

The contact angle measurements were performed at 25 °C with a DataPhysics OCA 15+ system (DataPhysics Instruments GmbH, Filderstadt, Germany) on a thin polymer film. For

the preparation of the film, the polymer melt was smoothed out to a plane surface on a microscope glass slide at 70 °C. With a dosing rate of 0.5 $\mu\text{L}/\text{min}$, a small drop of water with a volume of 1 μL was dispensed on the polymer film. After an equilibration time of 30 s, the measurements were conducted. Each sample was tested with ten drops at different positions of the polymer film. Contact angle values were calculated with the OCA 15+ software. The Young-Laplace method was chosen for the fitting approximation.

3.1.5 OSCILLATORY RHEOLOGY

The rheological behaviour of the PGA-based polymers was determined with a Malvern Kinexus Lab+ rheometer (Malvern Panalytical GmbH, Nuremberg, Germany). To simulate the physiological properties of the polymers at body temperature, the experiments were conducted at 37 °C. Additionally, the measurements were performed at 23 °C for PGA-S65, PGA-S90 and PGA-B45-S35. For the measurements, a plate-plate (parallel plate) geometry with a plate diameter of 40 mm was used and the gap size was set to be 0.2 mm.

The plate-plate geometry was chosen because loading of the high substituted FA-PGAs (PGA-B75, PGA-B45-S35) to a cone-plate setup could not successfully be done. Due to the high solidity of the polymers at 37 °C the cone was breaking the polymer bulk integrity. Consequently, measurements with the cone-plate setup were not possible. Another reason for the parallel plate setup was that measurements of smaller sample volumes compared to the cone-plate setup were feasible.

The PGA backbone and the pure stearyl PGAs were loaded onto the plate geometry at 37 °C. For the polymers containing behenic acid, loading was performed at 70 °C before equilibrating at measurement temperature.

Firstly an amplitude sweep test was conducted at a set frequency of 1 Hz over a shear strain range from 0.01% to 100%, to detect the linear viscoelastic region (LVER) of the polymers. Thereafter, a frequency sweep test at a shear strain within the LVER of 0.015% and over a frequency range from 0.1 Hz to 10 Hz was performed. The obtained data were evaluated using the rSpace software for Kinexus (Version 1.75, Malvern Panalytical GmbH, Nuremberg, Germany).

3.1.6 ELECTRON PARAMAGNETIC RESONANCE (EPR)

EPR experiments with PGA-B45 and PGA-B45-S35 were conducted to gain insight into the penetration behaviour of water into the polymer and their microviscosity. Since the FA-PGAs are diamagnetic and EPR silent, the addition of stable free radicals, so-called spin probes, is necessary. Tempol-d17 (4-Hydroxy-TEMPO-d17) was chosen as a spin probe for the EPR measurements, due to its sharper signals in comparison to the undeuterated Tempol. Therefore, a stock solution of the spin-probe Tempol-d17 in methanol was added to 200 mg of FA-PGA resulting in a Tempol-d17 concentration of 1.0 mmol/kg. The organic solvent was then removed under vacuum in a vacuum drying oven (VD 53, BINDER GmbH, Tuttlingen, Germany) at 25 °C for 24 h. Afterward, the dried mixture was milled using a CryoMill (Retsch GmbH, Haan, Germany) to powder the sample and to ensure homogeneity. The milling was conducted for 3 x 1.5 min with a vibration frequency of 30 Hz after pre-cooling the sample to -197 °C with liquid nitrogen for 5 min. Subsequently, the powdered sample was filled into the sample holder at 70 °C, which is above the melting temperature of the fatty acid side chains. After cooling down to room temperature, this resulted in a homogenous sample with a plane surface capping off with the cavity of the sample holder.

The prepared sample holders were exposed to 20 mL of Sørensen's phosphate-buffered saline (PBS) pH 7.4 preserved with 0.02 % (w/v) sodium azide in a shaking water bath (SW 23, JULABO GmbH, Seelbach, Germany) at 37 °C and 60 rpm. At defined time points the samples were withdrawn from the buffer and dabbed carefully with a paper towel to remove the remaining PBS from the surface.

EPR measurements were carried out with a 1.1 GHz (L-band) EPR spectrometer (Magnettech GmbH, Berlin, Germany) connected with a re-entrant resonator operating at a microwave frequency of 1.1 - 1.3 GHz. The sample holders were placed onto a positioning device (Figure 6) to ensure a reproducible measurement position and measured with the following parameters: magnetic field center 48.9 mT, scan range 10 mT, scan time 60 s, modulation amplitude 0.1 mT. Evaluation of the spectra and peak amplitudes was done with the MultiPlot 2.0 software (Magnettech GmbH, Berlin, Germany). For the calculation of the order parameter (S-parameter), the software "Nitroxide Spectra Simulation-

Freeware Version. 4.99–2005" ("Jozef Stefan" Institute, Department of Solid State Physics, Ljubljana, Slovenia) was used [117].

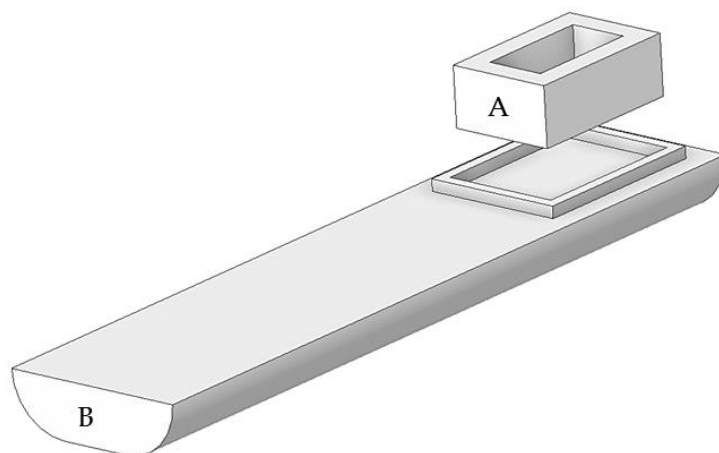


Figure 6: Sample holder (A) and positioning device (B) used for EPR measurements. The internal dimensions of the sample holder are 10 mm x 5 mm x 4 mm (length x width x height).

The sample holder and positioning device were designed and 3D-printed for this purpose. 3D printing was performed with a German RepRap X350pro using a PLA filament with a diameter of 1.75 mm (all German RepRap GmbH, Feldkirchen, Germany). The inner dimensions of the sample holder were set to be 10 mm x 5 mm x 4 mm (length x width x height) which equals a volume of 200 mm³.

3.2 PREPARATION AND CHARACTERIZATION OF MICROPARTICLES

3.2.1 PREPARATION OF MICROPARTICLES

Microparticles were prepared according to a solvent evaporation method similar to previously described processes [118][119]. The general setup of the preparation is displayed in Figure 7.

100 mg of polymer were dissolved in 2 mL methylene chloride (DCM) and injected into 300 mL of 0.5% (w/v) aqueous polyvinyl alcohol (PVA) solution under stirring with a paddle (75 mm x 19 mm). For the preparation of loaded microparticles, various percentages (w/w; related to the polymer mass) of the thiamine derivatives were dissolved in the polymer solution prior to injection.

The injection was performed using a Syringe Pump Model 11 (Harvard Apparatus, Holliston, MA, USA) and a 2.5 mL GASTIGHT® syringe equipped with a 23 gauge metal hub needle (Hamilton Germany GmbH, Graefelfing, Germany) with an injection rate of 5.2 $\mu\text{L}/\text{min}$. Stirring was carried out with an IKA® RW 20 overhead stirrer (IKA Werke GmbH & Co. KG, Staufen im Breisgau, Germany) at 240 rpm (if not stated otherwise). After injection, the residual solvent was removed with a rotary evaporator. Subsequently, the suspension was washed three times with distilled water via centrifugation with a LABOFUGE® 300 (Heraeus, Hanau, Germany). Eventually, the particles were dried by lyophilization using a Christ Alpha 1-2 (Martin Christ Gefriertrocknungsanlagen GmbH, Osterode am Harz, Germany).

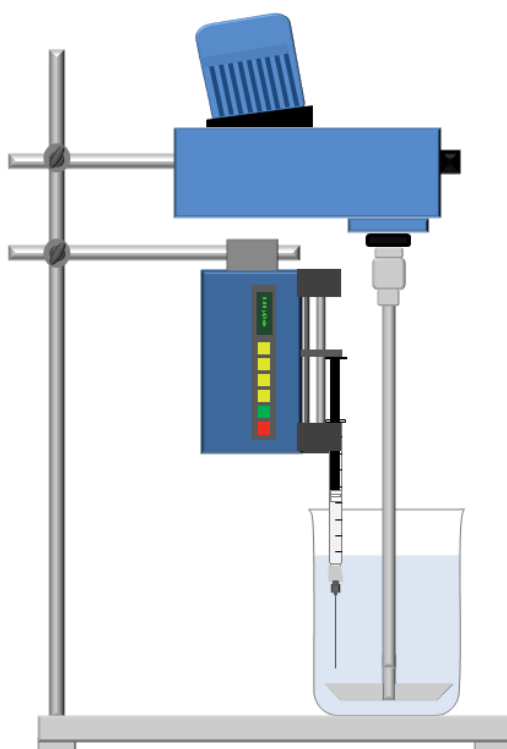


Figure 7: Experimental setup of the microparticle preparation process.

3.2.2 LASER DIFFRACTION ANALYSIS

Particle size distribution was determined by laser diffraction analysis with a Mastersizer 2000 equipped with a Hydro 2000 S dispersion unit (both Malvern Panalytical GmbH, Nuremberg, Germany). Each sample was measured in triplicate in distilled water. The data were evaluated with the Mastersizer 2000 software (Version 5.60) and the median $d(0.5)$, as

well as $d(0.1)$ and $d(0.9)$ values, are reported as a volume average in 4.2.2. The $d(0.1)$ and $d(0.9)$ values describe the upper size limit not reached by 10% resp. 90% of the particles. Additionally, the span was calculated as a parameter for the distribution width:

$$\text{Span} = \frac{(d(0.9) - d(0.1))}{d(0.5)} \quad \text{(Equation 1)}$$

3.2.3 SCANNING ELECTRON MICROSCOPY (SEM)

Scanning electron micrographs were taken with a Philips ESEM XL 30 FEG (Philips Electron Optics, Amsterdam, Netherlands). Before measuring, the samples were sputter-coated with a layer of chromium (approx. 30 nm) by ion beam deposition to improve the SEM imaging of non-conductive and beam-sensitive materials. Images were taken under high vacuum with an acceleration voltage of 2 kV.

3.2.4 DETERMINATION OF DRUG LOADING AND ENCAPSULATION EFFICIENCY BY HIGH-PERFORMANCE LIQUID CHROMATOGRAPHY (HPLC)

Drug loading and encapsulation efficiency (EE) of the thiamine derivatives were determined by high-performance liquid chromatography (HPLC). For the extraction of the API and to precipitate the polymer, 1 mg of loaded microparticles was dissolved in 1 mL methylene chloride, added to 9 mL of methanol and agitated on a Reax top apparatus (Heidolph Instruments GmbH & CO. KG, Schwabach, Germany) at 2000 rpm for 30 s. Subsequently, the precipitated polymer was separated by centrifugation with an IKA mini G (IKA-Werke GmbH & CO. KG, Staufen, Germany) at a fixed speed of 6000 rpm for 10 min. Each sample was prepared in triplicate.

Measurements were performed on an HPLC system equipped with a Waters Delta 600 Pump and controller, a Waters 717plus Autosampler, a Waters 2996 Photodiode Array Detector (Waters Corporation, Milford, MA, USA). DBT was analyzed with an XTerra RP18 (150 mm x 3.9 mm; 5 μ m) column (Waters Corporation, Milford, MA, USA) and SBT with a NUCLEODUR® C18 ISIS (150mm x 3mm; 5 μ m) column (MACHERY-NAGEL GmbH & Co. KG, Dueren, Germany) at a column temperature of 30 °C.

Runs were executed for both APIs by gradient elution with the parameters shown in Table 6. Both substances were detected at a wavelength of 265 nm. DBT was eluted with a retention time of 12.53 min and SBT with a retention time of 17.05 min.

Table 6: Measuring parameters for the determination of drug loading and encapsulation efficiency of DBT and SBT by HPLC analysis.

Analyte	Dibenzoyl Thiamine	Sulbutiamine
Column	XTerra RP18 (150 mm x 3.9 mm; 5 µm)	NUCLEODUR® C18 ISIS (150 mm x 3 mm; 5µm)
Mobile Phase	A: Water/MeOH - 85/15 (v/v) B: MeOH	A: Water/ Mobile Phase B - 80/20 (v/v) B: MeOH/ACN - 70/30 (v/v) + 0.1% (v/v) TFA
Flow Rate	1 mL/min	0.4 mL/min
Injection Volume	20 µL	20 µL
Gradient Elution	0 min - 100% A → 100% B 10 min 10 min - 100% B 18 min 18 min - 100% B → 100% A 19 min 19 min - 100% A 34 min	0 min - 100% A → 100% B 10 min 10 min - 100% B 18 min 18 min - 100% B → 100% A; 19 min 0.5 mL/min 19 min - 100% A; 0.5 mL/min 34 min 34 min - 100% A; 0.5 mL/min 35 min → 100% A; 0.4 mL/min

Subsequently, the encapsulation efficiency was calculated with the following equation (Equation 2):

$$EE (\%) = \frac{(\text{total drug added} - \text{non-entrapped drug})}{\text{total drug added}} \times 100 \quad (\text{Equation 2})$$

3.2.5 X-RAY POWDER DIFFRACTION (XRD)

X-Ray patterns were acquired with an STOE STADI MP (STOE & Cie GmbH, Darmstadt, Germany) operating with Mo-K α radiation ($\lambda = 0.071073$ nm) and equipped with a curved primary Ge(111) monochromator and a DECTRIS MYTHEN 1 K strip detector. The rotating samples were measured in transmission mode from $2\theta = 5^\circ$ - 41° in 0.5° steps and an exposure time of 140 s, after powdering of the samples with a CryoMill (Retsch GmbH, Haan, Germany). The data obtained were evaluated with the STOE WinX^{POW} software package. For better graphical visualization, data was depicted from $2\theta = 5^\circ$ - 20° since the relevant DBT peaks appear in this area and no peaks were detected in the range from 20° - 41° .

3.2.6 IN VITRO RELEASE OF DIBENZOYL THIAMINE

To assess the release behaviour *in vitro*, 10 mg of microparticles loaded with 6% DBT (w/w) were placed in 50 mL PBS pH 7.4 containing 0.2% sodium dodecyl sulfate (SDS) and 0.02% sodium azide for preservation. The samples were agitated in a shaking water bath (60 rpm) under light protection at 37 °C. In regular time intervals, 1 mL release medium was taken for analysis and replaced with fresh buffer solution. The withdrawn samples were centrifuged with an IKA mini G (IKA Werke GmbH & Co. KG, Staufen im Breisgau, Germany) for 10 min to separate potentially withdrawn particles. Eventually, the samples were analyzed with an Agilent 1100 Series HPLC system (Agilent Technologies Inc., Santa Clara, CA, USA) equipped with a NUCLEODUR® C18 ISIS (150mm x 3mm; 5 μ m) column. The used HPLC method was the same as described in 3.2.4 but with a flow rate of 0.4 mL/min.

For further evaluation by residual analysis, the general setup was the same. At the time of sample taking the entire amount of particles was separated by centrifugation with a LABOFUGE® 300 (Heraeus, Hanau, Germany), washed three times with distilled water and lyophilized before analyzing it by HPLC (3.2.4). All release experiments were performed three times.

Previously, the saturation concentration of DBT and the stability of DBT in the dissolution medium were evaluated. Therefore, 50 mg of DBT were added to 100 mL of PBS pH 7.4 with or without surfactant and stirred with a magnetic stirrer (IKA C-MAG HS 7, IKA

Werke GmbH & Co. KG, Staufen im Breisgau, Germany) for 48 h. After the centrifugation of the sample with a LABOFUGE® 300 (Heraeus, Hanau, Germany), the saturation concentration was detected with the HPLC method described above. As surfactants Tween® 20, Tween® 80, Kolliphor® HS 15 and SDS in the concentrations of 0.2% (w/w) and 0.5% (w/w) were examined. For the stability testing of DBT in PBS pH 7.4 containing 0.2% SDS, a DBT solution of 50 µg/mL was stored in a water bath at 37 °C for 14 days. At regular time intervals, a sample was withdrawn and analyzed via HPLC.

3.2.7 CYTOTOXICITY

Toxicity assays for PGA-B45, PGA-B75 and PGA-B45-S35 microparticles were carried out with 3T3 (mouse embryonic fibroblasts) - and NHDF (normal human dermal fibroblasts) - cell lines. Therefore, the cells were seeded into 96-well plates (TPP® tissue culture test plate, TPP Techno Plastic Products AG, Trasadingen, Switzerland) and incubated in 100 µL cell culture medium at 37 °C and 5% CO₂ for 24 h in a Heraeus HeraCell CO₂ incubator (Thermo Fisher Scientific Inc., Waltham, MA, USA). The composition of the cell culture medium for the NHDF cells was Dulbecco's Modified Eagle's Medium D5796 (DMEM, without sodium pyruvate containing 10% (v/v) fetal calf serum and 1% (v/v) penicillin-streptomycin solution (all Sigma-Aldrich Chemie GmbH, Taufkirchen, Germany). For 3T3 cells DMEM D6429 (with sodium pyruvate) was used instead of DMEM D5796. Table 7 shows the quantities of the seeded cells. No cells were seeded in the first of the 12 columns of each well plate to determine the blank value of the cell culture medium.

Table 7: Cell quantities and concentrations (c) per time point, cell line and well plate size.

cell line	time point [h]	96-Well Plate			24-Well Plate		
		cells/well	volume/well [mL]	c [cells/mL]	cells/well	volume/well [mL]	c [cells/mL]
3T3	4; 24	1.0×10^4	0.1	1.0×10^5	6.0×10^4	0.5	1.2×10^5
	96	5.0×10^3	0.1	5.0×10^4	3.0×10^4	0.5	6.0×10^4
NHDF	4; 24	2.0×10^4	0.1	2.0×10^5	1.2×10^5	0.5	2.4×10^5
	96	5.0×10^3	0.1	5.0×10^4	3.0×10^4	0.5	6.0×10^4

After incubation of the cells for 24 h, 100 μL cell culture medium were added to columns 1 (blank) and 2, whereas column 3 was treated with 100 μL of a 0.05% (v/v) Triton[®] X 100 solution. Hence, column 2 remained untreated as a negative control of viable cells and column 3 served as a positive control of completely inhibited cells. The remaining columns were treated by adding 100 μL of a microparticle suspension in cell culture medium leading to final polymer concentrations of 1, 5, 10 and 20 mg/mL. Subsequently, the well plates were incubated for another 4, 24 and 96 h. Each sample was prepared for each time point and cell line in triplicate.

The determination of the cell viability was done by resazurin reduction assay. Therefore, 20 μL of 440 μM resazurin solution were added to each well and incubated for 2 h. Fluorescence intensities were measured with the Cytation[™] 5 cell imaging reader (BioTek Instruments Inc., Winooski, VT, USA) using the RFP filter set with an excitation wavelength of 531 nm and an emission wavelength of 593 nm. The cell viability was calculated as a percentage of the negative control (untreated cells) after subtraction of the blank value.

To determine if the physical pressure of the microparticles on the cells had an impact on the cell viability, another experimental setup was implemented for the PGA-B75 microparticles (Figure 8). Thus, 3T3 and NHDF cells were seeded into 24-well plates (Table 7) and incubated as mentioned before. 0.5 mL of cell culture medium were added to column 1 (blank) and 2 (negative control) and 0.5 mL of a 0.05% (v/v) Triton[®] X 100 solution to column 3 (positive control). Besides, 0.3 mL of culture medium were pipetted into the remaining wells equipped with ThinCert[™] cell culture inlays with a pore size of 3 μm (Greiner Bio-One GmbH, Frickenhausen, Germany). A volume of 0.2 mL of the PGA-B75 microparticle suspension in cell culture medium was added into the ThinCerts[™] and the well plates were incubated for 4 and 24 h. The final polymer concentration was 20 mg/mL. After incubation, the ThinCerts[™] containing the microparticles were removed and the medium was withdrawn completely. 1 mL of 44 μM resazurin solution was added in each well and the fluorescence intensity was measured with the Cytation[™] 5 cell imaging reader as described above. Due to the high amount of polymer necessary for the experiment, the measurements for each sample were performed only twice for each time point and cell line.

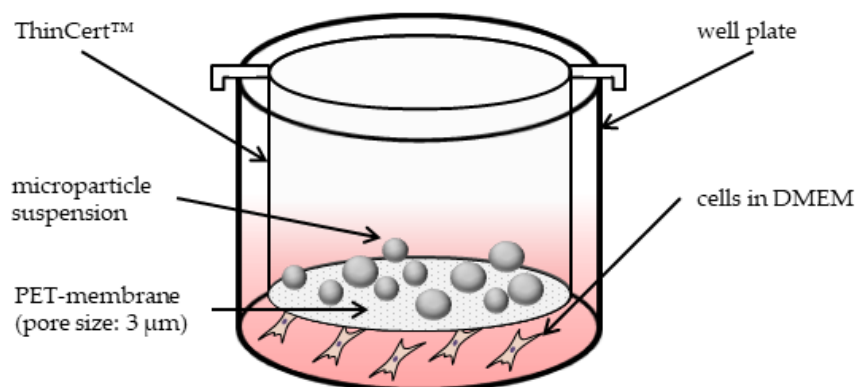


Figure 8: Experimental setup for toxicity assays with cell culture inserts.

3.2.8 ELECTRON BEAM STERILIZATION

As a sterilization method, electron beam irradiation was chosen. Therefore, PGA-B75, DBT and PGA-B75 microparticles were irradiated by a 10 MeV linear accelerator MB 10-30 MP (MeveX, Stittsville, ON, Canada) on a moving tray (95 cm/min). All samples were treated with a total dose of 25 kGy portioned into two separate doses of 12.5 kGy each. The beam current was 250 mA at a pulse frequency of 450 Hz with a pulse duration of 8 μs. To assess polymer degradation and inactivation of the API, GPC measurements (3.1.2) and HPLC analysis (3.2.4) were performed.

3.2.9 *IN VITRO* RELEASE OF DIR

For the *in vitro* release of the fluorescent dye DiR, PGA-B75 was used as a polymer matrix. Instead of the thiamine derivative, DiR was incorporated as a model drug during the microparticle preparation. Therefore, 80 μL of a DiR stock solution (0.025 mg/mL DCM) were added to the polymer solution (50 mg/mL DCM). Further preparation steps were done according to 3.2.1. The final nominal concentration of DiR in the PGA-B75 microparticles was 0.002% (w/w). Each sample was prepared in triplicate.

10 mg of DiR loaded microparticles were placed on a Greiner Bio-One ThinCert™ (Frickenhausen, Germany) with a translucent PET membrane (pore size 3 μm) in a 24 well plate. The samples were exposed to 2 mL PBS 7.4 containing 0.2% SDS and 0.02% sodium azide for preservation and agitated (60 rpm) under light protection in a shaking water bath at 37 °C. At defined time points the release medium was withdrawn and measured with

the fluorescence spectrometer as described in 3.2.11. Additionally, the ThinCerts™ containing the microparticles were removed from the well plate and analyzed with the fluorescence imager according to 3.2.10. Subsequently, the ThinCerts™ were placed back in the well plate and fresh buffer solution was added. The investigation was terminated after 85 days consistent with the *in vivo* release experiment.

3.2.10 FLUORESCENCE IMAGING

In vitro fluorescence imaging was carried out with the Maestro™ *in vivo* imaging system (Cambridge Research & Instrumentation Inc., Hopkinton, MA, USA). A near-infrared (NIR) filter set with a 710 nm to 760 nm excitation filter and an 800 nm long-pass emission filter was used to detect the DiR signal. The image cubes were acquired in 10 nm steps in the range of 780 to 950 nm and evaluated with the Maestro™ software (Version 2.10.0). The exposure time was automatically set to the optimum value (autoexposure) and the total fluorescence signal was correlated to the respective value by the software.

3.2.11 FLUORESCENCE SPECTROSCOPY

Fluorescence measurements were conducted on a FluoroMax-4 spectrofluorometer (HORIBA Jobin Yvon GmbH, Bensheim, Germany). The DiR signal was detected by single point acquisition at an excitation wavelength of 750 nm and an emission wavelength of 780 nm. All samples were measured in a 10 mm quartz cuvette. The obtained data were analyzed using the FluorEssence™ software (HORIBA Jobin Yvon GmbH, Version 3.8.0.60).

3.2.12 *IN VIVO* CHARACTERIZATION

3.2.12.1 ANIMAL CARE

All *in vivo* experiments were approved (Approval No. 42502-2-1529 MLU) by the local authorities of Saxony-Anhalt, Germany. Furthermore, they complied with the guidelines of the Federation for Laboratory Animal Science Associations (FELASA). The *in vivo* studies were performed on four male and four female hairless, immunocompetent SKH1-Elite mice (SKH1-*Hr^{Hr}*, Charles River, Sulzfeld, Germany) bred by the center for basic research (ZMG) of the Martin Luther University of Halle-Wittenberg. The initial average age of the mice was 6 months and they were kept under controlled conditions (12 h light/dark cycle, 24 °C, 65% RH, feed and water *ad libitum*) in groups of a maximum of five animals.

3.2.12.2 SAMPLE PREPARATION

Based on the *in vitro* characterization of the FA-PGA microparticles, PGA-B75 microspheres were chosen for the *in vivo* study. Therefore, two different microparticle formulations were prepared under aseptic conditions.

To study polymer degradation *in vivo* a fluorescence-labeled PGA-B75-DY782 was used for formulation A. The preparation of the microparticles was done according to 3.2.1. For the synthesis of the fluorescent-labeled PGA, 1 mg of fluorescent dye DY-782 was labeled to 100 mg of PGA-B75 by Prof. Kreßler's research group at the Institute of Chemistry (Martin Luther University of Halle-Wittenberg, Germany) as described in [66]. To purify the product of synthesis, the polymer was dialyzed against water for 24 h using a dialysis membrane (Carl Roth GmbH & Co. KG, Karlsruhe, Germany) with a molar mass cut-off of 1 kDa. Subsequently, further dialysis steps against DMF (24 h) and THF (48 h) were performed and the final product was dried under nitrogen flow.

To study the release behaviour of the DDS *in vivo*, DiR loaded microparticles (0.002% (w/w)) were prepared as described in section 3.2.9 (formulation B). Thereby, the incorporated fluorescent dye DiR was functioning as a model drug.

3.2.12.3 INJECTIONS AND ANESTHESIA

For the injection of the formulations, the mice were divided into two groups. Both treatment groups (A+B) consisted of four mice (two male and two female). Group A was treated with the fluorescence-labeled PGA-B75-DY782 microparticles and group B with the DiR loaded PGA-B75 microparticles.

The mice were anesthetized with 2.5% (v/v) of isoflurane (Forene®, AbbVie Deutschland GmbH & Co. KG, Wiesbaden, Germany) in oxygen at a flow of 3 L/min with the XGI-8 Gas Anesthesia System (Caliper LifeScience, Waltham, MA, USA) and MIDMARK® MatrX VIP 3000® Isoflurane Vaporizer (Midmark, Dayton, OH, USA). 200 µL of the microparticle suspension (20 mg/mL) were slowly injected subcutaneously into the nuchal fold (24 G cannula). Aqueous sucrose solution 10% (m/v) was used as a dispersant. The mice were kept in anesthesia (2.5% (v/v), 0.25 L/min), during the multispectral fluorescence imaging.

On day 32 of the study, one male mouse of treatment group A had to be removed from the experiment due to an ocular disease, which was not related to the administered formulation. Furthermore, one male mouse of treatment group B had to be withdrawn from the experiment on day 56 due to neoplasia at a bite wound unrelated to the applied formulation and remote from the injection site. The experiment was conducted for a maximal period of 84 days as approved by the relevant authorities (Approval No. 42502-2-1529 MLU).

3.2.12.4 MULTISPECTRAL FLUORESCENCE IMAGING

Measurements were performed at defined time points on an IVIS® Spectrum *In Vivo* Imaging System (PerkinElmer Inc., Rodgau, Germany) in the epi-illumination fluorescence mode at auto exposure. To detect the NIR dyes DiR and DY-782 a filter pair with a 745 nm excitation filter (30 nm bandwidth) and an 800 nm emission filter (20 nm bandwidth) was used. The four mice were placed on a tempered stage (37 °C) to prevent a decrease of the body temperature during the measurement. The field of view was set to “D”. Image and data processing was carried out with the PerkinElmer® Living Image® 4.7.3 software. Furthermore, the brightness was set to 100, contrast to 1.5 and opacity to 100 using the “rainbow” color table in reverse scale. The binning was set to 1 and the smoothing to “none”. To cut off the autofluorescence of the mice the minimum of the color scale was set to 5.0×10^7 (p/sec/cm²/sr)/(μW/cm²). The maximum of the color scale was set above the maximal detected radiant efficiency of all taken fluorescence images to 2.0×10^9 or 1.25×10^{10} (p/sec/cm²/sr)/(μW/cm²) for the detection of DY-782 and DiR, respectively.

For the evaluation of the experiment, the intensity values of day 1 were set to 100% since after 24 hours the system was in balance and reproducible measurements were possible. By that time the suspension medium was completely absorbed from the mouse tissue and the microparticles were condensed on the site of injection.

3.3 PREPARATION AND CHARACTERIZATION OF PREFORMED IMPLANTS

3.3.1 PREPARATION OF PREFORMED IMPLANTS

FA-PGA implants were formed with a custom-made heating press (Figure 9) manufactured by the workshop of Precision Mechanics at the Institute of Chemistry (Martin Luther University of Halle-Wittenberg). For the preparation PGA-B45, PGA-B75 and PGA-B45-S35

were chosen as a matrix since they are able to form solid implants at both room and body temperature. Prior to compression, a mixture of powdered FA-PGA and 6% DBT (w/w) was prepared using a CryoMill (Retsch GmbH, Haan, Germany) with six milling cycles each for 2.5 min at 20 Hz. Thereafter, 40 mg of the mixture were filled in the cylindrical cavity of the heating press (diameter 5.5 mm) and tempered for 15 min at a temperature above the melting temperature of the fatty acid side chains. The set temperatures were 41 °C for PGA-B45-S35, 50 °C for PGA-B45 and 53 °C for PGA-B75. After tempering, the polymers were compressed with a cylindrical Teflon stamp loaded with 1 kg for 5 minutes. The compressed implants were cooled down for 1 hour at room temperature and finally ejected from the heating press.

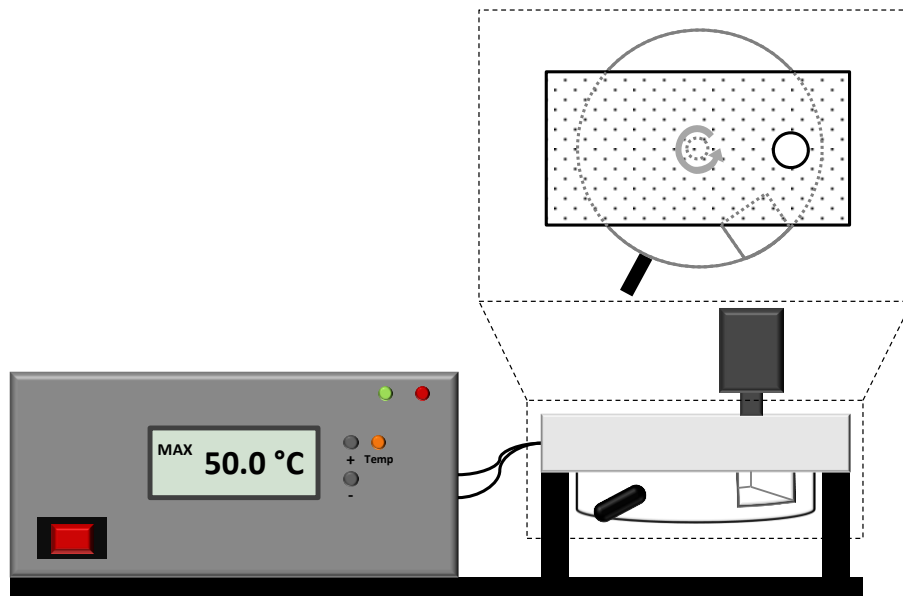


Figure 9: Schematic illustration of the heating press.

3.3.2 LIGHT MICROSCOPY

For visualizing the prepared implants, an Olympus SZX9 reflected-light microscope equipped with a UC30 camera was used. The pictures were processed with OLYMPUS Stream Motion software (all Olympus Europa SE & Co. KG, Hamburg, Germany).

3.3.3 TEXTURE ANALYSIS

To analyze the mechanical properties of the FA-PGA implants, the required force to press a metal cylinder with a constant velocity into the samples was recorded. The measurements were carried out with a CT3™ Texture Analyzer (AMETEK GmbH / B.U. Brookfield, Hadamar-Steinbach, Germany). Therefore, the implant was placed onto the sample table

and compressed by the measurement tool with a velocity of 0.01 mm/s at 23 °C. As a measurement body, a cylinder with a diameter of 2 mm was used (accessory TA39). The trigger force was set to be 0.01 N and the target distance 1.0 mm. For data recording and processing, the accompanying TexturePro CT software (Version 1.7 Build 35) was used.

3.3.4 DETERMINATION OF DRUG LOADING AND DRUG DISTRIBUTION BY HIGH PERFORMANCE LIQUID CHROMATOGRAPHY (HPLC)

Drug loading and drug distribution in the FA-PGA implants were determined with the HPLC method described in section 3.2.4. Therefore, the samples were divided into four fractions (A1, A2, A3 and B) with a scalpel. Subsequently, each fraction was analyzed separately via HPLC and the standard deviation of the obtained values was calculated.

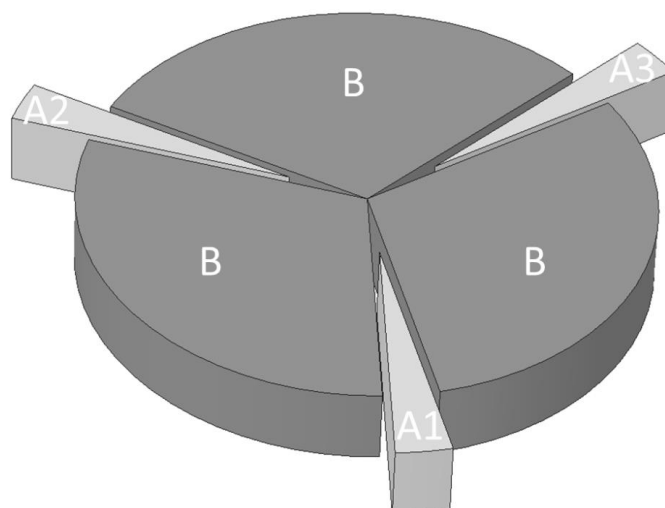


Figure 10: Schematic illustration of preformed implants divided into fractions A1, A2, A3 and B.

3.3.5 *IN VITRO* RELEASE OF DIBENZOYL THIAMINE

The *in vitro* release of DBT from the FA-PGA implants was conducted in 20 mL PBS pH 7.4 containing 0.2% SDS and 0.02% sodium azide for preservation. Therefore, the implants loaded with 6% DBT (w/w) were placed in 20 mL brown glass vials and incubated with release medium at 37 °C and mild agitation (60 rpm) in a shaking water bath under light protection. At predetermined time points, the release medium was fully exchanged with fresh buffer solution and analyzed via HPLC as described in 3.2.6. The sampling interval did not exceed three days.

4 RESULTS AND DISCUSSION

4.1 CHARACTERIZATION OF BULK POLYMERS

4.1.1 DIFFERENTIAL SCANNING CALORIMETRY (DSC)

DSC measurements of the bulk polymers were conducted to investigate the thermal properties of the various FA-PGAs with particular regard to their physiological application at 37 °C body temperature. As apparent from the resulting thermograms in Figure 11, PGA is an amorphous polymer with a glass transition temperature (T_g) at -30.2 °C. By esterification of the pendant hydroxyl groups of the PGA backbone with fatty acids, comb-like polymers are obtained. For comb-like polymers, the formation of self-organized layered structures and a phase separation between the amorphous backbone and crystalline side chains have been reported [72,120–122]. In that regard, grafting of the backbone with fatty acids led to the occurrence of endothermic peaks in the heating traces. These endothermic events are caused by the melting of the acyl side chains and appear gradually over a temperature range of about 10 °C. Compared to the pure fatty acids, the melting points of the alkyl side chains occurred at considerably lower temperatures. These observations are referable to the packing mode and crystal order of the different substances. Due to the high crystallinity and regularity of the pure stearic- and behenic acid in comparison to the FA-PGAs, higher energy is required for melting. With both, the increase in chain length and the acylation degree of the polymer, a more ordered packing mode and an increase in the crystal order are presumed [123]. Therefore, higher melting temperatures (T_m) were detected with increasing substitution degree and increasing length of the acyl side chain. A summary of glass transition and melting temperatures is shown in Table 8

Alongside the endothermic peaks in the heating traces, glass transitions were observed in the thermograms of the FA-PGAs as well. These temperatures were also dependent on the acylation degree of the polymer backbone and were increasing correspondingly. Hence, the increasing T_g originates from a decrease in the mobility of the polymer chains due to sterical interferences of the acyl side chains. This phenomenon agrees with previously published research [85,124]. For PGA-S90, the T_g was not distinctly detectable since the step in the baseline of the thermograms was becoming less pronounced with higher crystallinity of the polymers. The presence of both a glass transition and a melting point indicates a

semi-crystalline behaviour for the FA-PGAs with an amorphous polymer backbone and crystalline side chains.

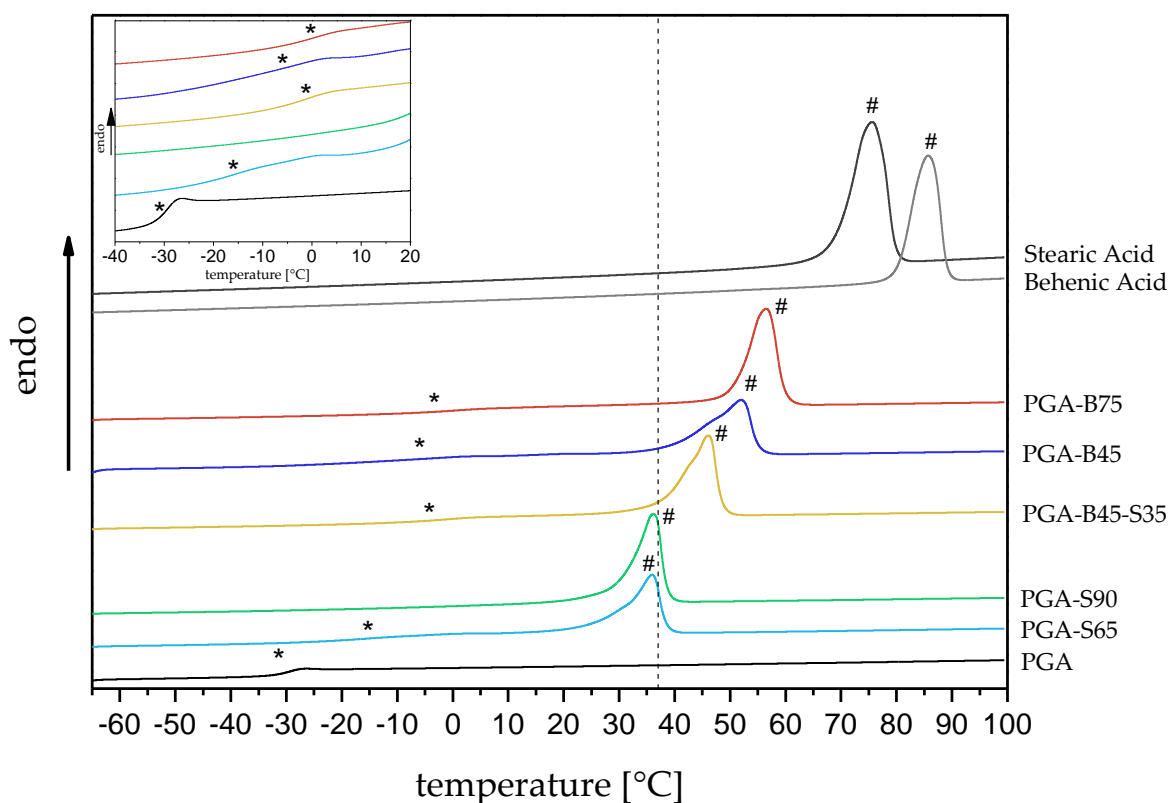


Figure 11: DSC thermograms of fatty acids, PGA and FA-PGAs. The symbols (*, #) indicate the glass transition and the melting points in the second heating curves; the vertical dotted line represents body temperature (37 °C).

The thermal behaviour of the FA-PGAs at body temperature is decisive for the applicability *in vivo* as it will presumably influence other properties such as rheological parameters, drug release and water penetration inside the polymer. For the stearic acid substituted PGAs the melting temperatures were around 36 °C whereas they were well above 37 °C for the PGAs containing behenic acid. Based on the melting temperatures of the acyl side chains, it was questionable if the pure stearyl PGAs, which are solid at room temperature, are still able to form solid DDSs in a physiological environment at 37 °C. Therefore, more detailed investigations of the macroviscosity of these polymers at body temperature were conducted in the subsequent section (4.1.4).

Table 8: Glass transition (T_g) and melting temperatures (T_m) of fatty acids, PGA and FA-PGAs.

Substance	T_g [°C]	T_m [°C]
PGA	-30.2	NA
PGA-S65	-15.2	35.8
PGA-S90	ND	36.2
PGA-B45	-8.1	55.8
PGA-B75	-1.6	59.6
PGA-B45-S35	-2.3	46.2
Stearic acid	NA	75.5
Behenic acid	NA	85.7

4.1.2 STABILITY TESTING

A storage stability test was implemented to determine the storage conditions for the bulk polymers and to gain evidence on possible quality variations under the influence of temperature and humidity. In addition, it could give a first indication of the shelf life of future DDSs. The examined storage conditions and the packaging in a container closure system were based on the ICH guidelines “Stability Testing of New Drug Substances and Products” [116] which are an essential directory for the pharmaceutical industry.

Therefore, the molecular weight of the bulk polymers was used as a quality parameter during storage (Figure 12). Concerning the storage in the refrigerator at 4 °C neither PGA nor the FA-PGAs showed any significant alteration in the molar mass or the polydispersity index (PDI). Thus, all examined bulk polymers were stable over the testing period of 3 months while stored in the refrigerator.

Exaggerated storage conditions at 40 °C and 75% RH were investigated as well to increase the rate of possible chemical degradation and to assess the quality of the polymer for longer storage terms. The results showed that no substantial effects on the molecular weight or PDI could be detected for the FA-PGAs whereas the pure PGA revealed a decrease of the number average molar mass and an increase of the PDI between days 7 and 28. These values imply a higher number of shorter polymer chains and a broader molecular weight distribution, hence, a higher heterogeneity in the PGA sample. Accordingly, hydrolysis

triggered by high temperature and humidity could be a probable cause for the degradation of the polymer backbone. Modification of the backbone with fatty acids delays these effects. This could be attributed to the higher lipophilicity and the shielding of the cleavable ester bonds of the backbone by the side chains.

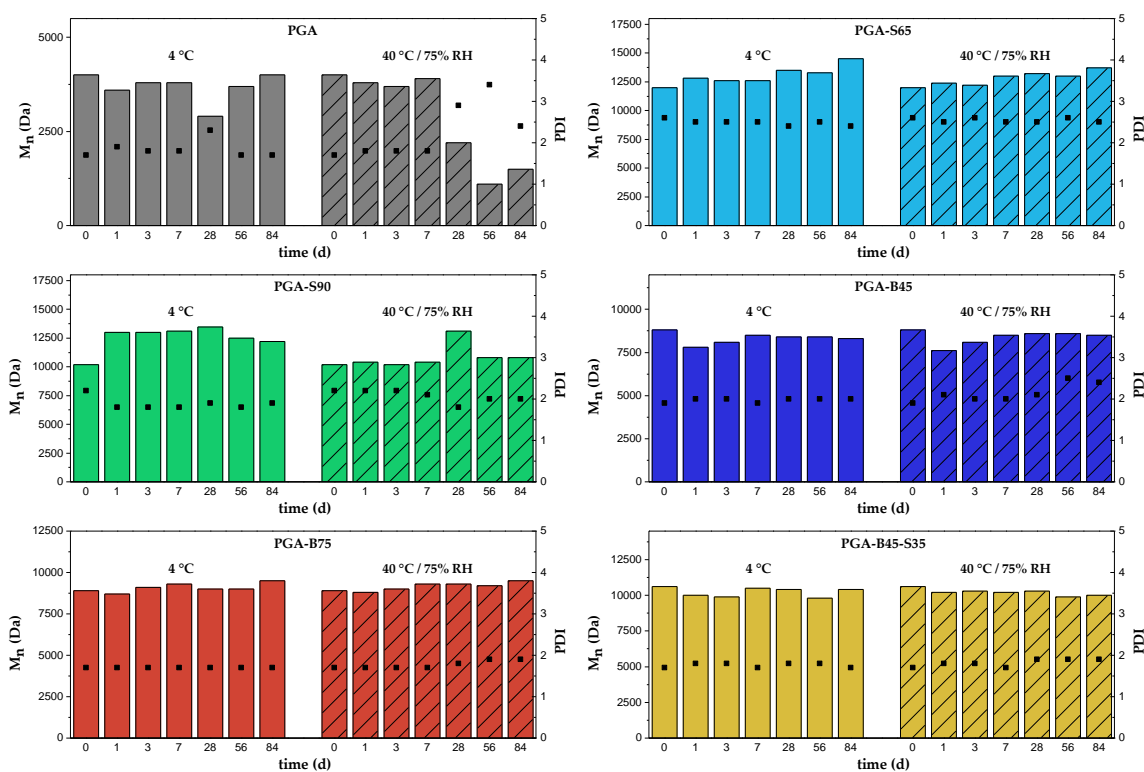


Figure 12: Number average molar masses (M_n) and polydispersity indices (PDI) of bulk polymers during storage at two different storage conditions. Columns indicate the M_n , dots represent the PDI.

Concluding from this data, the storage conditions for PGA were set to 4 °C for a maximum of 3 months to prevent changes in the molecular weight distribution. Although no changes occurred for the FA-PGAs even at accelerated conditions, storage conditions were set to be the same as for PGA. To determine the possible storage duration for the modified PGAs exactly, further long-term studies at 4 °C have to be conducted. Nevertheless, it can be stated that the shelf life of these FA-PGAs at 4 °C is above 3 months.

4.1.3 STATIC CONTACT ANGLE

Static contact angle θ measurements between water and the polymer surface were undertaken to examine the influence of the grafting of the PGA backbone on the wettability of the polymer. The higher the affinity with water the lower the static contact angle. Hence, low θ values correlate to hydrophilic and high θ values to hydrophobic surfaces.

Nevertheless, the threshold between hydrophilicity and hydrophobicity is not strictly to be set at 90° [125]. The hydrophilicity of the polymer is a relevant parameter to estimate its behaviour during *in vitro* or *in vivo* experiments in an aqueous environment and to predict its interactions with the API.

Table 9: Mean static contact angle values and standard deviations of measurements of water droplets on FA-PGAs and PGA. Experiments were performed with double distilled water ($1 \mu\text{L}$) after 30 s of droplet placement at 25°C .

Polymer	Contact Angle θ [$^\circ$]	Standard Deviation [$^\circ$]
PGA	40.1	4.1
PGA-S65	88.1	0.7
PGA-S90	91.5	3.4
PGA-B45	85.1	5.2
PGA-B75	95.8	2.4
PGA-B45-S35	89.1	3.5

The resulting θ values are displayed in Table 9. Since the static contact angle is a time-dependent variable, all measurements were conducted 30 s after droplet placement on the polymer film to obtain comparable values. PGA showed a rather hydrophilic character with a mean θ value of 40.1° due to its free hydroxyl groups. While not water-soluble, it swelled in water to a high degree [73].

For the FA-PGAs an increase in the θ values was observed up to a contact angle of 95.8° for PGA-B75. Moreover, higher contact angles were detected with increasing substitution degrees. Grafting of the polymer backbone with acyl side chains reduces the number of free hydroxyl groups and therefore, the hydrophilic portion of the polymer declines. Furthermore, the presence of lipophilic substituents in the polymer structure and the low availability of the remaining hydroxyl groups due to spatial rearrangements reinforce the change in the θ values [124]. Hence, the extent of the decrease in hydrophilicity depends on the acylation degree of the polymer backbone. Additionally, the surface wettability of the fatty acid-modified PGAs is also dependent on the length and consequently the hydrophobicity of the substituted side chain. Consequently, a total θ increase of 55.7° was

measured after grafting the PGA backbone with 75 mol% of behenic acid (C₂₂) whereas an increase of just 51.4° was detected for PGA-S90 (90 mol% C₁₈).

4.1.4 MACROVISCOSITY

Rheological measurements were conducted to investigate the macroviscosity of the bulk polymers. Rheology studies the flow and deformation of matter, thus, allowing to assess the behaviour of the examined material under physiological stress. Rheological properties affect the processability of the polymers, i.e. by melt extrusion or 3D printing, and their resistance to physiological stress, for example during or after injection into the subcutaneous tissue. The DSC measurements raised the question whether PGA-S65 and PGA-S90 are able to form solid DDSs in a physiological environment. To answer that and to obtain relevant data for planned *in vivo* studies, the experiments were performed at 37 °C.

The viscosity describes the resistance of the sample to deformation, hence, the relationship between viscous stress and the deformation rate. It is the most important rheological characteristic of a material. In oscillatory rheology, the viscosity is given as a function of the frequency - the complex viscosity η^* . For Newtonian fluids, the shear stress is linearly correlated to the deformation rate. Polymers are mostly non-Newtonian fluids, which show shear-thinning due to the disentanglement of macromolecules under shear strain. They combine elastic and viscous characteristics and are therefore described as viscoelastic [126]. The elastic portion of the viscoelastic behaviour is thereby represented by the storage modulus G' , which indicates the deformation energy stored in the material. G'' - the loss modulus - characterizes the energy lost through internal friction of the flowing material and therefore the viscous portion. Whether the elastic or the viscous portion predominates is indicated by the proportion of G' and G'' [127]. The proportion of storage and loss modulus is represented by the loss angle δ . For ideal-elastic systems, the loss angle is 0°, while the value is 90° for ideal-viscous materials. Consequently, viscoelastic materials that combine both characteristics show δ values between 0° and 90°, with 45° being the threshold that indicates equal fractions of viscous and elastic portions.

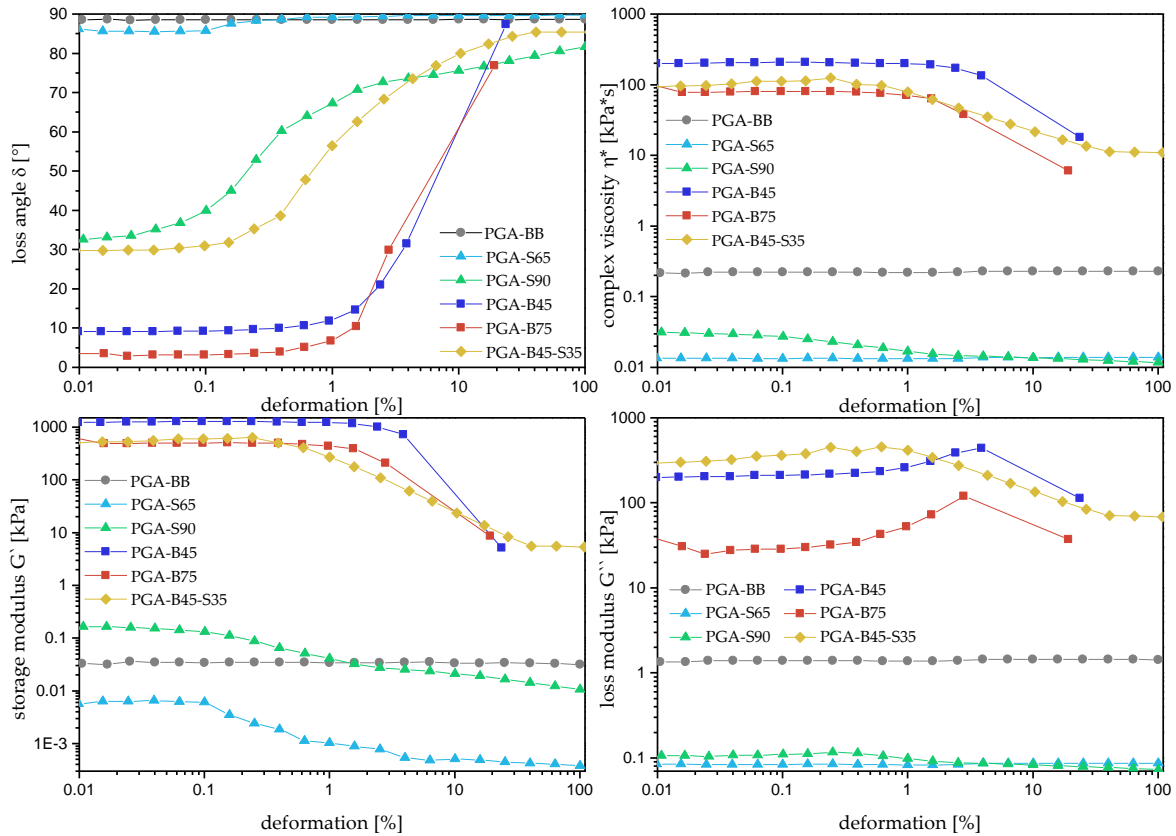


Figure 13: Amplitude sweep test at a set frequency of 1 s^{-1} . Deformation dependence of loss angle δ , complex viscosity η^* , storage modulus G' and loss modulus G'' at a temperature of $37 \text{ }^\circ\text{C}$.

Figure 13 displays an amplitude sweep test performed at a set frequency of 1 s^{-1} . For PGA-B45 and PGA-B75 data are shown up to a deformation of 20% only, since thereafter the texture broke down completely and the measurement was stopped. The purpose of an amplitude sweep test is to obtain information about the stability of the sample's structure while increasing the shear stress. It aims at determining the linear viscoelastic region (LVER) of the FA-PGAs. Furthermore, it allows the characterization of the rheological behaviour after the applied stress has exceeded this region, and consequently, yielding of the internal structure occurs. The region in which the internal sample structure is not dependent on the amplitude of the deformation and therefore is stable is defined as the LVER. In the LVER the storage modulus G' and loss modulus G'' are constant [128]. During the amplitude sweep, the moduli of all modified PGAs changed their plateau value at a certain deformation, while the PGA backbone was able to sustain its structure over the whole range. Furthermore, the loss angle δ , with a value of almost 90° , and the complex viscosity remained constant for the polymer backbone. This indicates an almost ideal-viscous behaviour for the PGA which acts virtually like a Newtonian fluid. As stated prior,

this behaviour is unusual for a polymer and is probably caused by the low molar mass which is below the entanglement molar mass. The stearyl PGAs showed linear viscoelasticity up to 0.1% deformation. For the behenoyl PGAs and the double substituted polymer, an LVER of up to approximately 0.3% was observed. The values of G' and G'' and their ratio in the LVER give an idea about the consistency of the material. If the sample has gel-like or solid characteristics and behaves like a viscoelastic solid at the set frequency the value of G' exceeds G'' . This applies for PGA-S90, PGA-B45, PGA-B75 and PGA-B45-S35. However, if $G' < G''$, as for PGA-S65, the material is a viscoelastic liquid with fluid properties.

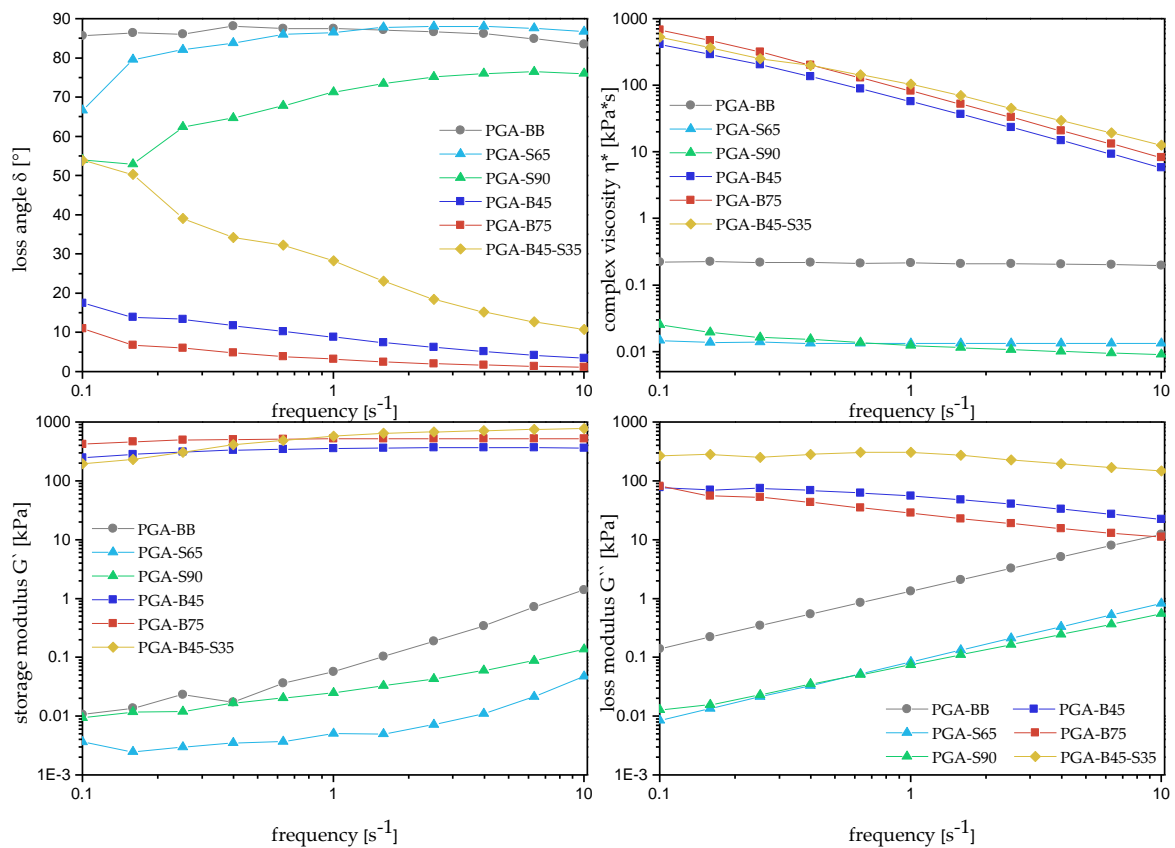


Figure 14: Frequency sweep test at 37 °C. The dependence of loss angle δ , complex viscosity η^* , storage modulus G' and loss modulus G'' on the shear rate at a default deformation of 0.015%.

Subsequently, a frequency sweep test was performed to give insight into the time-dependent behaviour of the material and the inner structure of the polymers (Figure 14). Thus, the deformation was set at a value of 0.015% which is in the range of the LVER for all investigated polymers. To measure the inherent material properties, it is essential to keep the deformation inside the LVER during the measurement, so that the polymer structure

remains unaltered and comparable results are obtainable. Figure 14 shows that the non-grafted PGA had a loss angle of almost 90° and a constant complex viscosity over the whole frequency range. These data are in agreement with the results of the amplitude sweep test and suggest the properties of a Newtonian fluid for the polymer backbone. During a frequency sweep the storage modulus G' is often unsteady for fluid materials, while it is nearly constant for solid samples. The PGAs grafted with only stearic acid showed an increase of the storage modulus with higher frequencies, whereas G' was virtually frequency-independent for all behenoyl PGAs. Hence, the constant G' values indicate a solid-like behaviour for the behenic acid substituted polymers at 37°C . Moreover, the δ values of PGA-B45 and PGA-B75 were below 45° over the whole frequency range, i.e. the elastic portion predominates the rheological properties. PGA-S65 and PGA-S90 on the other hand showed loss angles above 45° during the experiment and therefore revealed a highly viscous character. Interestingly, for the double substituted PGA-B45-S35, the viscous properties predominated at low frequencies, hence, at slow changes of stress. However, there was a shift to an elastic character at higher frequencies. As depicted by the decrease of the complex viscosity η^* , all behenoyl PGAs and to a small degree also PGA-S90 showed shear-thinning. Thereby, the entangled polymer chains disentangle and orientate along the flow direction. Furthermore, the η^* values of the stearyl PGAs were below the polymer backbone. This phenomenon could result from the molten acyl side chains, which act as a lubricant and, hence, facilitate the flow of the polymer chains. Furthermore, this lubricant effect may also be responsible for the higher loss angle values of PGA-B45-S35 at low frequencies. This assumption would presuppose that the stearyl side chains in the double substituted polymer are partly melting at body temperature. In comparison, the high complex viscosities of PGA-B45 and PGA-B75 suggest that the acyl side chains, meaning the crystalline polymer portion, impede the flow of the polymer chains. To flow freely, the polymer needs space between the individual macromolecules [129]. This free space is reduced by the crystalline side chains. Additionally, the acyl groups interfere with each other and therefore high η^* values were detected.

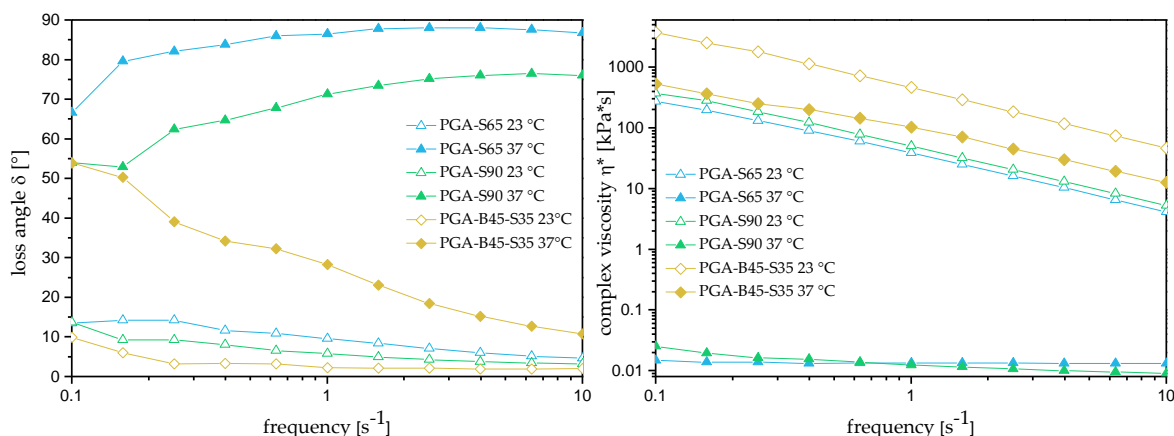


Figure 15: Comparison of loss angle δ and complex viscosity η^* for PGA-S65, PGA-S90 and PGA-B45-S35 at 23 °C and 37 °C during a frequency sweep test at a default deformation of 0.015%.

To evaluate if the high loss angle values and low complex viscosities of PGA-S65 and PGA-S90 were actually caused by the melting of the stearyl side chains, another frequency sweep test was conducted at 23 °C room temperature inside the LVER (amplitude sweep test at 23 °C, supplementary data Figure S1). Additionally, the rheological behaviour of PGA-B45-S35 was tested at 23 °C to examine the linkage between the relatively high δ values at low frequencies and the substituted stearic acid. According to the DSC data in section 4.1.1, the melting temperature of the stearyl side chains is not reached at that temperature and therefore they are still in a crystalline state. Figure 15 displays the loss angles and complex viscosities at 23 °C and 37 °C. The δ values at 23 °C were considerably lower compared to the values at 37 °C. Hence, PGA-S65 and PGA-S90 showed an elastic behaviour at room temperature, while the viscous portion predominated at body temperature. In contrast to the values at 37 °C, the loss angle of PGA-B45-S35 was greatly below 45 °C over the whole frequency range. The complex viscosity values at 23 °C were above the values at 37 °C for all investigated FA-PGAs, whereby the differences were considerably higher for PGA-S65 and PGA-S90. The obtained rheological data show that the polymers behaved substantially differently at both investigated temperatures. With exceeding temperatures above the melting point of the stearyl side chains, the evaluated FA-PGAs showed lower complex viscosities and an increase in the viscous portion leading to higher loss angle values. Furthermore, the low δ values of PGA-B45-S35 at 23 °C compared to the higher values at 37 °C reveal a partial melting of the stearyl side chains at body temperature.

In summary, the melting of the stearic acid side chains has a crucial influence on the rheological properties of the FA-PGAs. PGA-S65 and PGA-S90 behave fluid-like at 37 °C and therefore are not able to form completely solid DDSs at body temperature. Consequently, the form stability after injection into the body cannot be guaranteed, which reduces the suitability of these polymers for the formulation of microparticles or preformed implants. Furthermore, the low viscosity is expected to have a large influence on the drug release as well, considering the higher diffusion coefficients resulting from melting of the stearyl side chains. Nevertheless, the pure stearyl PGAs are still promising materials for the formulation of other DDSs, such as nanoparticles [71]. The grafting of the PGA backbone with behenic acid made it possible to control the structure of the material. The behenoyl side chains increased the elastic portion of the material and led to higher viscosities. Thus, the behenoyl PGAs are suitable to form solid systems at body temperature.

4.1.5 WATER PENETRATION AND MICROVISCOSITY

To gain insight into the processes occurring within the polymer during incubation in buffer at 37 °C EPR measurements were performed. This non-invasive spectroscopic method allows the detection of paramagnetic compounds inside the sample [130–132]. EPR is based on the interaction of magnetic moments caused by electrons with externally applied magnetic fields. The magnetic moment of an electron originates from its “spin”. For suitable interaction with the electromagnetic field, hence, to be EPR-active, the electron has to be unpaired. Otherwise, the net magnetic moment would be zero because of the oppositely orientated spin. EPR-active species include free radicals or metal ions. Therefore, the nitroxide radical Tempol-d17 was added to the bulk polymers as a spin probe, since these polymers themselves contain no paramagnetic species and consequently are EPR silent. An exemplary EPR spectrum of Tempol-d17 in double distilled water is shown in Figure 16. Information about the local environment of the spin probe are provided from the shape of the spectrum and the obtained parameters. The splitting of the EPR signal of Tempol-d17 into three lines is called hyperfine splitting and is caused by the interaction of the unpaired electron with the magnetic spin of the neighbouring nitrogen nucleus. For fast motions of the spin probe in low viscous environments, e.g. in water, the anisotropy of the hyperfine interaction is averaged and therefore, similar signal amplitudes (I) for all three peaks are

observed (Figure 16). With increasing viscosity of the medium, anisotropy becomes visible because of the slower molecule motion. The peak to peak line widths (ΔB_{pp}) increase for all peaks, but most dominant for the third line, and therefore, different signal amplitudes are observed. If the motion is very slow (e.g. in solids), the anisotropy determines the shape of the spectrum and so-called powder spectra are observed [133]. Moreover, with increasing polarity of the surrounding of the spin probe, the distance between the three peaks (hyperfine splitting constant a_N) increases [134].

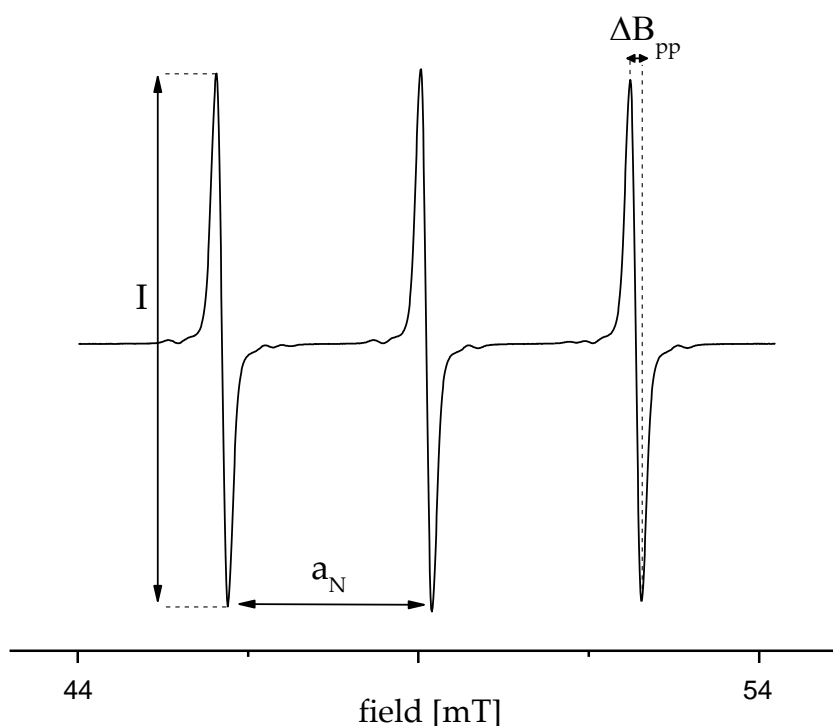


Figure 16: L-Band spectrum of Tempol-d17 in double distilled water at room temperature. I marks the signal amplitude, a_N the hyperfine splitting constant and ΔB_{pp} the peak to peak line width.

In order to examine to which extent water penetrates into the bulk polymer, PGA-B45 and PGA-B45-S35 were investigated in the 3D-printed sample holder (section 3.1.6). The sample holder ensured consistent positioning during the experiment and water penetration from just one direction into the bulk. Thus, comparability and interpretability of the measurements were improved.

Since the preparation of the EPR samples included the melting of the semicrystalline FA-PGAs, the sample aggregated as a dense solidified polymer melt. A similar structure is to be expected for FA-PGAs applied as melt-pressed implants (section 3.3.1) or melt-extruded implants. Hence, the EPR experiments allow conclusions about the water

penetration behaviour into melt-based FA-PGA formulations. The translation of these results to microparticle formulations has to be interpreted carefully since the microparticle preparation was done by a solvent evaporation method (section 3.2.1) and the microparticle structure may therefore be considerably more porous [135,136]. Due to this consideration and their utilization for the preparation of the preformed implants, PGA-B45 was chosen as a behenoyl PGA and PGA-B45-S35 was selected to study the influence of the stearyl side chain on the penetrability.

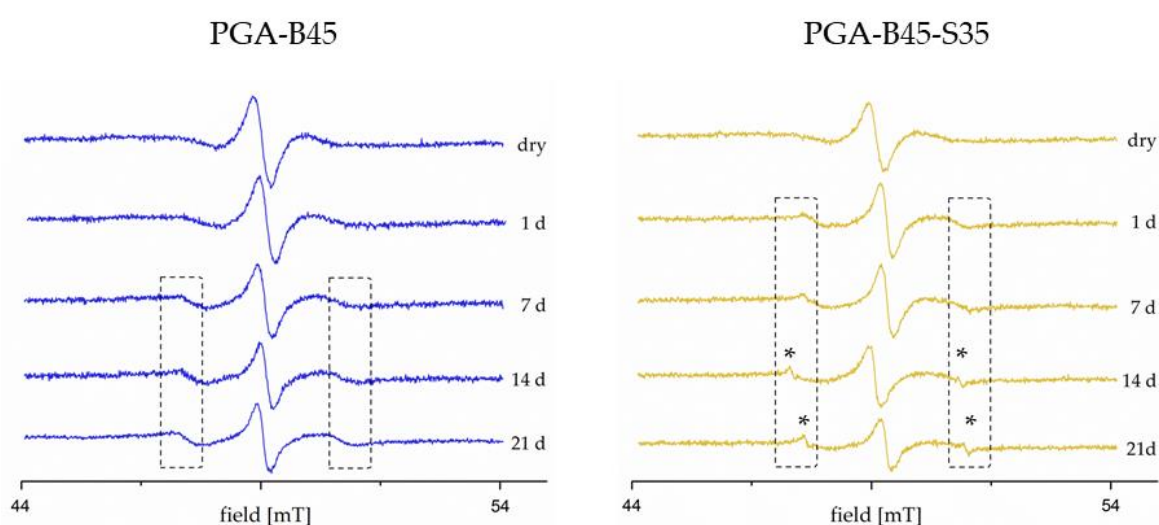


Figure 17: EPR spectra of PGA-B45 and PGA-B45-S35 samples loaded with Tempol-d17 during incubation in PBS pH 7.4 at 37 °C at different time points. The appearing mobile signal of the spin probe is highlighted by the dotted boxes, highly mobile signals are highlighted by the star symbol (*).

Figure 17 displays the L-Band EPR spectra for the investigated FA-PGAs over a period of 21 days. The dry spectra for both PGA-B45 and PGA-B45-S35 showed only a broad signal which can be attributed to the highly, but not completely, immobile Tempol-d17. This was expected since the motion of the spin probe is restricted in the solid polymer matrix. After incubation in buffer at 37 °C for seven days, a superposition of small signals with narrow lines appeared in the PGA-B45 spectrum. These signals remained constant for the investigated time and indicate an increase in the mobility of the spin probe. Since the mobile signals were only slightly pronounced and did not increase over time, a clear assignment to an aqueous environment was not possible. For PGA-B45-S35, a superposition of small and sharp signals appeared already after one day of exposure to phosphate buffer. Throughout the next 20 days, the peaks became sharper and the signals increased while remaining generally low. These sharp signals (*) with line widths of 0.1 mT indicate the

presence of water which increases the mobility of the spin probe. The increase of the mobile peak amplitude suggests that more water was penetrating the polymer over the course of the experiment. Furthermore, the release of Tempol-d17 out of the sample led to a decrease in the signal amplitude of the immobile peak for both polymers.

In summary, both polymers showed increasing mobility of the spin probe during incubation in PBS at 37 °C. The highly mobile signals in the PGA-B45-S35 spectra can be assigned to aqueous micro-domains. Overall, the mobile signals constituted only a small percentage of the total signal, hence, the amount of penetrated water was generally low. Visually, no swelling of the samples was recognizable. Since PGA-B45-S35 has a higher acylation degree and, according to the static contact angle measurements, higher lipophilicity compared to PGA-B45, a lower penetrability was expected. The contrary results suggest that the stearyl side-chain enhanced the water penetration into the polymer. Including the results from the DSC measurements in section 4.1.1 and the rheology experiments from the previous chapter, partial melting of the C₁₈-side chains of PGA-B45-S35 and consequently, a change in the microviscosity could explain this phenomenon. Therefore, the order parameter (S-parameter) was calculated from the EPR spectra to assess changes in the microviscosity of the FA-PGAs.

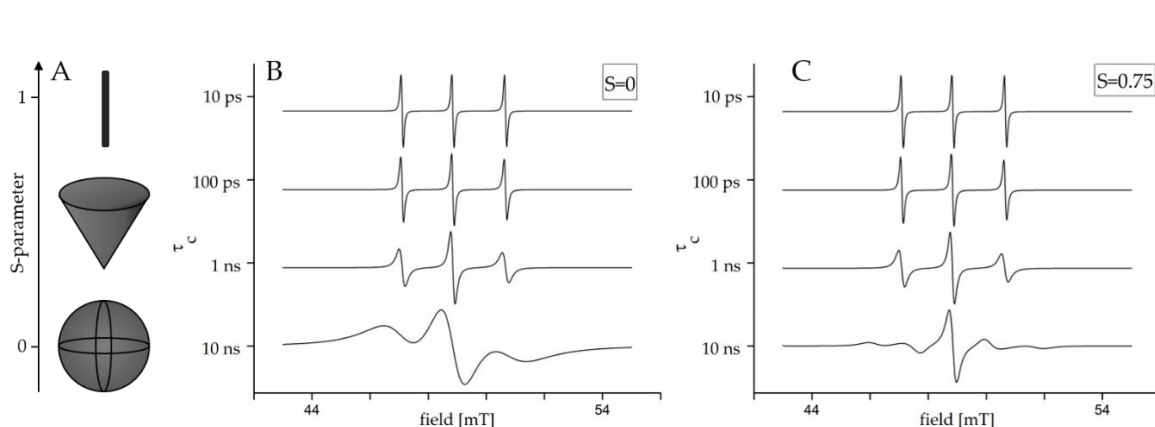


Figure 18: (A) Schematic illustration of the range of tumbling motion of the spin probe depending on the S-parameter, (B+C) Simulated L-Band EPR spectra of Tempol-d17 for different S-parameter values at various rotational correlation times (τ_c).

The order parameter is a measure of the fluidity of the microenvironment in which the spin probe is incorporated. It indicates the degrees of freedom and the range of the tumbling motion of the spin probe [137,138]. In a rigid environment ($S = 1$), the motion is strongly

restricted. Whereas, $S = 0$ in a homogenous solution with free motion of the spin probe [139]. Figure 18 illustrates the range of the tumbling motion and the spectral changes for different S -parameters of Tempol-d17. It is depicted that only for rotational correlation times (τ_c) above 1 ns spectral changes are visible. At faster motions, the anisotropy of the hyperfine splitting is averaged while signal changes appear for different S -parameters at slower motions. For an S -parameter of 0.75, almost only the immobile signal is present in the spectrum at a τ_c of 10 ns (Figure 18C). For low S -values, relatively broad signals appear, which correlate to the increasing range of motion of Tempol-d17 in the sample (Figure 18B). Therefore, shifting of the order parameter reveals changes in the microviscosity of the sample.

The S -values for PGA-B45 and PGA-B45-S35 during incubation in buffer medium were derived from the obtained EPR-spectra. In Figure 19 the changes in the order parameter for the investigated FA-PGAs are depicted. A decrease of the order parameter values for both polymers is visible. Thus, Tempol-d17 is able to move more freely due to a softening of the polymer structure throughout the experiment. For PGA-B45-S35 lower values in general and a rapid decline of the S -parameter were detected. These results support the assumption, that the stearyl side chains of the PGA-B45-S35 are already partially melting at 37 °C and therefore lead to a decrease of the microviscosity and an increase of the fluidity of the sample.

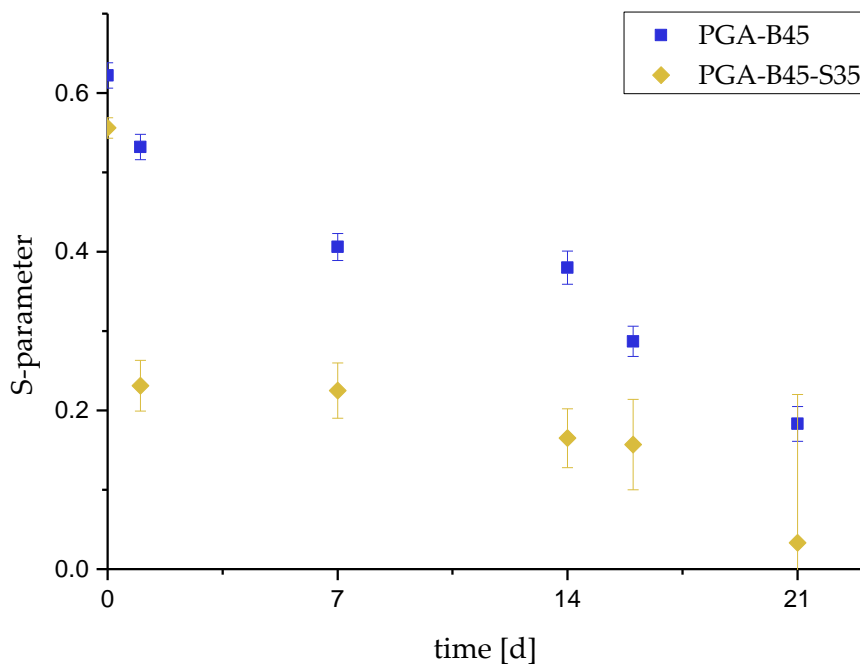


Figure 19: S-parameter values of PGA-B45 and PGA-B45-S35 samples loaded with Tempol-d17 during incubation in PBS pH 7.4 at 37 °C.

Based on the presented data, the EPR measurements showed that the water penetration into the melt-prepared FA-PGA samples is generally low due to the hydrophobic nature of these polymers. Only small signals appeared throughout the experiment indicating the presence of water. Despite its higher acylation degree, PGA-B45-S35 revealed higher penetrability than PGA-B45 because of the partial melting of the stearyl side chains. The resulting changes in the microviscosity and the higher fluidity of the PGA-B45-S35 at 37 °C were also observed by the examination of the order parameter. Concerning the administration of these polymers as DDSs, the differences in water penetration and microviscosity could likely influence the drug release from the formulation.

4.2 PREPARATION AND CHARACTERIZATION OF MICROPARTICLES

4.2.1 PREPARATION OF MICROPARTICLES

The FA-PGA microparticles were prepared by a solvent evaporation method. Thereby, a solution of FA-PGA with or without API in methylene chloride was emulsified in an aqueous continuous phase. The disperse phase was injected with a syringe pump to accomplish reproducible results. PVA was added to the continuous phase to stabilize the emulsion and a paddle apparatus was used for stirring to maintain a constant and

preferably laminar flow. After evaporation of the organic phase, the microparticle suspension was lyophilized. With this procedure, FA-PGA microparticles could be obtained for all investigated polymers. Furthermore, the incorporation of thiamine derivatives was successful. The influence of different process parameters and the incorporation of the drug on the particle size distribution will be investigated in the following section.

4.2.2 SIZE DISTRIBUTION

The size distribution of the microparticles was measured by static light scattering also known as laser diffraction. In laser diffraction scattering intensities are measured as a function of the scattering angle and the wavelength of the light [140]. It is one of the most common methods for particle size measurements in the sub-micron to millimeter range due to its high reproducibility, fast operation and broadly applicable size range [140,141]. The obtained size distributions are characterized by the $d(0.1)$, $d(0.5)$ and $d(0.9)$ values. Besides, the span is given as a measure of the width of the distribution (3.2.2, Equation 1). Small span values indicate narrow size distributions, whereas broad particle size distributions lead to high span values. The influence of several process parameters and the incorporation of DBT on the size distribution of the microparticles was investigated in the following sections.

4.2.2.1 INFLUENCE OF STIRRING SPEED AND POLYMER CONCENTRATION

Various process parameters, such as agitation speed and polymer concentration, can influence the particle size distribution [119]. The width of the distribution and the size of the particles, however, have an impact on the drug release and the injectability through cannulas. For subcutaneous injections, the recommended cannula size is 23 gauge which is equivalent to an inner diameter of 0.34 mm [142]. Consequently, particle sizes considerably below 300 μm are required to ensure injectability.

To evaluate the effect of these parameters on the particle size of FA-PGA microparticles, the preparation process was conducted at various agitation velocities (240 rpm, 275 rpm and 300 rpm) and with two different polymer concentrations (50 mg/mL and 25 mg/mL) for stirring at 275 rpm. The process parameter screening was conducted only with the behenoyl PGAs since the polymer synthesis is time-consuming and high amounts of polymer were

needed for the screening experiments. However, a transfer of the obtained results to the stearyl PGAs is most probable.

Figure 20 displays a characteristic volume-weighted particle size distribution of microparticles prepared at a stirring speed of 240 rpm. The distribution graphs indicate that monomodal size distributions were achieved for all FA-PGAs. Since the particle size impacts the release behaviour, monomodal size distributions are preferable to achieve constant and reproducible drug release [143,144]. Besides, monomodal distributions indicate a controllable preparation method. The particle size distributions remained monomodal for all FA-PGAs after the adjustment of stirring velocity and polymer concentration during the process parameter screening.

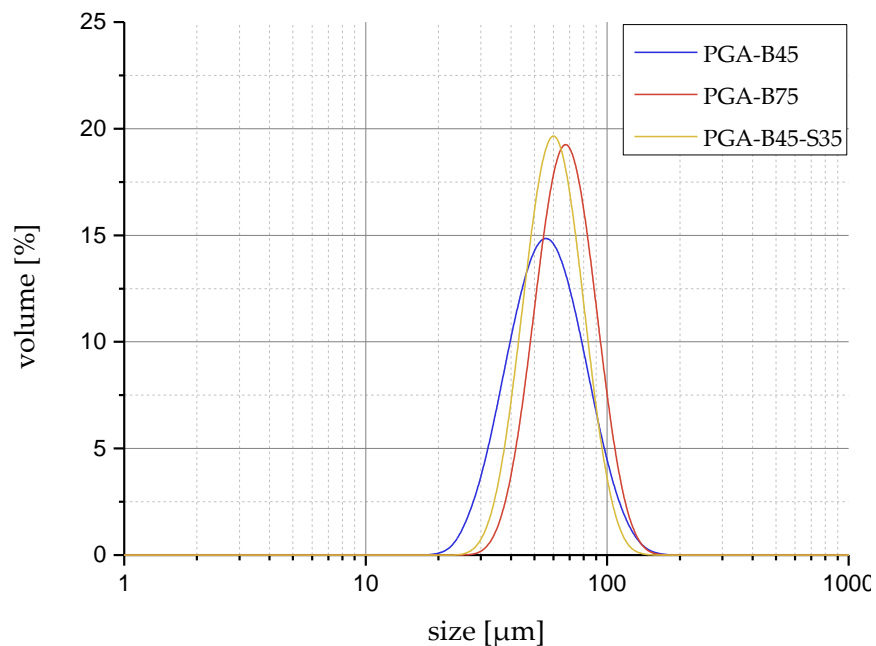


Figure 20: Exemplary volume-weighted particle size distribution graphs of PGA-B45, PGA-B75 and PGA-B45-S35 microparticles prepared at a stirring speed of 240 rpm.

The span and $d(0.5)$ values for all screened parameters are shown in Figure 21. A decrease in the median was observed for all investigated FA-PGA microparticles by increasing the stirring speed from 240 rpm to 275 rpm. The $d(0.5)$ values of PGA-B45 for example were reduced from 58.7 μm to 45.2 μm , which is a size reduction of 23%. For PGA-B75 a reduction of the $d(0.5)$ value from 71.8 μm to 53.0 μm and for PGA-B45-S35 from 61.2 μm to 53.7 μm was measured. This was expected since higher agitations velocities, hence higher energy

input, lead to an earlier tearing of the droplet from the cannula point and greater comminution of the disperse phase into small droplets.

With a further increase in the agitation velocity to 300 rpm, no clear additional decrease in particle size could be detected. A possible explanation is, that either the additional energy input is not sufficient for additional disruption of the droplets or the surfactant is not able to stabilize the resulting smaller droplet sizes and re-coalescence is occurring [146,147].

Moreover, the polymer concentration in the disperse phase was decreased with the stirring speed unaltered at 275 rpm. Thereby, the median values for PGA-B75 and PGA-B45-S35 decreased while the $d(0.5)$ value of PGA-B45 remained almost constant. A reduction of the particle size through a decrease in polymer concentration caused by lower viscosity of the organic phase has also been reported for PLGA microparticles [148]. Since the reduction of the polymer concentration did not cause a particle size reduction for all FA-PGAs, the screening of further stirring velocities with the lower polymer concentration was renounced. Furthermore, the span values did not change distinctly through the alteration of the process parameters. For PGA-B45 the span values were in the range of 0.9 to 1.1, whereas the PGA-B75 and PGA-B45-S35 microparticles were slightly narrower distributed with values around 0.7.

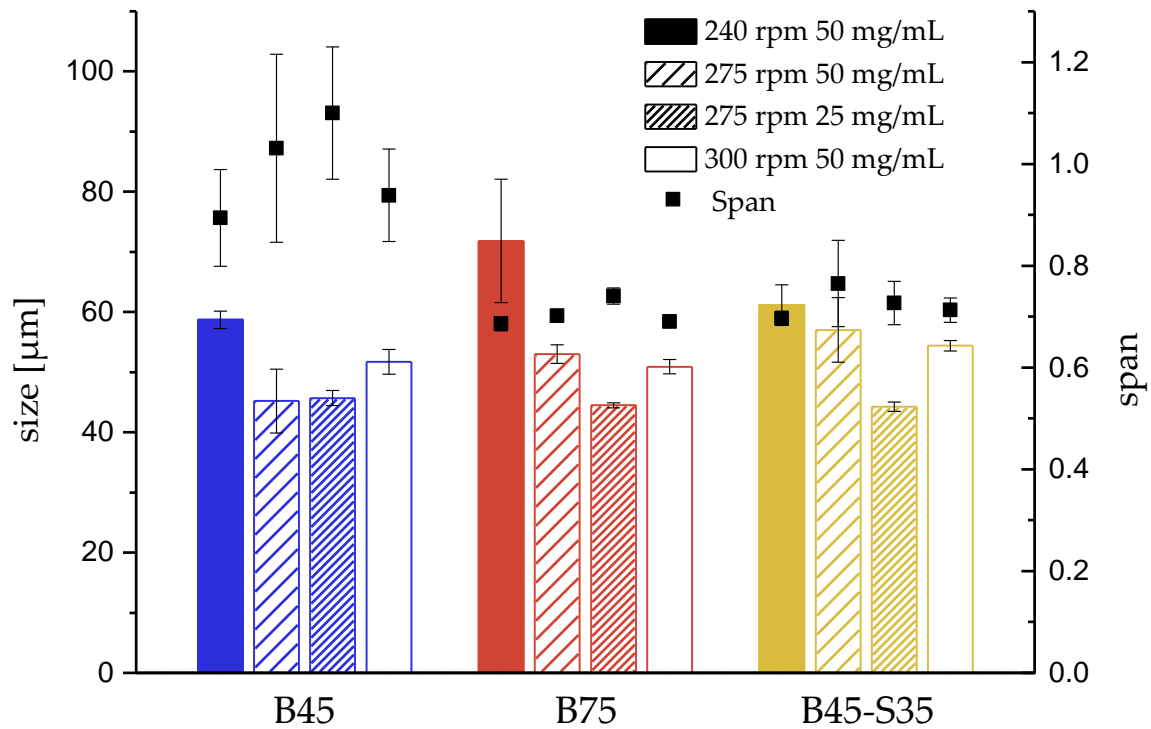


Figure 21: The influence of stirring speed and polymer concentration on the size distribution of PGA-B45, PGA-B75 and PGA-B45-S35 microparticles. The columns indicate the $d(0.5)$ values, the dots the width of the distribution.

In summary, both the stirring speed and the polymer concentration showed an influence on the particle size. An increase in the stirring velocity from 240 rpm to 275 rpm and a decrease in the polymer concentration resulted in smaller particle sizes. All microparticles showed monomodal size distributions and had particle sizes considerably below 300 μm to ensure injectability. This study aims to formulate microparticles for controlled and sustained release of DBT. Therefore, the stirring speed was set to 240 rpm for the following experiments, since larger particle sizes generally lead to longer release times. As an exception, to evaluate the effect of the particle size on the release behaviour in detail (section 4.2.6), two varying particle size distributions were chosen for the *in vitro* release experiments. Consequently, DBT was incorporated in microparticles prepared at 240 rpm and 275 rpm in the subsequent section. Considering the higher particle yields for 50 mg/mL compared to 25 mg/mL, 50 mg/mL was chosen as the polymer concentration for both stirring velocities.

4.2.2.2 INFLUENCE OF DRUG LOADING

To evaluate whether the loading of DBT influences the size distribution of FA-PGA microparticles, particles loaded with nominally 6% DBT were prepared and measured via laser diffraction. A drug load of 6% (w/w) was chosen to assure the amorphous state of the API. The value was based on preliminary microscopic tests. Subsequently, the exact threshold for the presence of the amorphous state of DBT in the particles was investigated via XRD (4.2.5). Figure 22 displays the size distribution values of FA-PGA microparticles loaded with DBT compared to drug-free placebo particles prepared at varying stirring velocities. The incorporation of DBT into the microparticles considerably increased the median particle size for the preparation at 240 rpm. An increase of about 20 μm was detected for the behenoyl PGAs, while for PGA-S65 and PGA-S90 microparticles the median particle size more than doubled. These differences could either arise from process technological distinctions or variations in the molecular alignment of polymer and API. As to that, changes in the viscosity or surface tension of the disperse phase caused by the addition of DBT to the solution could influence the tearing of the droplet from the cannula point, hence, the particle size [149]. Furthermore, possible steric interference of the drug molecule with the polymer side chains and therefore a more expansive inner particle structure could explain this phenomenon as well. Interestingly, no clear differences between the median particle sizes of loaded and placebo particles were detected at a stirring speed of 275 rpm. A possible explanation is that the greater agitation compensates the physicochemical distinctions of the disperse phases and the tearing of the droplet remains unaltered by the addition of DBT. Similar results have been published on PLGA microparticles containing progesterone [150]. The span values of the drug-loaded and placebo particles did not differ distinctly, hence, the width of the size distribution was not altered by the incorporation of DBT.

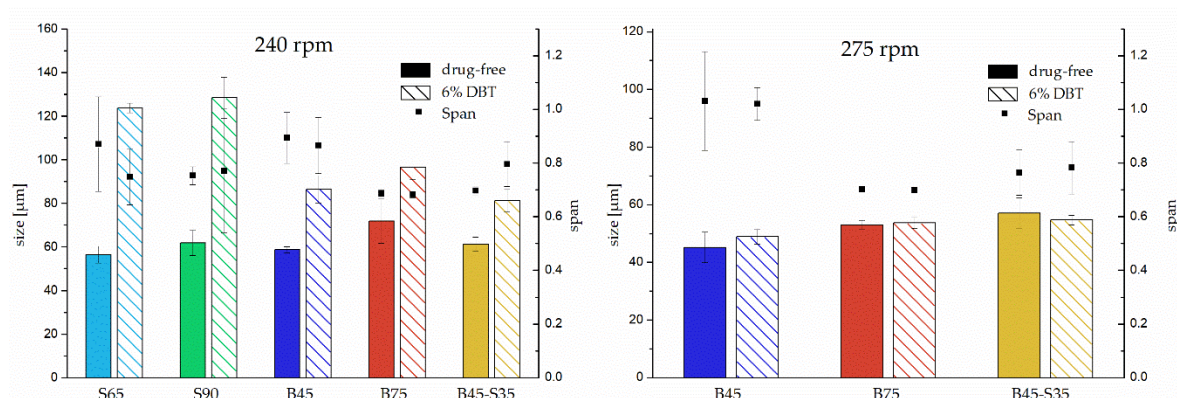


Figure 22: Influence of loading of nominally 6% DBT on the particle size distribution. The columns indicate the d(0.5) values, the dots the width of the distribution. Left: Stirring speed of 240 rpm during microparticle preparation. Right: Stirring speed of 275 rpm during microparticle preparation.

The exact size distribution values of the microparticle formulations used in the following experiments are shown in Table 10. All FA-PGA microparticles loaded with DBT were still considerably smaller than 300 μm and therefore injectable. However, PGA-B45, PGA-B75 and PGA-B45-S35 formed smaller particles with median particle sizes below 100 μm, thus, are favorable for injection. The values suggest that with increasing acylation degree of the PGA backbone larger particles were formed. By increasing the substitution degree of stearic acid from 65 mol% to 90 mol%, the median particle size rose from 123.7 μm to 128.3 μm. The same effect was observed for behenoyl PGA microparticles. For PGA-B45 a d(0.5) value of 86.4 μm was measured whereas the value increased to 96.5 μm for PGA-B75. Similar effects were also described for the formation of FA-PGA nanoparticles [65,71]. The influence of the substitution degree on the particle size was observed for both placebo and drug-loaded particles. However, the length of the acyl group had no distinct effect on the particle size distribution. The d(0.5) value of the stearyl PGAs was about 30 μm higher than the one of the behenic acid substituted polyesters. It was anticipated that FA-PGAs substituted with longer side chains form bigger particles. Against this expectation, the PGAs grafted with C₂₂-acyl chains formed smaller particles than the polymers acylated with C₁₈-chains. Moreover, the smallest particle sizes were measured for the double substituted PGA-B45-S35. Possible explanations could be varying viscosities and interfacial tensions during particle preparation or differing packing structures in the particle core, which are dependent on the type of fatty acid, or the composition of the substituted fatty acid blend.

Table 10: Size distribution values of FA-PGA microparticles loaded with nominally 6% DBT at a stirring speed of 240 rpm and 275 rpm.

Stirring Speed: 240 rpm				
Polymer	d(0.1) [μm]	d(0.5) [μm]	d(0.9) [μm]	Span
PGA-S65	86.6 \pm 3.1	123.7 \pm 2.2	179.2 \pm 11.3	0.748 \pm 0.104
PGA-S90	90.0 \pm 12.9	128.3 \pm 9.4	187.8 \pm 14.2	0.771 \pm 0.231
PGA-B45	57.0 \pm 5.5	86.4 \pm 6.3	131.6 \pm 8.9	0.865 \pm 0.104
PGA-B75	69.1 \pm 4.4	96.5 \pm 5.4	134.9 \pm 7.1	0.683 \pm 0.012
PGA-B45-S35	55.0 \pm 5.2	81.2 \pm 5.2	119.5 \pm 5.8	0.796 \pm 0.084
Stirring Speed: 275 rpm				
Polymer	d(0.1) [μm]	d(0.5) [μm]	d(0.9) [μm]	Span
PGA-B45	30.4 \pm 1.4	48.9 \pm 2.5	80.3 \pm 5.4	1.020 \pm 0.061
PGA-B75	38.0 \pm 1.3	53.7 \pm 1.9	75.6 \pm 2.7	0.698 \pm 0.006
PGA-B45-S35	37.6 \pm 0.8	54.7 \pm 1.7	80.5 \pm 6.0	0.783 \pm 0.098

4.2.3 PARTICLE MORPHOLOGY

Particle morphology affects various mechanisms of drug delivery, such as polymer degradation and the kinetics of the drug release [151–153]. Furthermore, knowing the shape of the particle is of great importance for the validity of the particle size measurements [154]. Scanning electron micrographs were taken to study the morphology of the FA-PGA microparticles and to support the results gained by laser diffraction analysis.

The SEM images are shown in Figure 23. As already observed in chapter 4.2.2.2, the behenoyl PGAs formed smaller microspheres than PGA-S65 and PGA-S90. It is visible that all FA-PGAs formed uniformly spherical particles. The evaluation theory of laser diffraction analysis assumes the particles to be perfectly spherical [140]. Consequently, a spherical shape is required to obtain valid results. Thus, the results from the size distribution measurements were confirmed to be valid.

In addition, no defined pore structure was visible on the microparticle surface. The formation of pores during microparticle preparation is influenced by the rate of solvent removal and therefore the rate of particle hardening [148]. The rate at which the solvent is removed correlates with the disperse phase to continuous phase ratio (D/C ratio). Low D/C

ratios result in fast solvent removal and therefore in lower porosity and smoother surfaces [155,156]. Thus, the absence of pores on the particle surface complies with the low D/C ratio of 1/150 during microparticle preparation. However, the absence of pores on the surface does not imply the general absence of pores inside the polymer matrix.

Moreover, the SEM images indicate an effect of both substitution degree and the fatty acid on the particle morphology. Higher substitution degrees and therefore higher crystallinity led to rougher particle surfaces. Hence, PGA-S90 formed microspheres with clearly rougher surfaces (Figure 23 B) than PGA-S65 (Figure 23 A). In addition, the selection of the fatty acid side chain affected the surface morphology. Behenic acid had a greater impact on the roughness of the particle surface than stearic acid. Consequently, despite the lower acylation degree, the PGA-S65 microspheres (Figure 23A) remained considerably smoother than the PGA-B45 particles (Figure 23C). Furthermore, no DBT crystals were detected on the particle surfaces. This indicates the incorporation of the drug in its amorphous form. Further investigations regarding API crystallinity inside the microspheres were conducted in section 4.2.5.

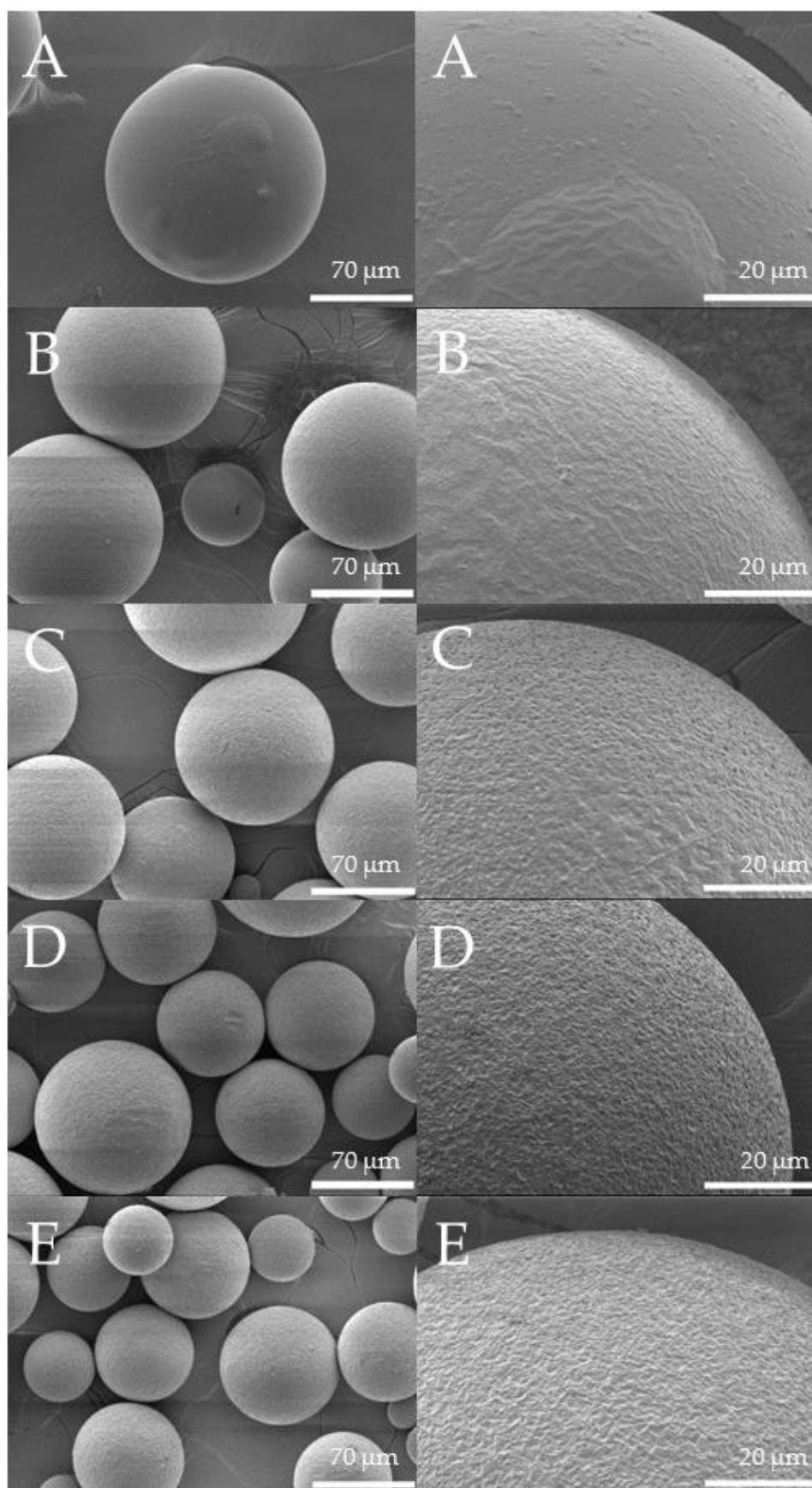


Figure 23: Representative scanning electron micrographs of FA-PGA microparticles loaded with nominally 6% DBT. (A) PGA-S65, (B) PGA-S90, (C) PGA-B45, (D) PGA-B75, (E) PGA-B45-S35.

4.2.4 ENCAPSULATION EFFICIENCY

Microencapsulation is described as a process of embedding solid particles or droplets of liquids or gasses in an inert shell, which in turn isolates and protects them from the external environment [157]. This process is utilized for a variety of reasons such as the protection of sensitive substances and to achieve controlled release of the encapsulated material. The extent to which the substance is embedded into the particle is defined as encapsulation efficiency. Different factors during the microparticle preparation are influencing the encapsulation efficiency. Some of these factors are the solubility of the polymer and the API in the organic phase, the solubility of the organic solvent in the continuous phase, the rate of solvent removal and the interaction between drug and polymer [158,159]. By grafting the PGA backbone with fatty acids, the physicochemical properties of the polymer change and therefore the drug-polymer interaction is altered. Consequently, the modification of the PGA backbone is one possibility to control the encapsulation efficiency. To examine the effect of the acylation of PGA on the encapsulation efficiency, two vitamin B₁ derivatives were incorporated into FA-PGA microparticles. HPLC analysis was used to measure the drug entrapment. The two thiamine derivatives differ in hydrophilicity (see logP values in 2.2) with DBT being more lipophilic than SBT.

Table 11: Encapsulation efficiencies of Dibenzoyl Thiamine (DBT) and Sulbutiamine (SBT) in FA-PGA microparticles loaded with nominally 6% (w/w) of API.

Polymer	Encapsulation Efficiency [%]	
	DBT	SBT
PGA-S65	78.2 ± 5.5	71.1 ± 4.4
PGA-S90	85.6 ± 5.9	62.9 ± 6.1
PGA-B45	47.5 ± 1.3	66.3 ± 3.3
PGA-B75	84.2 ± 5.3	77.8 ± 4.5
PGA-B45-S35	87.8 ± 3.3	67.5 ± 1.3

Table 11 depicts the encapsulation efficiency values for the investigated FA-PGAs. Concluding from the obtained values, the entrapment percentages correlate with the hydrophilicity of the polymer used. For PGA-S90, PGA-B75 and PGA-B45-S35 microparticles, encapsulation efficiencies of >80% were measured incorporating DBT into the polymer matrix. According to the water contact angle measurements (4.1.3), these polymers had θ values around 90° and were the most lipophilic of the investigated

FA-PGAs. Considering that the water contact angle was measured on the polymer surface, it is not possible to transfer those values directly to the particle core. However, the general differences in hydrophobicity of these materials still pertain to the bulk of the particles. For this reason, it is comprehensible that the encapsulation efficiency of the lipophilic DBT was the lowest (47.5%) in the most hydrophilic polymer PGA-B45 and that the values increased with advancing lipophilicity. The maximum encapsulation efficiency of DBT was measured for PGA-B45-S35 (87.8%), even though the three most lipophilic PGAs showed only minor differences.

The incorporation of the slightly less lipophilic thiamine derivative SBT into the microparticles confirmed the influence of the polymer's hydrophobic interactions. An increase of the encapsulation efficiency for the most hydrophilic PGA-B45 to 66.3% was measured, whereas the values for the more lipophilic FA-PGAs declined. The value of the previously most suitable PGA-B45-S35, for example, decreased from 87.8% to 67.5%. Interestingly, the maximum entrapment percentage was detected for PGA-B75 at 77.8%, although this polymer had the highest water contact angle measured, hence, had the most lipophilic surface. This example shows, that the direct transfer of the θ values from the surface to the inner particle is not adequate to explain the entrapment of the drug. Other factors on a molecular level affect the encapsulation efficiency as well, i.e. the molecular weight of the polymer and potentially steric hindrance caused by the polymer structure [159,160]. In this particular case, the biggest drop in encapsulation efficiency was measured for PGA-S90 and PGA-B45-S35 with 20.3% and 22.7% respectively. These are the investigated FA-PGAs with the highest acylation degree. As a possible reason, the esterification of a high amount of free hydroxyl groups in the PGA backbone led to a reduction in free space for the incorporation of SBT in the polymer matrix. Similar observations were made for FA-PGA nanoparticles by Kallinteri et al. [65]. The precondition for this explanation would be that SBT is sterically more demanding than DBT since this effect was not observed for the incorporation of DBT.

In summary, the grafting of the PGA backbone and therefore the alteration of its physicochemical properties affected the effectiveness of the incorporation of the two vitamin B₁ derivatives. Through the modification of the polymer backbone, it is possible to

control the affinity of the polymer to the drug, thus, the encapsulation efficiency. The modification of PGA customized to the requirements of the API is easily conceivable.

4.2.5 X-RAY POWDER DIFFRACTION (XRD)

X-ray powder diffraction measurements were conducted to investigate the physical state of the drug inside the DDS. XRD is one of the most frequently used and one of the most conclusive methods for the detection and quantification of crystallinity [161]. Crystalline materials provoke sharp Bragg peaks in the X-ray diffraction patterns. The absence of these distinct peaks indicates the presence of an amorphous state [162]. The amorphous state of a pharmaceutical compound is characterized by the lack of long-range order symmetry operators (translational, orientational and conformational order) which are found in crystalline compounds. Hence, the individual molecules exist in a random orientation to one another and various conformational states [163]. The present physical state of the drug is of great relevance due to the different dissolution behaviours of crystalline and amorphous states. An amorphous drug has an improved apparent solubility, hence, an enhanced bioavailability towards its crystalline counterpart [164,165]. Since a major portion of new drug candidates developed via high-throughput screening and combinatorial chemistry is characterized by low aqueous solubility, the amorphization of drugs is an important strategy for the pharmaceutical industry to improve bioavailability [6,161]. DBT with a solubility of < 0.1 mg/ml in PBS pH 7.4 is classified as practically insoluble according to the European Pharmacopoeia [166]. Therefore, the incorporation of DBT in its amorphous form into the microspheres would be desirable. PGA-B45, PGA-B75 and PGA-B45-S35 microspheres were selected for these measurements as the most promising FA-PGA candidates for controlled release.

Initially, the characteristic diffraction pattern of DBT and the limit of detection for the crystalline API in presence of the polymer had to be identified. Therefore, X-ray traces of DBT and physical mixtures of DBT with the various FA-PGAs in different percentages were acquired. The results are displayed in Figure 24. As expected, DBT caused a definite diffraction pattern indicating its crystalline structure. The most characteristic peaks of DBT appear at 8.4° and 11.1°. These specific Bragg peaks were also detected in the physical mixtures. The detection limit of DBT in the physical mixtures with PGA-B45 and PGA-B75 was at 10% drug content, whereas it was higher for the mixture with PGA-B45-35 at 15%.

A possible explanation of the slightly poorer detection limit in PGA-B45-S35 could be the high crystallinity of the specific FA-PGA itself. As a result of the semi-crystalline behaviour of the FA-PGAs, the Bragg reflexes of DBT could be overlapped by the polymer's diffraction pattern. Further distinctive peaks in the X-ray traces of the mixtures at 5.3° and 9.7° are caused by the different FA-PGAs (XRD traces of pure FA-PGAs, supplementary data Figure S 2). Similar diffraction patterns of stearic acid-modified PGAs were reported by Weiss et al. [72].

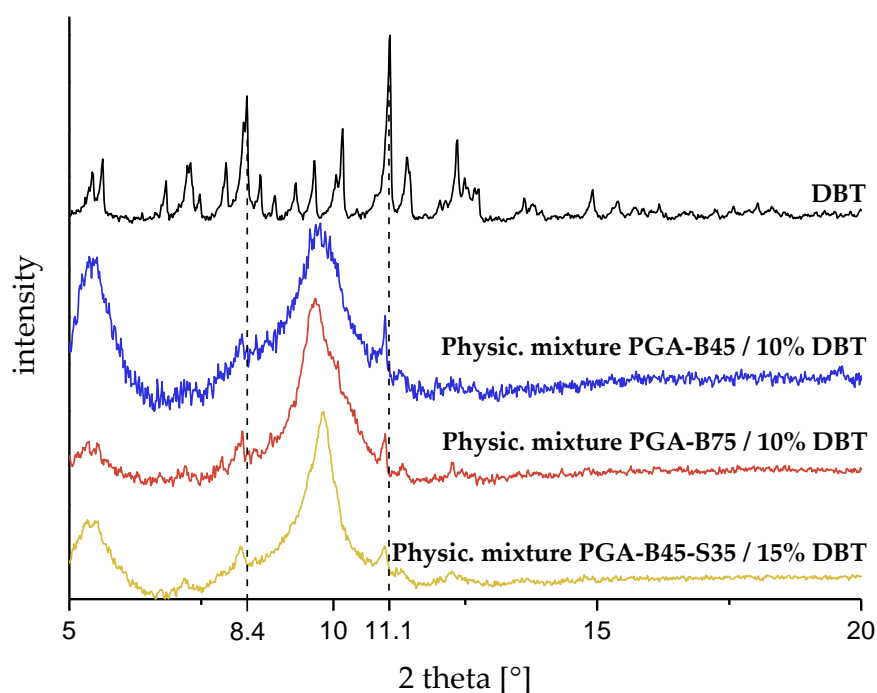


Figure 24: X-Ray powder diffraction traces of DBT and of physical mixtures of DBT with different FA-PGAs. The dotted line indicates the most characteristic DBT-peaks.

Subsequently, the threshold for the presence of amorphous DBT in FA-PGA microparticles was detected. Therefore, the amount of drug incorporated into the particles was increased until crystalline DBT reflexes appeared in the X-ray traces. Figure 25 displays the diffraction patterns for the powdered polymeric microparticles. The threshold for the presence of amorphous DBT is indicated by the lower curves. No sharp Bragg peaks of crystalline DBT are visible there, which suggests the incorporation of DBT in its amorphous state. With increasing DBT concentration the characteristic diffraction patterns of DBT at 8.4° and 11.1° emerged as shown by the second curves in Figure 25. For PGA-B45 and PGA-B75 microparticles, the threshold was detected at 23% and 25% drug loading respectively. However, signals indicating crystalline DBT appeared already at incorporation

percentages >16% for PGA-B45-S35 microspheres. Consequently, the amorphous state of DBT had higher stability in PGA-B45 and PGA-B75 functioning as a polymeric matrix than in the double substituted PGA-B45-S35.

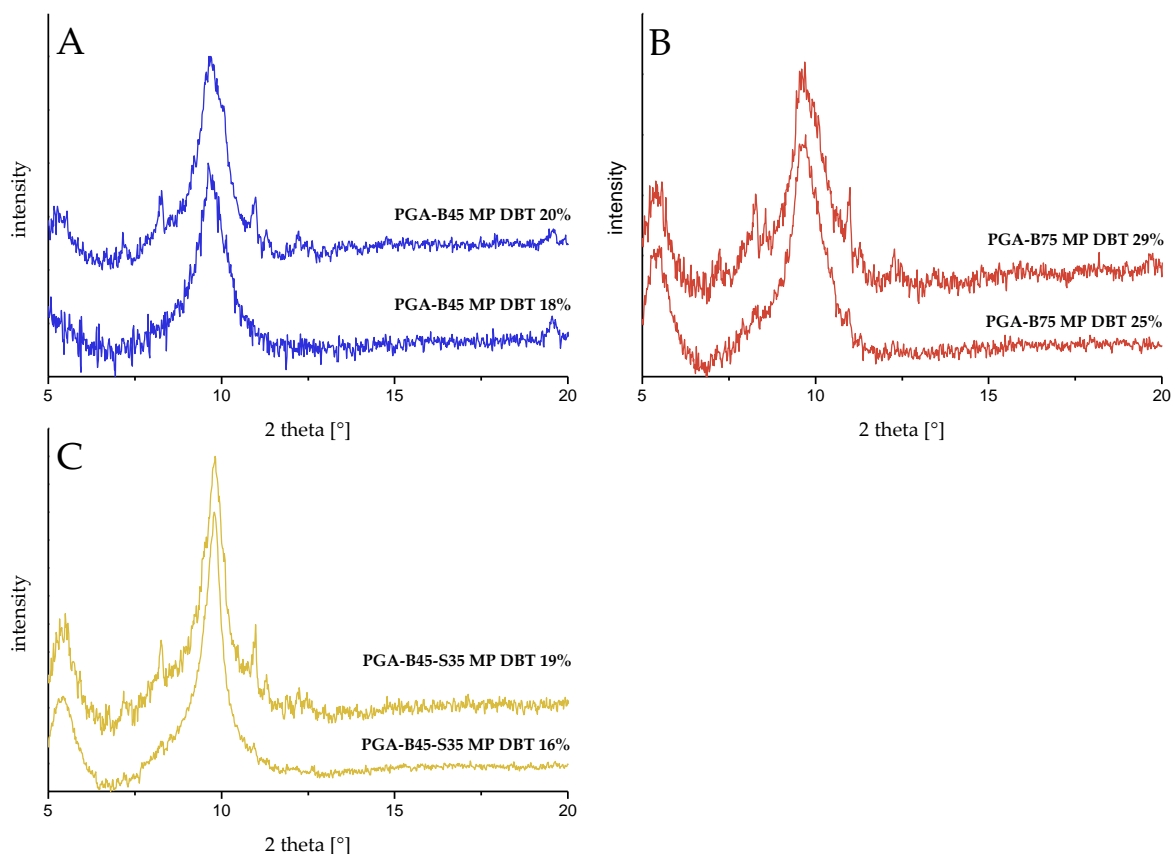


Figure 25: X-Ray traces of powdered FA-PGA microparticles loaded with different amounts of DBT. The lower curve shows the threshold for the absence of crystalline patterns. (A) PGA-B45, (B) PGA-B75, (C) PGA-B45-S35.

The polymer plays a key role in the stability of the amorphous state in a DDS. Several parameters such as the glass transition temperature, molecular weight, molecular mobility, and solubility affect the crystallization behaviour of APIs in solid dispersions [163]. The drug solubility determines the upper limit of drug concentration, in which the drug exists in a molecularly dispersed state and no crystallization or phase separation will occur [161]. Various drug-polymer interactions, such as hydrogen bonds or Van der Waals forces, are responsible for the solubility of the drug in the polymer [167,168]. Thus, the hydrogen bonding between the free hydroxyl groups of the PGA backbone and DBT could be a possible explanation for the different crystallization behaviours of DBT in the FA-PGAs. Due to its high acylation degree, PGA-B45-S35 has fewer free hydroxyl groups available for hydrogen bonding. Therefore, the strength of interaction might be not sufficient enough to

inhibit the crystallization of DBT to the same degree as in the other FA-PGAs. Consequently, the solubility of DBT in PGA-B45-S35 would be poorer which could explain the lower threshold for the presence of DBT in its amorphous form.

4.2.6 *IN VITRO* RELEASE EXPERIMENTS

In vitro release experiments are a valuable tool to assess the release performance of the DDS under reproducible conditions and to ensure the physiological availability of the drug. Thereby, *in vitro* tests provide first insights into the release duration and release rate during the development of the drug product. Especially for parenteral depot formulations, these parameters are crucial since a prolonged and controlled drug release is intended. The results from the *in vitro* experiments are indispensable for the preparation of release tests *in vivo*. To establish some correlation to the release behaviour *in vivo* a rational approach to the experiment is essential. Initially, the test parameters had to be determined. Since the test environment should be as close as possible to the actual release conditions *in vivo*, the experiment was conducted at 37 °C body temperature. Furthermore, the selection of release medium and release duration is discussed in the following sections.

4.2.6.1 SELECTION OF RELEASE MEDIUM

In general, the use of aqueous release media with physiological pH values is recommended [169–171]. Therefore, phosphate-buffered saline pH 7.4 was chosen.

According to the Noyes-Whitney equation, the rate at which a solid substance dissolves in its own solution is proportional to the difference between the concentration of that solution and the saturation concentration (c_s) [172]. Hence, it is essential to stay substantially below c_s during the release experiments in order to maintain constant drug dissolution rates. Therefore, it is vital to comply with the so-called “sink” conditions to detect realistic release rates [173,174]. Sink conditions are maintained if the drug concentration in the medium does not exceed 10% to 30% of c_s [169]. Especially for poorly water-soluble drugs with low saturation concentrations the preservation of perfect sink conditions during the study is difficult. Due to the poor solubility of DBT in PBS pH 7.4, the modification of the release medium was necessary. Different approaches, such as the use of partially organic media, biphasic systems or the addition of surfactants to the release medium, have been pursued [175–177]. Since the use of organic release media seems to be questionable, the saturation

concentration of DBT in PBS pH 7.4 with the addition of different surfactants was determined [178].

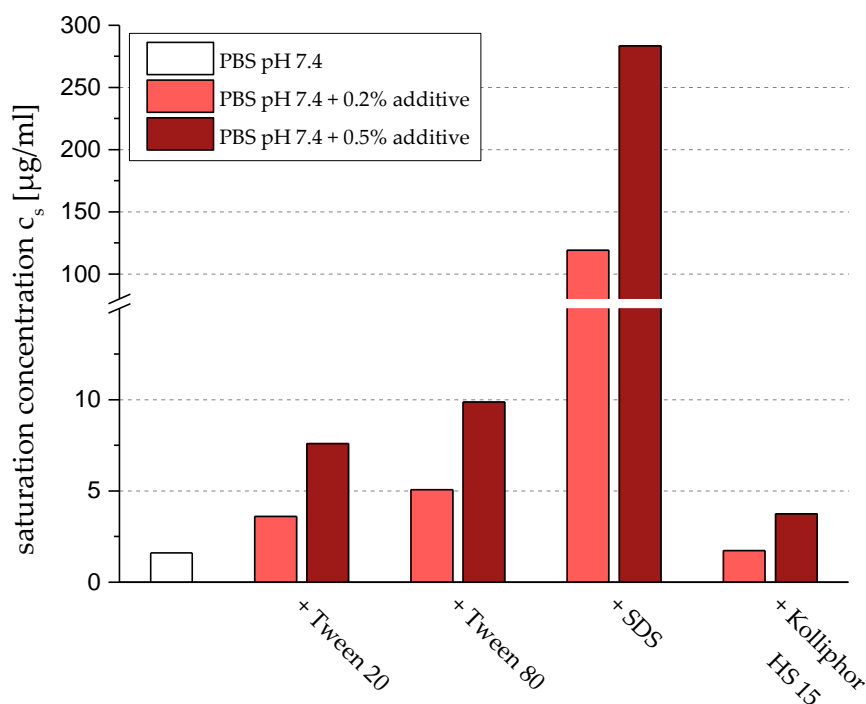


Figure 26: Saturation concentration of DBT in PBS pH 7.4 with different additives.

The results are displayed in Figure 26. Due to its low c_s of 1.6 µg/mL, DBT is classified as practically insoluble in PBS pH 7.4 according to the European Pharmacopoeia [166]. The poor solubility made a conventional release experiment within sink conditions effectively impossible. Therefore, Tween® 20, Tween® 80, SDS and Kolliphor® HS 15 in two different concentrations were added to improve solubility. All surfactants increased the saturation concentration of DBT, except for the addition of 0.2% Kolliphor® HS 15. As expected, higher detergent concentrations had a greater impact on c_s . The most effective additive was SDS, which increased the solubility of DBT to 119.1 µg/mL for 0.2% of SDS and to 283.5 µg/mL for 0.5%. Therefore, SDS was chosen for the solubility enhancement of DBT. Besides, the addition of SDS to the dissolution medium has already been investigated in the literature and has been recommended for *in vitro* release experiments of sparingly water-soluble drugs [176,178,179]. The enhancement of c_s to 119.1 µg/mL was sufficient to maintain sink conditions ($< 10\% c_s$) during the whole study with the aforementioned experimental setup (section 3.2.6). Therefore, the lowest suitable SDS concentration (0.2%) was chosen in accordance with FDA- and EMA-guidelines [170,171].

4.2.6.2 SELECTION OF SAMPLING TECHNIQUE AND DURATION OF RELEASE EXPERIMENTS

Release experiments of microparticulate DDSs raise the problem of sample taking. For the withdrawal of the sample, the microparticles have to be separated from the release medium. The most common sampling methods are the dialysis method and the sample and separate (SAS) method [180,181]. Regarding the SAS method, the microparticles are added directly to the buffer medium and are separated by filtration or centrifugation before sample taking. It allows a direct and rather precise measurement of the *in vitro* release. In the case of the dialysis method, the microparticle suspension is introduced into a dialysis bag which is placed in the release medium. Drug release is measured due to diffusion through the dialysis membrane into the buffer. The dialysis method has the advantage of physical separation between particles and medium but can be misleading due to the membrane diffusion kinetics [143]. Therefore, the SAS method was chosen as a sampling technique for this study, and the sample was withdrawn after allowing the particles to sediment. The major drawback of this method is that it is hardly possible to accomplish total buffer replacement. Consequently, the drug is constantly in contact with the release medium, hence, the stability of the drug has to be guaranteed for the time of the experiment.

To determine the maximum duration of the release experiments, the stability of dissolved DBT in the release medium had to be assessed. Figure 27 exhibits the stability of DBT in PBS pH 7.4 containing 0.2% SDS at 37 °C. After 24 h the concentration started to decrease which reveals the instability of DBT in its solvent. On day four the DBT concentration had dropped to 87.5% and on day 14 only 57.3% of the initial concentration was measured. Consequently, the conventional experimental setup was not suitable for long-term measurements due to the poor stability of DBT in the release medium. As a compromise between the validity of the results and the gained insight into the release rate of the microparticles, a release duration of four days was agreed on. To enable the measurement of the release over a longer period, a residual analysis was conducted for the most promising formulations. In this approach, the microparticles are removed from the release medium completely and the residual drug amount inside the microparticles can be analyzed. Therefore, it is possible to elude the stability problems of DBT. Since the residual analysis is a destructive technique it requires large amounts of microparticles. For this

reason, the sampling frequency was set to be lower and not every formulation was investigated this way.

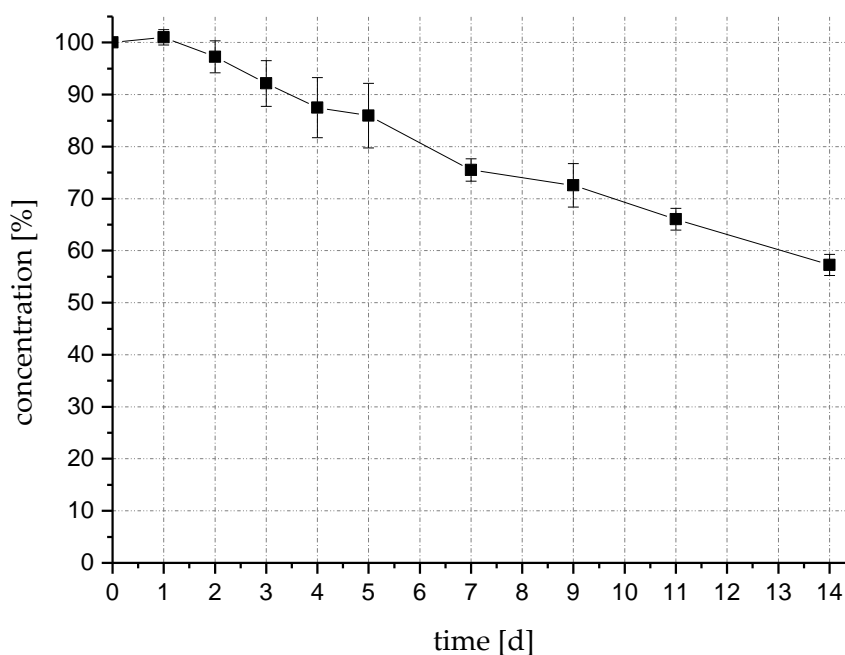


Figure 27: Stability of DBT in PBS pH 7.4 + 0.2% SDS at 37 °C.

4.2.6.3 *IN VITRO* RELEASE OF DIBENZOYL THIAMINE

The *in vitro* release of DBT was investigated for FA-PGA microparticles with different size distributions to assess the influence of particle size on the release rate. Therefore, particles were prepared with different stirring velocities, larger particles at 240 rpm and smaller particles at 275 rpm, as mentioned in 4.2.2.2.

Release profiles of particles prepared at 240 rpm are shown in Figure 28. Major differences in the release patterns of the FA-PGAs became apparent. The stearyl PGA microparticles showed a fast drug release and liberated DBT within the first two hours completely. However, extended periods of drug release were observed for the polymers modified with behenic acid. The high release rates of PGA-S65 and PGA-S90 can be explained by the melting of the stearic acid side chains of the polymer backbone at 37 °C (see DSC measurements 4.1.1) which led to a softening of the polymer structure. As a consequence, the water penetration into the particle increases, and higher diffusion coefficients occur. As

already expected, the quick drug release diminishes the suitability of the stearyl PGAs for the formulation of parenteral depot systems.

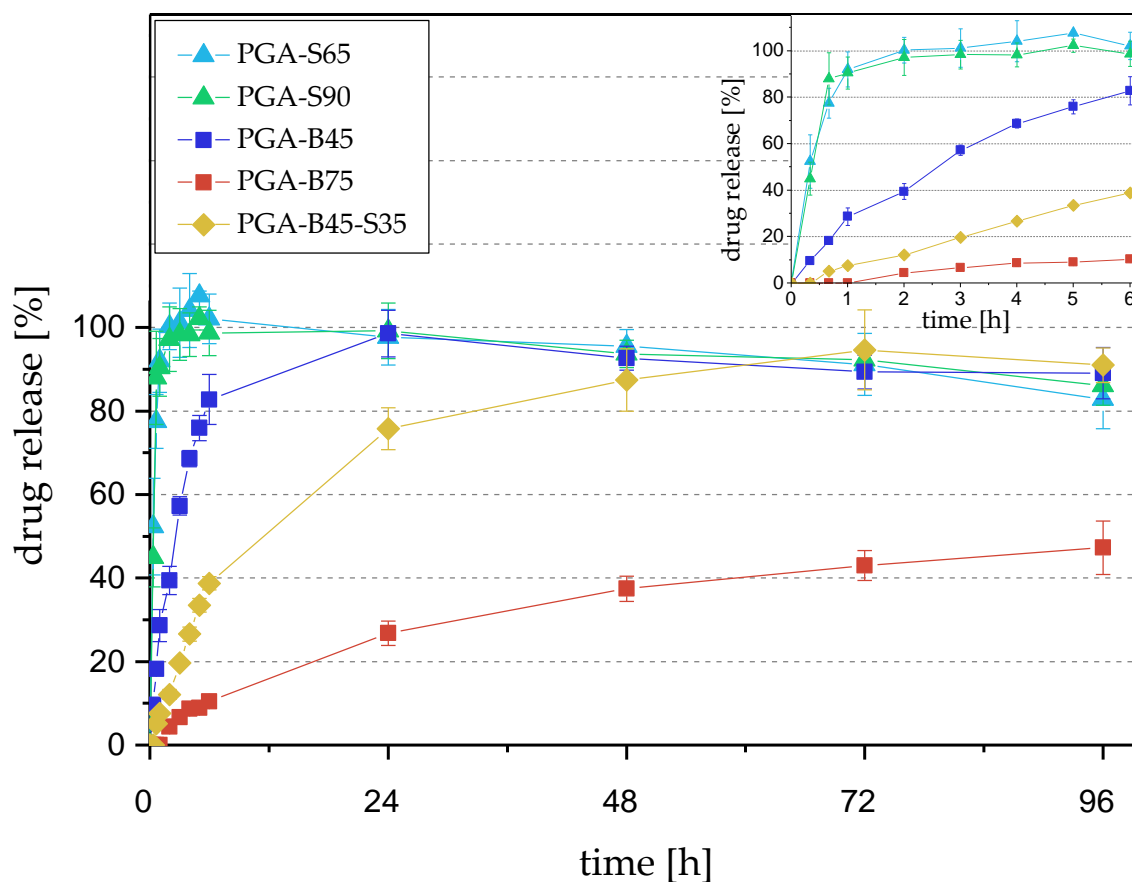


Figure 28: *In vitro* release of FA-PGA microparticles loaded with nominally 6% DBT in PBS pH 7.4 + 0.2% SDS over a period of four days at 37 °C. The microspheres were prepared with a stirring velocity of 240 rpm.

A prolongation of the drug release was achieved through grafting of the PGA backbone with behenic acid. For low substitution degrees, the release period was only extended slightly, whereas higher substitution percentages led to a considerably longer drug release. PGA-B45 microparticles showed a drug release over a prolonged time span compared to the stearyl PGAs despite the lower acylation degree. Nevertheless, PGA-B45 released DBT within the first 24 hours probably due to its comparatively high hydrophilicity. Examining the higher substituted PGA-B75 it became apparent that the increase in the acylation degree of the polymer affects the release behaviour distinctly. The PGA-B75 microspheres released only 47.3% of the total DBT amount during 96 h and showed the lowest release rate of the investigated FA-PGA microparticles. Regarding PGA-B45-S35, the DBT release was completed after 72 hours. Despite its overall higher acylation degree of 80%, a shorter period of drug release was observed compared to PGA-B75. This observation suggests that

the stearic acid acts as a release accelerator in the double substituted polymer due to its lower melting temperature. The partial melting of the fatty acid side chains was already discussed in the rheology and EPR section and could be the reason for higher diffusion coefficients inside the polymer matrix. Therefore, it is possible to regulate the release behaviour by simultaneous grafting of different fatty acids. Furthermore, the visible decline of the release curves after the complete DBT release can be attributed to the poor stability of DBT in the release medium.

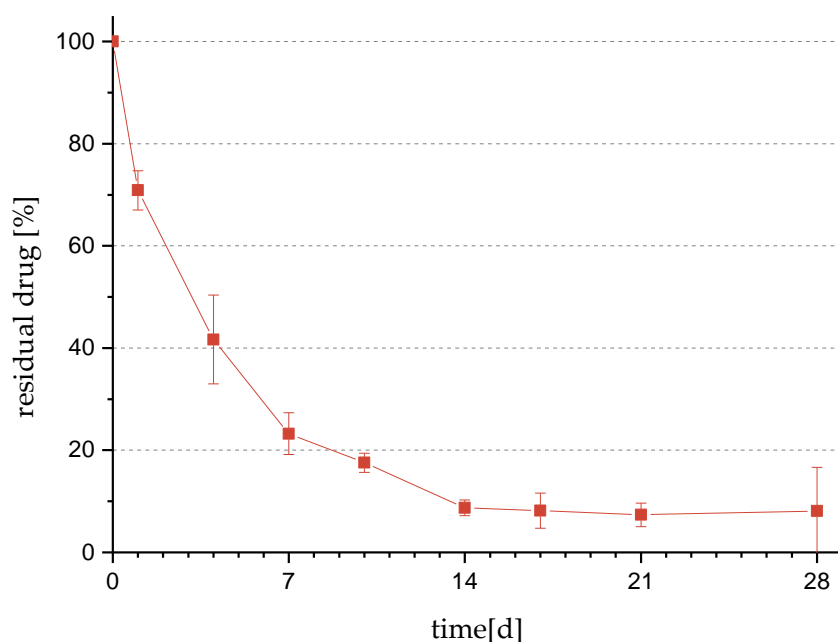


Figure 29: Residual drug content of PGA-B75 microparticles loaded with nominally 6% DBT after incubation at 37 °C in PBS pH 7.4 + 0.2% SDS. The microspheres were prepared with a stirring velocity of 240 rpm.

Figure 29 illustrates the results obtained from the residual analysis. It shows that the PGA-B75 microparticles released the API over a period of 14 days. No distinctive burst release could be detected for the PGA-B75 particles with either method. The general release patterns of both methods coincide. Small variations in the exact values originate from the stability problems of DBT in the conventional experimental setup. To assess whether degradation processes influenced the drug release from the microspheres, PGA-B75 particles were incubated in PBS pH 7.4. Subsequently, the molar mass was analyzed via GPC to conclude about potential ester hydrolysis. As displayed in Figure 30, no degradation occurred during the experiment. No distinct changes could be observed in the molecular weight and PDI respectively. Due to the relative stability of ester bonds in aqueous media ($t_{0.5} = 3.3$ years) *in vitro* and the high lipophilicity of PGA-B75, this is not

surprising [182]. Therefore, the influence of degradation on the *in vitro* release behaviour of PGA-B75 microspheres can be excluded. Hence, presumably diffusion processes through the polymer matrix or pores account for the release profile to a large degree.

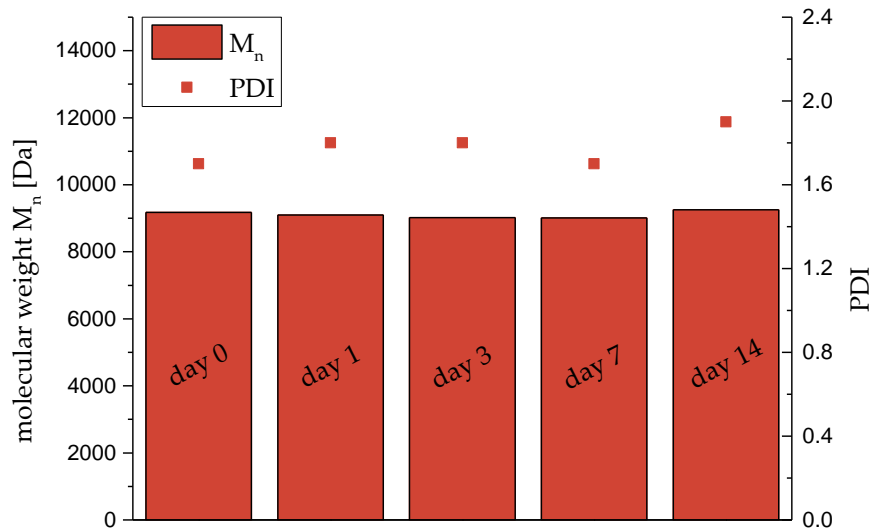


Figure 30: Degradation behaviour of PGA-B75 microspheres prepared at 240 rpm over 14 days incubated in PBS pH 7.4 at 37 °C. The columns indicate the number averaged molecular weight (M_n), the dots represent the PDI.

To investigate the effect of the particle size on the release behaviour of FA-PGA microparticles, PGA-B45, PGA-B75 and PGA-B45-S35 microspheres were also prepared with a stirring velocity of 275 rpm. The stearyl PGAs were excluded from this study due to their high release rate in the previous experiment.

Figure 31 summarizes the results of the *in vitro* release of DBT from FA-PGA microparticles with smaller particle sizes. It was observed that the release rate increased considerably for all investigated polymers due to the reduction of the particle size. The PGA-B45 particles ($d_{0.5} = 48.9 \mu\text{m}$) released DBT within three hours completely while the drug release for the bigger particles ($d_{0.5} = 86.4 \mu\text{m}$) ended at 24 hours. For PGA-B45-S35 the release duration was decreased from three days to two days. While the PGA-B75 microspheres with a median particle size of $96.5 \mu\text{m}$ released only 47.3 % DBT over four days, the smaller particles ($d_{0.5} = 53.7 \mu\text{m}$) liberated 84.6 % within the same time interval. Due to the instability of DBT in the buffer medium, the value was afterward rectified to 100% by the residual analysis (Figure 32). An increase in the release rate with decreasing particle size was also mentioned in the literature [148,149,183]. The longer release periods for larger FA-PGA microparticles are probably resulting from a smaller cumulative surface, hence, less

interaction with water. Furthermore, the distance for the drug to diffuse out of the particle is greater for larger particle diameters.

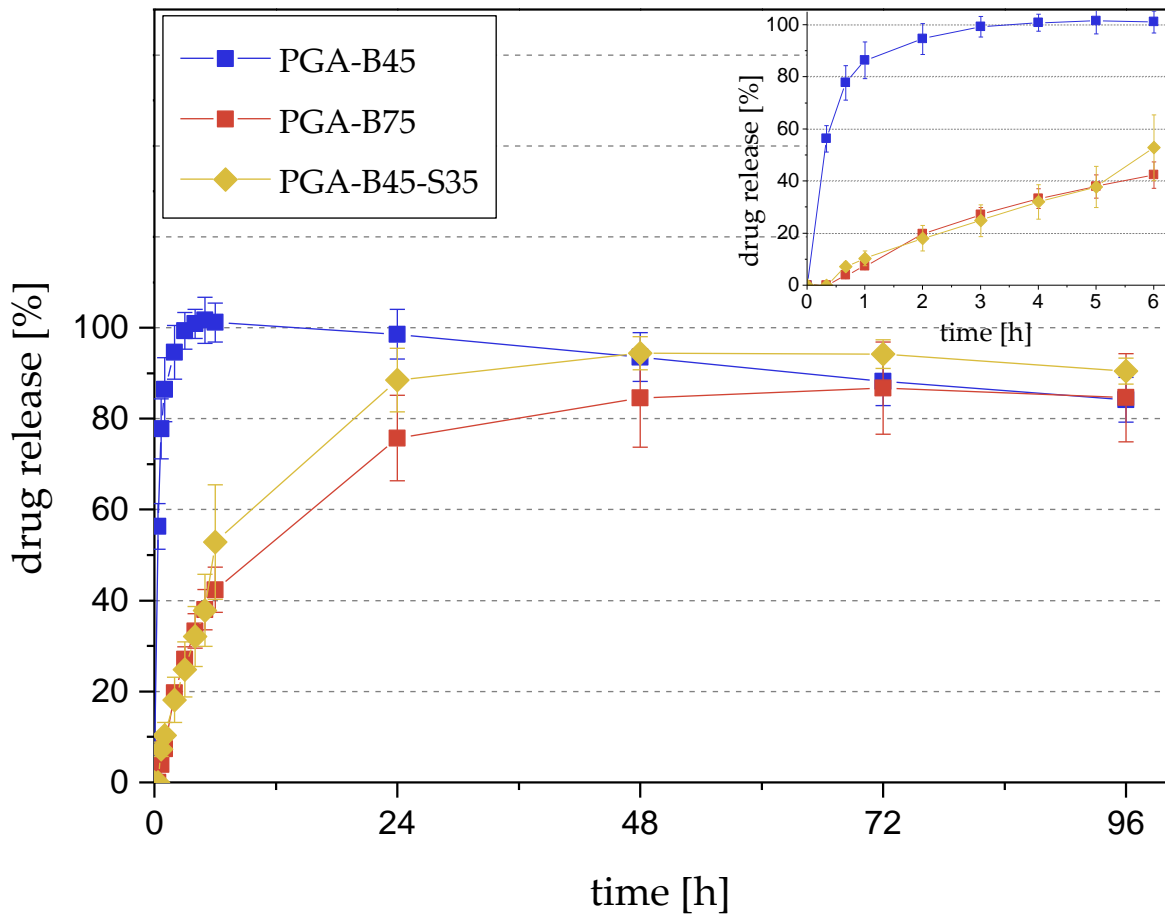


Figure 31: *In vitro* release of FA-PGA microparticles loaded with nominally 6% DBT in PBS pH 7.4 + 0.2% SDS over a period of four days at 37 °C. The microspheres were prepared with a stirring velocity of 275 rpm.

In summary, the release profile of DBT from FA-PGA microparticles was affected by the selection of the fatty acid and the substitution degree. Stearoyl PGA microspheres released the drug faster than the behenoyl PGA particles. With increasing substitution degree, the release rate decreased. The simultaneous substitution of the two fatty acids allows accelerating the release of the lipophilic DBT compared to an equally substituted behenoyl PGA. Therefore, the release rate can be adjusted without reducing the substitution degree, hence, the encapsulation efficiency. Furthermore, it is possible to regulate the release rate through the particle size distribution. Smaller particles showed faster drug release. Moreover, the *in vitro* release was not influenced by degradation but merely by diffusion processes based on the data for PGA-B75.

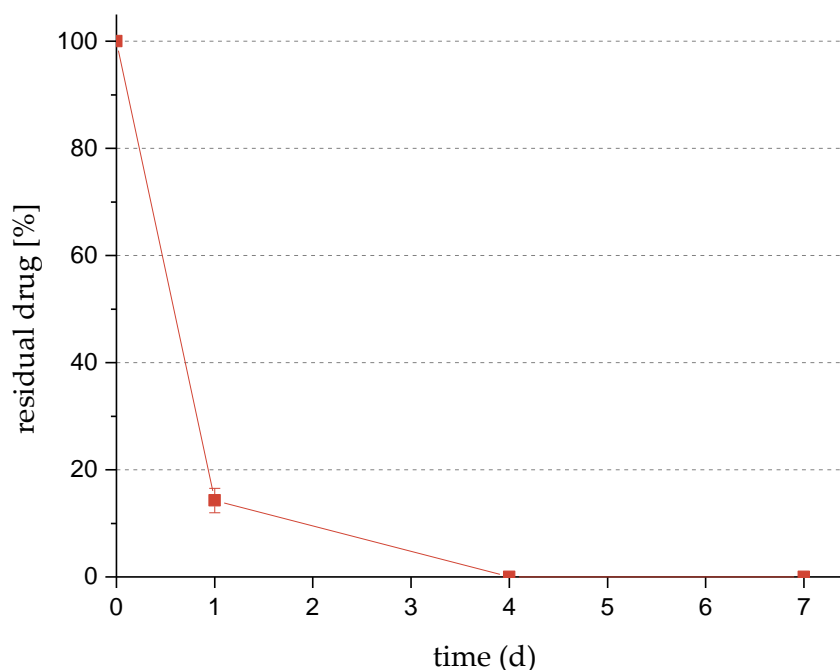


Figure 32: Residual drug content of PGA-B75 microparticles loaded with nominally 6% DBT after incubation at 37 °C in PBS pH 7.4 + 0.2% SDS. The microspheres were prepared with a stirring velocity of 275 rpm.

4.2.7 COMPARISON TO PLGA

Poly(lactic-co-glycolic acid) (PLGA) copolymers are the most extensively studied commercially available biodegradable polymers. The possibility to alter the ratio of lactic acid/glycolic acid and the molecular weight of these macromolecules made PLGA the most widely used biodegradable polymer with variable physicochemical properties [184]. Nevertheless, PLGA has some disadvantages such as the potential formation of a highly acidic pH-microclimate and complex degradation and release profiles [43,44,182,185,186]. Therefore, constantly new biodegradable materials such as modified PGA are investigated as alternatives for PLGA. To assess the release behaviour of FA-PGA microparticles in a greater context, the *in vitro* release of DBT out of PLGA microspheres was conducted for comparison. The PLGA microparticles were prepared as stated in section 3.2.1.

Table 12 summarizes the main characteristics of the PLGA microparticles loaded with 6% DBT. Microparticles were prepared with three different EXPANSORB® polymers varying in molecular weight. All investigated PLGAs had a lactic acid/glycolic acid ratio of 50/50. The measured size distributions of the PLGA particles were similar to the FA-PGA microspheres. This is important for the comparability of the *in vitro* release experiments since the particle size affects the release rate as discussed previously. Median particle sizes between 82.8 µm and 116.7 µm were detected for the PLGA microspheres. All PLGA

copolymers showed good encapsulation efficiencies comparable with the higher substituted FA-PGAs.

Table 12: Characteristics of different PLGA microparticles loaded with nominally 6% DBT. The number averaged molecular weight (M_n) of the polymers and the size distribution parameters $d(0.5)$ and span as well as the encapsulation efficiency (EE) of the microparticles are given.

Polymer	M_n [Da] ^a	$d(0.5)$ [μm] ^b	Span ^b	EE [%] ^c
DLG 50-2A	6046	105.7 \pm 11.8	0.772 \pm 0.120	78.3 \pm 5.5
DLG 50-3A	13554	116.7 \pm 10.6	0.675 \pm 0.012	90.7 \pm 3.5
DLG 50-5A	27370	82.8 \pm 8.8	0.682 \pm 0.014	84.6 \pm 2.9

^a Obtained from GPC data

^b Measured with laser diffraction analysis

^c Determined via HPLC analysis

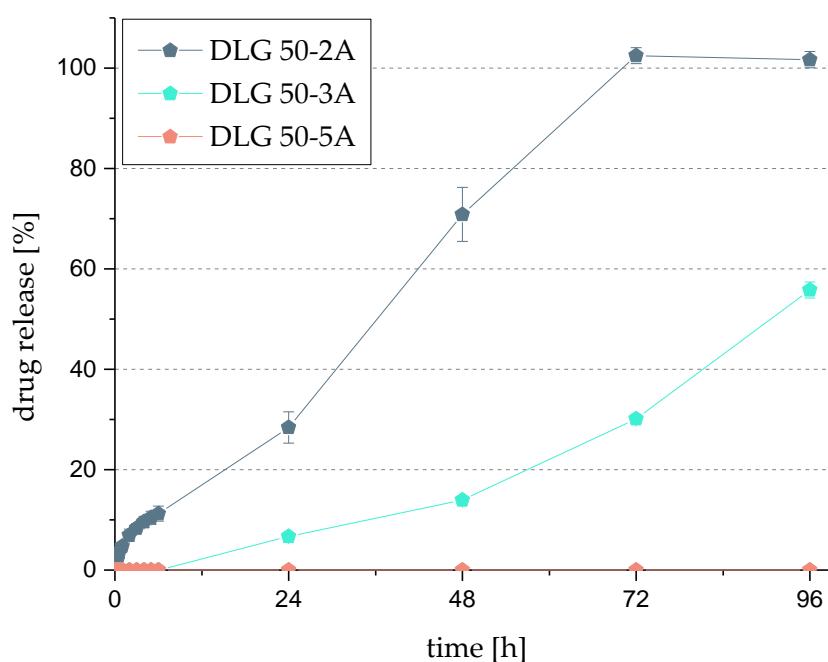


Figure 33: *In vitro* release of PLGA microparticles loaded with nominally 6% DBT in PBS pH 7.4 + 0.2% SDS over a period of four days at 37 °C.

Figure 33 displays the *in vitro* release of DBT from PLGA microparticles over four days. DLG 50-2A with a molecular weight of 6.0 kDa showed the highest release rate and released DBT within three days. With increasing molecular weight, the release rate decreased. For DLG 50-3A microparticles ($M_n = 13.6$ kDa) a short lag phase of at least six hours was detected. After 96 h 55.8% of DBT were released. The PLGA copolymer (DLG 50-5A) with the highest molecular weight of 27.4 kDa showed no DBT release during the experiment.

For DLG 50-3A and DLG 50-5A microparticles, a residual analysis was performed to investigate the release behaviour over a longer time span (Figure 34). The DLG 50-3A microparticles released DBT within seven days. Including a lag phase of four days, the DBT release of DLG 50-5A was virtually completed after ten days.

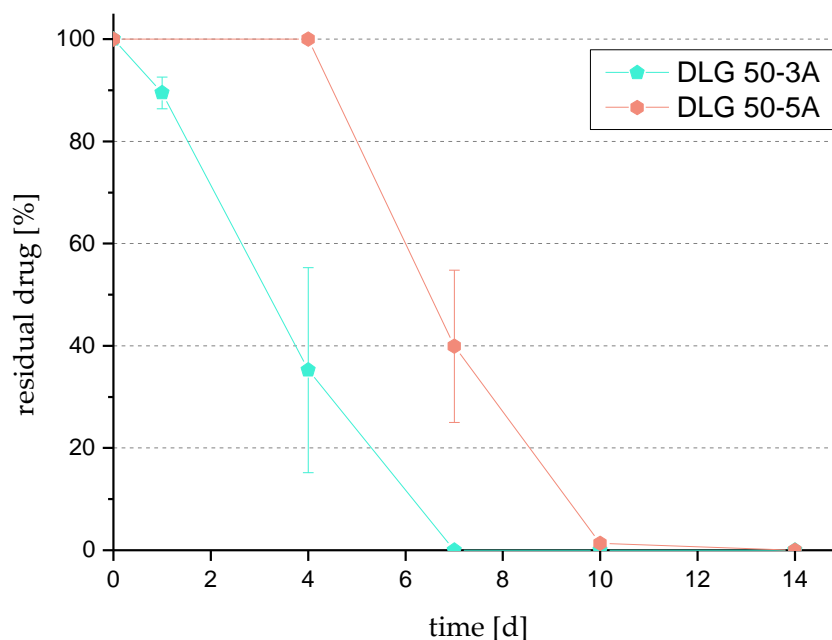


Figure 34: Residual drug content of PLGA microparticles loaded with nominally 6% DBT after incubation at 37 °C in PBS pH 7.4 + 0.2% SDS.

In many cases, a triphasic release profile is reported for PLGA microparticles [31,57,187]. An initial burst release is followed by a lag phase and a secondary release phase. The three phases are caused by initial drug diffusion, followed by matrix hydration and finally bulk degradation. The causes for burst release are diverse. A frequent reason for this is the release of API trapped on the particle surface especially observed for high drug loadings [188]. In this particular case, no distinct burst release was detected, hence, the release patterns were biphasic. This could be explained by the low drug loading percentage of 6% which did not provoke the attachment of DBT on the particle surface. The lag phase is dependent on the hydration of the polymer matrix. While for DLG 50-2A microparticles no lag phase was observed, increasing periods without drug release were detected for DLG 50-3A and DLG 50-5A. Consequently, the lag phases increased depending on the molecular weight of the polymer. The influence of molecular weight on the degradation and release behaviour of PLGA particles has been extensively discussed in the literature [189–192]. Hydration of the polymer and the rate of degradation decrease with increasing

molecular weight. Therefore, longer lag phases are observed for longer PLGA chains. After hydration, the drug release is affected by diffusion through the polymer matrix and degradation processes. The slight increase in the release rate of DLG 50-2A and DLG 50-3A after 24 to 48 hours could indicate the beginning of polymer degradation. However, all PLGA microparticles showed rather constant and linear release profiles except for the respective lag phases.

Compared to the FA-PGA microparticles the PLGA microspheres showed a more linear drug release. Constant drug release rates are favourable to avoid non-therapeutic concentrations and peaks in the drug plasma curves. Future research could aim at the modulation of the release patterns of FA-PGA microparticles towards a near zero-order kinetic. The adjustment of the composition of the acyl side chains or the influence of the release behaviour through hydrophilic residues (e.g. PEG) is conceivable. However, for the FA-PGA microspheres, no lag phases were observed. Therefore, a constant drug release was possible which is preferable to achieve a direct therapeutic effect after the application of the DDS. Furthermore, the PGA-B75 microparticles released DBT over a longer period than the PLGA formulations. Even DLG 50-5A, which had the highest molecular weight of all investigated polymers, revealed a release duration of only six to seven days. Moreover, it showed the longest lag phase. Certainly, it is possible to achieve a longer release by adjusting the lactic acid/glycolic acid ratio of PLGA towards the lactic acid but that would presumably prolong the lag phase simultaneously. Despite its considerably lower molecular weight (approx. 10 kDa), the longer release duration of PGA-B75 could be explained by its higher lipophilicity compared to the PLGA formulations.

To summarize, the advantages and disadvantages of PLGA are well known. Regarding the release behaviour, small modulations towards a more linear drug release could consolidate the position of FA-PGA as an equivalent alternative for PLGA. Especially the PGA-B75 microparticles revealed promising *in vitro* results regarding constant DBT release over long periods.

4.2.8 CYTOTOXICITY

Cytotoxicity is an important parameter for the assessment of the biocompatibility of materials. Concerning prospective *in vivo* applications, the biocompatibility of the FA-PGA

microparticles had to be evaluated *in vitro* beforehand. For that reason, a resazurin reduction assay was performed. Thereby, the non-fluorescent blue resazurin is reduced to the fluorescent red resorufin in mitochondria of living cells [193,194]. By comparing the measured fluorescence intensity of the treated cells to the signal intensity of untreated cells conclusions can be drawn about cell death. The determination of cell death after direct or indirect contact with the material is one of the most valuable measures for toxicity [195,196]. To assess the cytotoxic properties of the microparticle formulations the resazurin reduction assay was conducted on two different cell lines - mouse embryonic fibroblasts (3T3) and normal human dermal fibroblasts (NHDF).

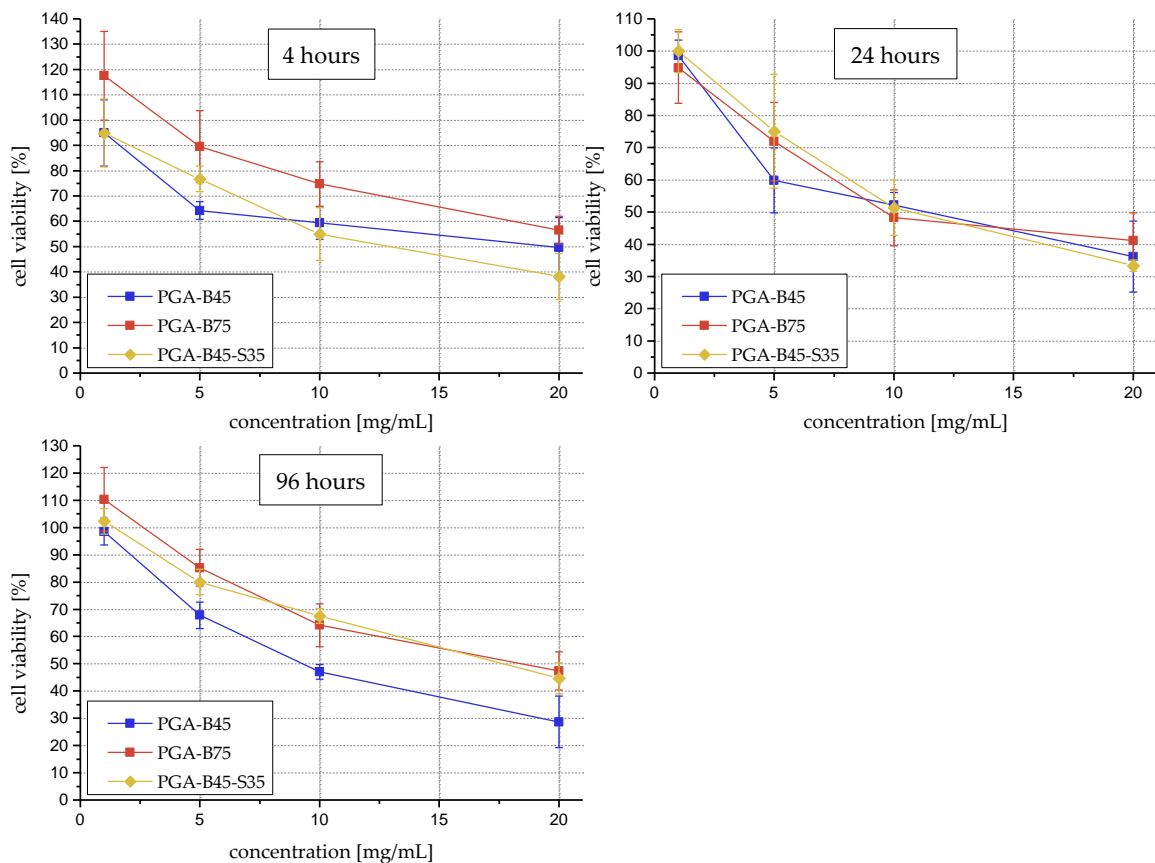


Figure 35: Cell viability of NHDF cells after incubation with different concentrations of FA-PGA microparticles for 4 h, 24 h and 96 h. Cell viability was determined fluorometrically by a resazurin reduction assay. The negative control value (untreated cells) was set as 100%.

Figure 35 displays the cell viability of NHDF cells after incubation with different concentrations of FA-PGA microparticles over 96 h. For the lowest investigated concentration of 1 mg/mL, no decrease in cell viability was detected. Higher concentrations affected the viability of the cells. At a concentration of 10 mg/mL, the half-maximal

inhibitory concentration was exceeded for PGA-B45 particles after 96 h. The half-maximal inhibitory concentration (IC_{50}) is the concentration needed to reduce cell viability by 50%. IC_{50} values are used to evaluate the cellular response to the material [197,198]. All investigated FA-PGA microparticles reduced the cell viability to < 50% at a concentration of 20 mg/mL. PGA-B75 and PGA-B45-S35 showed similar cytotoxic properties while PGA-B45, which has the lowest acylation degree, affected the cell viability the most. This observation coincides with research conducted on the hemolytic activity of modified PGA nanoparticles *in vitro* [67,86]. As a possible explanation, the larger quantity of free hydroxyl groups increased the amphiphilic character of the polymer. Furthermore, it was observed that the cell viability values initially decreased and increased in many cases subsequently. That implies that the cells were able to recover after initial stress. Moreover, at the lowest particle concentration, cell viability values over 100% were detected. The metabolization of the polymer by the cells resulting in enhanced cell activity and proliferation could possibly explain that phenomenon. Similar observations were made by Weiss et al. regarding stearyl PGA nanoparticles [67].

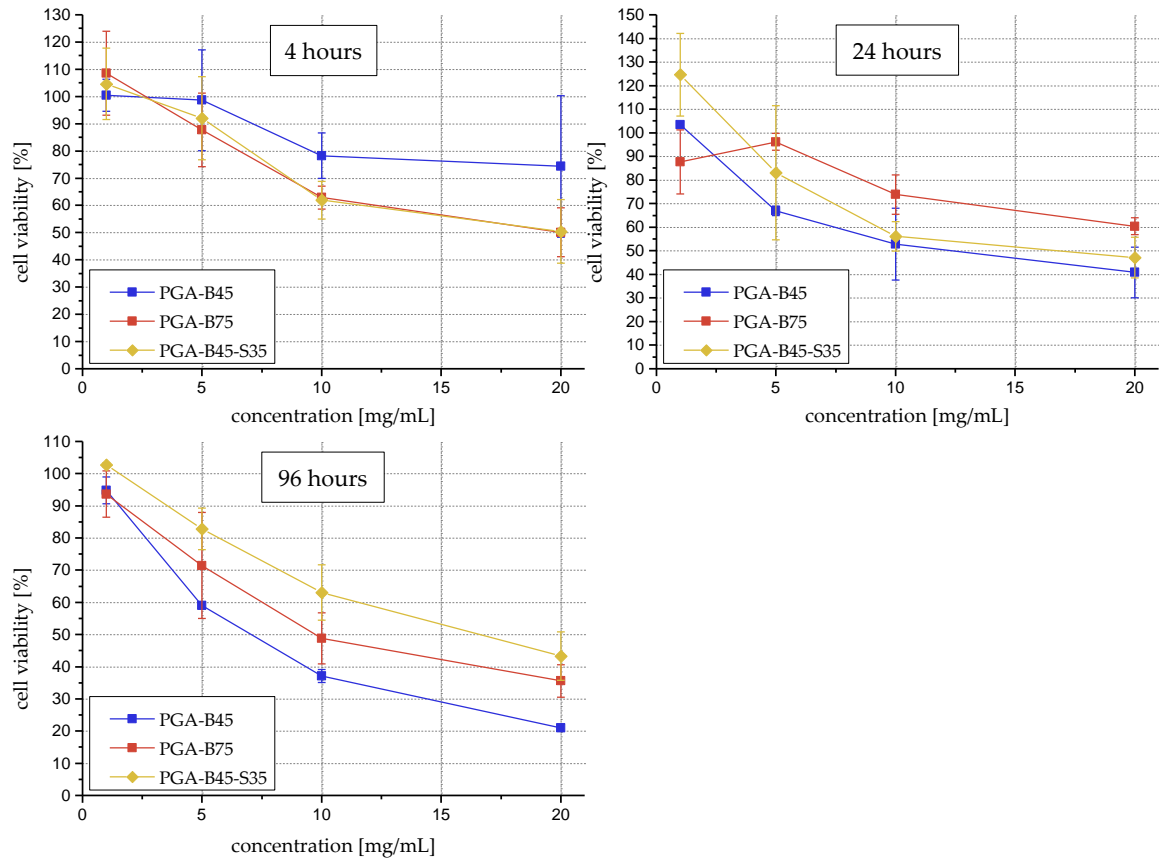


Figure 36: Cell viability of 3T3 cells after incubation with different concentrations of FA-PGA microparticles for 4 h, 24 h and 96 h. Cell viability was determined fluorometrically by a resazurin reduction assay. The negative control value (untreated cells) was set as 100%.

The investigation of cytotoxic effects on 3T3 cells revealed a similar pattern (Figure 36). Accordingly, the reduction of the cell viability was dependent on the particle concentration. While a concentration of 1 mg/mL did not impact the cells, the viability decreased with increasing concentration. Again, the PGA-B45 microparticles had the greatest effect. Regarding PGA-B45-S35, the 3T3 cells responded less strongly and the IC_{50} was not exceeded even for the higher concentration. For PGA-B45 and PGA-B75 a concentration of 10 mg/mL led to a reduction of the cell viability below 50%.

Although some of the results correlate with previously published data, the general cytotoxicity of the investigated FA-PGA microparticles was considerably higher. Previous *in vitro* studies on PGA nanoparticles showed no negative effects on cell viability [65,67,86]. That raised the question of whether the viability of the cells was only impacted by the material itself or if other experimental parameters had an effect as well. This was investigated in the following.

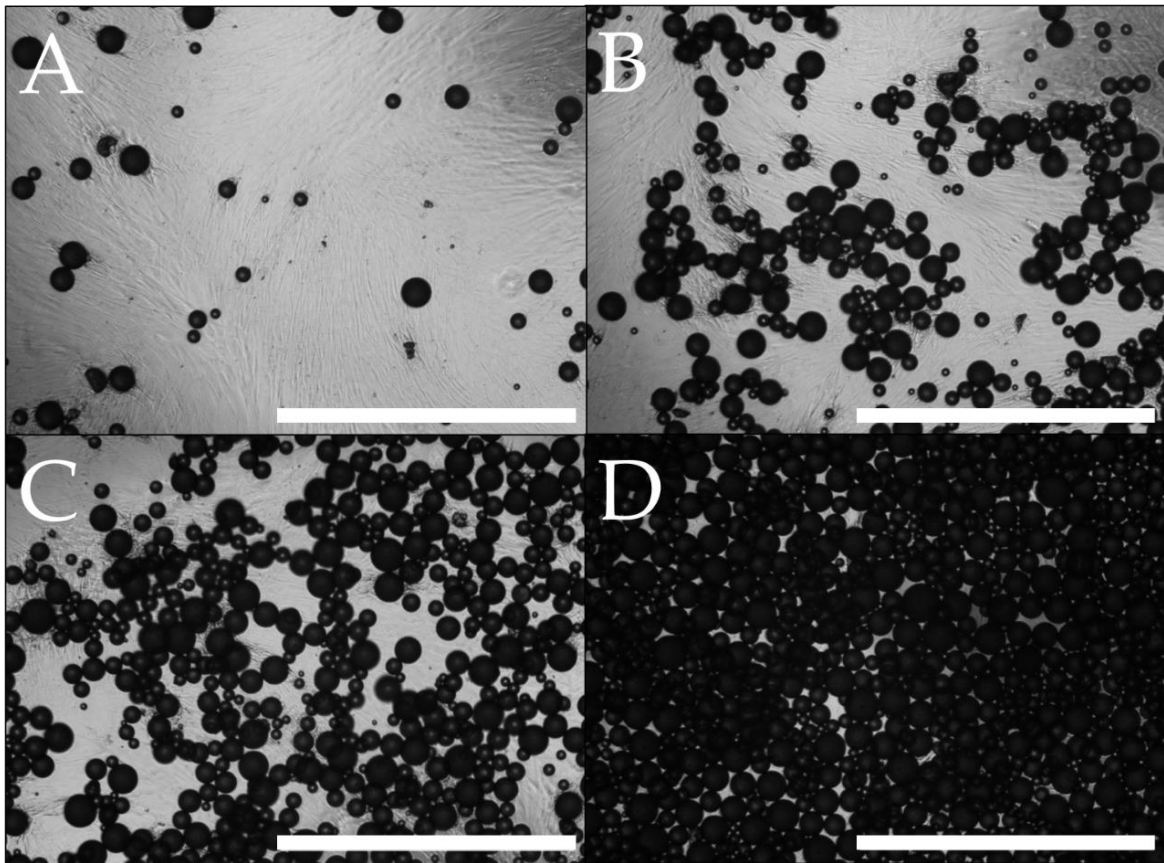


Figure 37: Exemplary images of NHDF cells and PGA-B75 microparticles after incubation for 96 h. Different particle concentrations are displayed: (A) 1 mg/mL, (B) 5 mg/mL, (C) 10 mg/mL, (D) 20 mg/mL. The white bar represents a distance of 1 mm.

Figure 37 displays exemplary microscopic images of the experimental setup. For the lower concentrations, an intact cell layer is visible below the microparticles. It becomes apparent that the cells are completely overlain by the microparticles at higher concentrations. These images suggest that by direct contact physical pressure is applied which could cause mechanical damage to the cells. Consequently, the mechanical damage would be misinterpreted as a cytotoxic effect [195,199]. To investigate this assumption an indirect approach with cell culture inserts (ThinCerts™) was chosen. Thereby, the cell material is physically separated from the particles by a permeable membrane but still in close contact with the test material. The indirect approach was conducted for the highest investigated particle concentration (20 mg/mL). Due to the high amount of material required for this setup, the test was only performed twice for each formulation, timepoint (24 h, 96 h) and cell line.

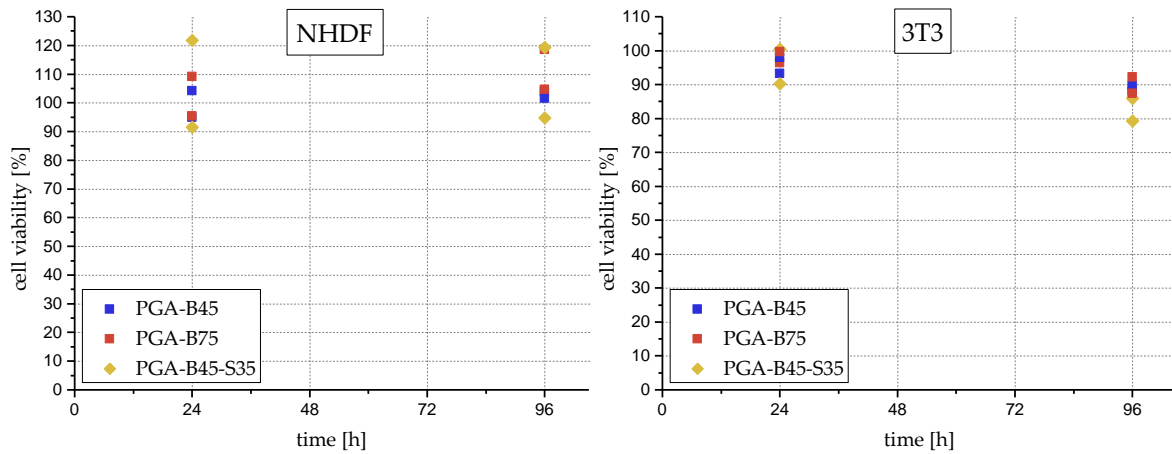


Figure 38: Cell viability of NHDF and 3T3 cells after incubation with 20 mg/mL of FA-PGA microparticles for 24 h and 96 h. ThinCerts™ were used to physically separate the particles from the cells. Cell viability was determined fluorometrically by a resazurin reduction assay. The negative control value (untreated cells) was set as 100%.

Figure 38 summarizes the cell viability results for the indirect approach. It becomes apparent that the effect of the FA-PGA microparticles on the cell viability was minor. For the NHDF cells, no distinct negative effect could be detected. The results obtained for the 3T3 cells might suggest a slight decrease in cell viability to approximately 85% to 90% after 96 h. Still, the effect was minor compared to the cytotoxic properties observed for direct cell-particle contact. Consequently, the physical pressure of the particles on the cells exaggerated the reduction of cell viability which therefore has to be interpreted carefully. The disparity between the two approaches suggests that the physical pressure led to either mechanical damage or a cell response due to insufficient gas or nutrient supply [200]. To conclude, based on the results from the indirect experimental approach FA-PGAs were well tolerated by the used cell models. The available literature data support this assessment [67,86]. Therefore, the FA-PGA microparticles were evaluated as drug delivery systems with good biocompatibility suitable for further *in vivo* investigations.

4.2.9 IMPACT OF ELECTRON BEAM STERILIZATION

A prerequisite for the application of parenteral DDSs is the sterility of the dosage form. According to EMA and FDA guidelines, steam sterilization, dry heat sterilization, ionization radiation sterilization and gas sterilization are the recommended sterilization methods [201,202]. Sterilization treatments involving high temperatures, i.e. dry heat and steam sterilization, are generally not suitable for polymeric microparticles. Thereby, glass transition or melting temperatures are exceeded and form stability can not be guaranteed.

Gas sterilization, most commonly with ethylene oxide, is due to potentially toxic residues only acceptable if no other method is available and is therefore mainly used for packaging materials [203]. Following the decision tree of the EMA guidelines, ionizing radiation is the most suitable sterilization method for the FA-PGA microparticles. Radiation sterilization by gamma radiation or electron beam (e-beam) is performed with radiation doses of ≥ 25 kGy. Since the transferred energy during sterilization can cause changes in the particle properties, the effect of the irradiation has to be investigated [204–206]. Since e-beam radiation provides higher dosing rates than gamma radiation, shorter exposure times can be set, thus, potential degradation of polymer and API is reduced [207,208]. Therefore, e-beam radiation with a dose of 25 kGy was chosen as a sterilization method.

Following the *in vitro* release experiments (section 4.2.6.3), PGA-B75 microparticles were selected as the most promising candidate for translation into *in vivo* testing. Consequently, the impact of electron beam sterilization on the molecular weight of PGA-B75, the content of DBT and the *in vitro* release behaviour of the microparticles had to be assessed. Figure 39 summarizes the results of the effect of sterilization on molecular weight and drug content. As depicted the e-beam irradiation affected the molecular weight distribution of PGA-B75. The PDI of the polymer increased, hence, the weight distribution became broader. This is also visible in the individual average molecular weights. The number averaged molecular weight (M_n) decreased from 8.9 kDa to 7.7 kDa due to irradiation, which indicates an increasing number of short polymer chains. On the contrary, the weight averaged molecular weight (M_w) of the sterilized sample increased from 15.4 kDa to 35.5 kDa compared to the non-sterilized sample. This implies longer and more massive polymer chains were detected in the sterilized samples. These changes in M_n and M_w are caused by the high energy transfer during sterilization. More precisely, radicals produced by ionizing radiation promote chain scission and crosslinking and therefore broaden the molecular weight distribution of the polymer [209–213]. Moreover, changes in the solubility of PGA-B75 were detected. After sterilization, insoluble residues were observed in DCM. Presumably, crosslinking led to insoluble polymer portions with high molecular weights. Regarding DBT, the sterilization process did not affect the API. No API degradation did occur either for the pure DBT or the microparticles. Recapitulating, electron beam radiation impacted the molecular weight of PGA-B75 while DBT remained unaffected.

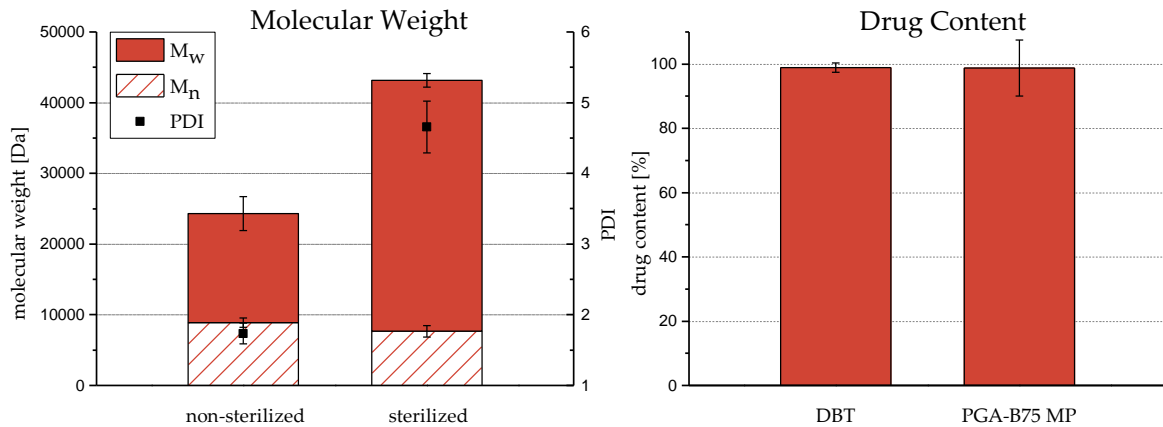


Figure 39: Impact of electron beam sterilization. Left: Influence on the weight (M_w) and number (M_n) averaged molecular weight and weight distribution (PDI) of PGA-B75 bulk polymer. Right: Drug content of pure DBT and PGA-B75 microparticles loaded with nominally 6% DBT after sterilization.

Additionally, the influence of the changes induced by e-beam sterilization on the *in vitro* release behaviour of PGA-B75 microparticles was investigated. Therefore, release experiments according to 3.2.6 were conducted. It became apparent that the irradiation did not affect the general release pattern of the microspheres (Figure 40). However, on average the e-beam sterilization led to a slight acceleration of the DBT release. Furthermore, considerably increased standard deviations were observed for the sterilized microparticles. The alteration of the release profile can be explained by the changes in the molecular weight distribution. Similar observations regarding the effect of irradiation on the release profile of microparticles are mentioned in the literature [205,214,215]. Due to the broadening of the molecular weight distribution, the deviations in the drug release increased. Moreover, the partial degradation of the polymer caused by the sterilization process led to a slight increase in the release rate.

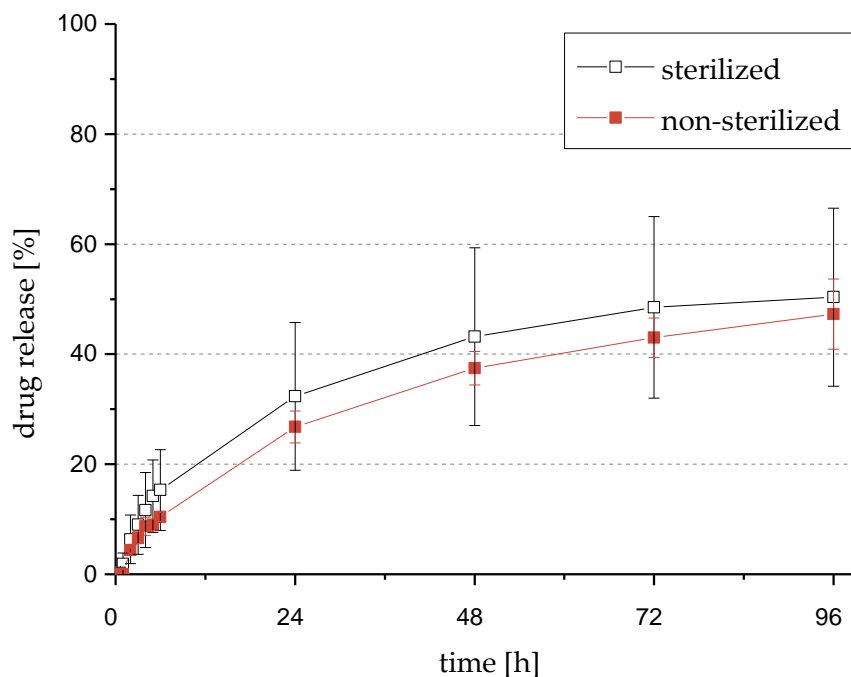


Figure 40: *In vitro* release of sterilized PGA-B75 microparticles loaded with nominally 6% DBT in PBS pH 7.4 + 0.2% SDS at 37 °C compared to non-sterilized particles.

In summary, e-beam radiation affected the properties of the microparticles. The broadening of the molecular weight distribution caused changes in solubility and release behaviour of the particles. This is concerning since the variability caused by the sterilization process is opposed to a controlled and consistent drug release. Therefore, e-beam radiation was assessed as inadequate for the sterilization of PGA-B75 microparticles. According to the decision tree of the EMA guidelines, the microspheres were prepared under aseptic conditions for further *in vivo* investigation.

4.2.10 IN VITRO RELEASE OF DiR

In view of the following *in vivo* investigations, the *in vitro* release of DiR from the PGA-B75 microparticles was assessed. Accordingly, the fluorescent dye DiR was incorporated into the microparticles as a highly lipophilic drug model. The evaluation of the quantitative release of a fluorescent dye can be challenging due to various effects influencing the fluorescence intensity. For example, solvent interactions, quenching effects and photobleaching can affect the obtained fluorescence signal [216]. To eliminate possible quenching effects, the range of concentration with a linear relationship between the amount of DiR and the total fluorescence intensity was detected prior to the experiment. Additionally, a DiR standard was measured along with the samples to identify potential

photobleaching. No bleaching was detected throughout the experiment. To improve the validity of the *in vitro* release investigation, two different measurement approaches for the detection of the DiR release were selected. The decrease in fluorescence intensity inside the microparticles was measured with the Maestro™ imaging system and the amount of DiR released to the medium was detected with the FluoroMax-4 spectrofluorometer (see methods section 3.2.10 and 3.2.11.).

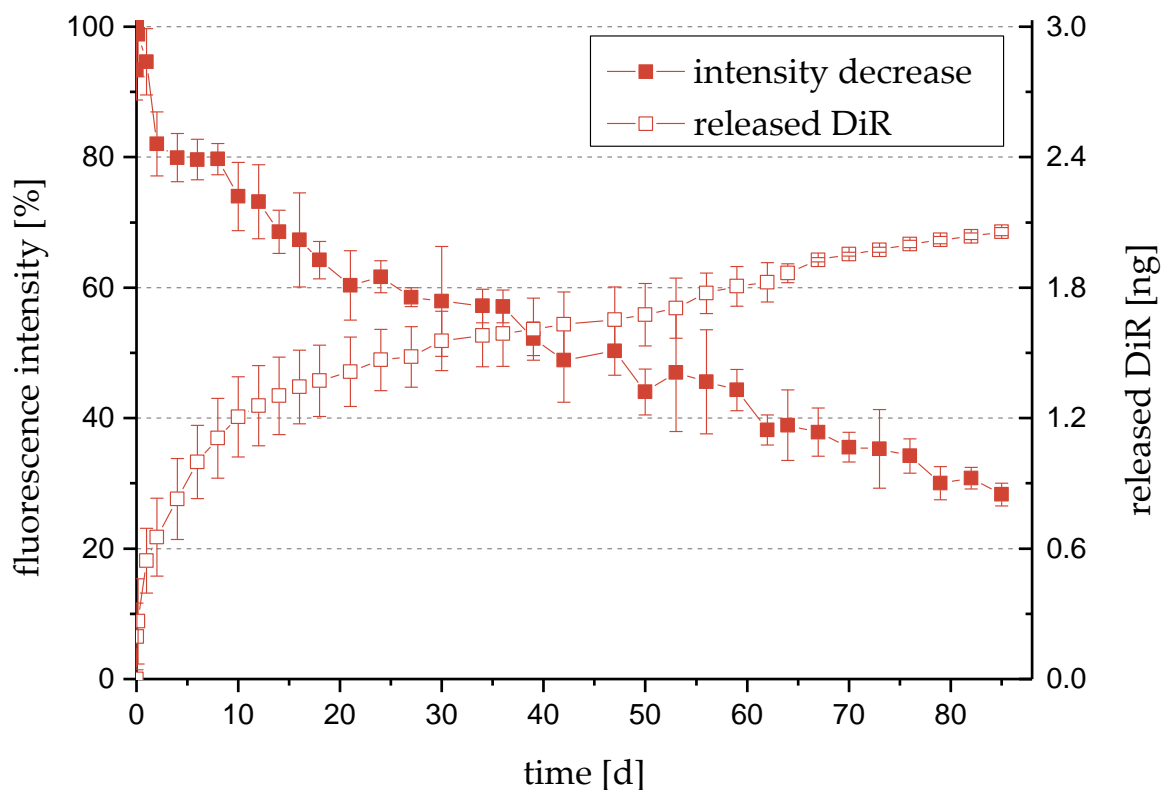


Figure 41: In vitro release of DiR from PGA-B75 microparticles in PBS pH 7.4 + 0.2% SDS over 85 days. The decrease in fluorescence intensity of the microparticles measured with the Maestro™ and the released amount of DiR obtained from fluorescence spectroscopic measurements are displayed.

Figure 41 summarizes the results obtained from the two measurement approaches. Within 85 days, the fluorescence intensity of the microparticles decreased to 28.3% which equates to 71.7% released DiR. A slightly higher release rate was observed for the first four days before it slowed down and stayed rather constant for the remaining period. The determination of the amount of DiR in the buffer medium revealed that 2.1 ng were released after 85 days. Both measurement approaches led to an almost identical release pattern with an initially higher liberation rate and a subsequent constant release. Consequently, the results obtained from the two methods confirm each other. Compared

to the liberation of DBT from PGA-B75 microparticles, the release rate of DiR was considerably lower. The low release rate of DiR can be attributed to its higher lipophilicity ($\log P = 17.4$) and therefore lower solubility in water [217]. Hence, the strong hydrophobic interactions with the lipophilic PGA-B75 resulted in long release durations. The slow liberation of DiR compared to the also lipophilic DBT highlights the impact of the API's physicochemical properties on the release profile. Therefore, the generalization of drug release from FA-PGA particles is not possible and each API has to be assessed individually regarding its release behaviour from the DDS to collect valid data.

4.2.11 IN VIVO FLUORESCENCE IMAGING

The research on novel DDSs aims ultimately at the administration of the drug product *in vivo*. This transfer from *in vitro* to *in vivo* is very challenging. Since *in vitro* investigations struggle to reproduce the physiological environment accurately, *in vivo* results often differ from the findings *in vitro*. Complex enzymatic degradation processes and other interactions between the drug formulation and its environment at the site of injection can only be exposed *in vivo*. Therefore, *in vivo* fluorescence imaging experiments were conducted on SKH1-*Hr^{hr}* mice. Hairless SKH1 mice were selected since their lack of hair and skin pigmentation makes them favourable for fluorescence imaging [218]. Following the previous *in vitro* characterization, PGA-B75 microparticles were chosen as the most promising controlled release formulation to gain some insight into the behaviour of FA-PGA particles *in vivo*. To visualize the microspheres at the injection site, NIR fluorescent dyes DiR and DY-782 were chosen for the investigation. Due to low absorption and tissue autofluorescence of the NIR range *in vivo*, the utilization of NIR dyes allows to minimized background interference and to improve penetration depth [219,220]. DiR was incorporated into the PGA-B75 microspheres as a lipophilic drug model to study the release behaviour. Furthermore, to observe polymer degradation, DY-782 was covalently bound to PGA-B75 and subsequently, microparticles were prepared with the dye-labeled PGA-B75-DY782. Eventually, the microparticle formulations were injected into the nuchal fold of the mice.

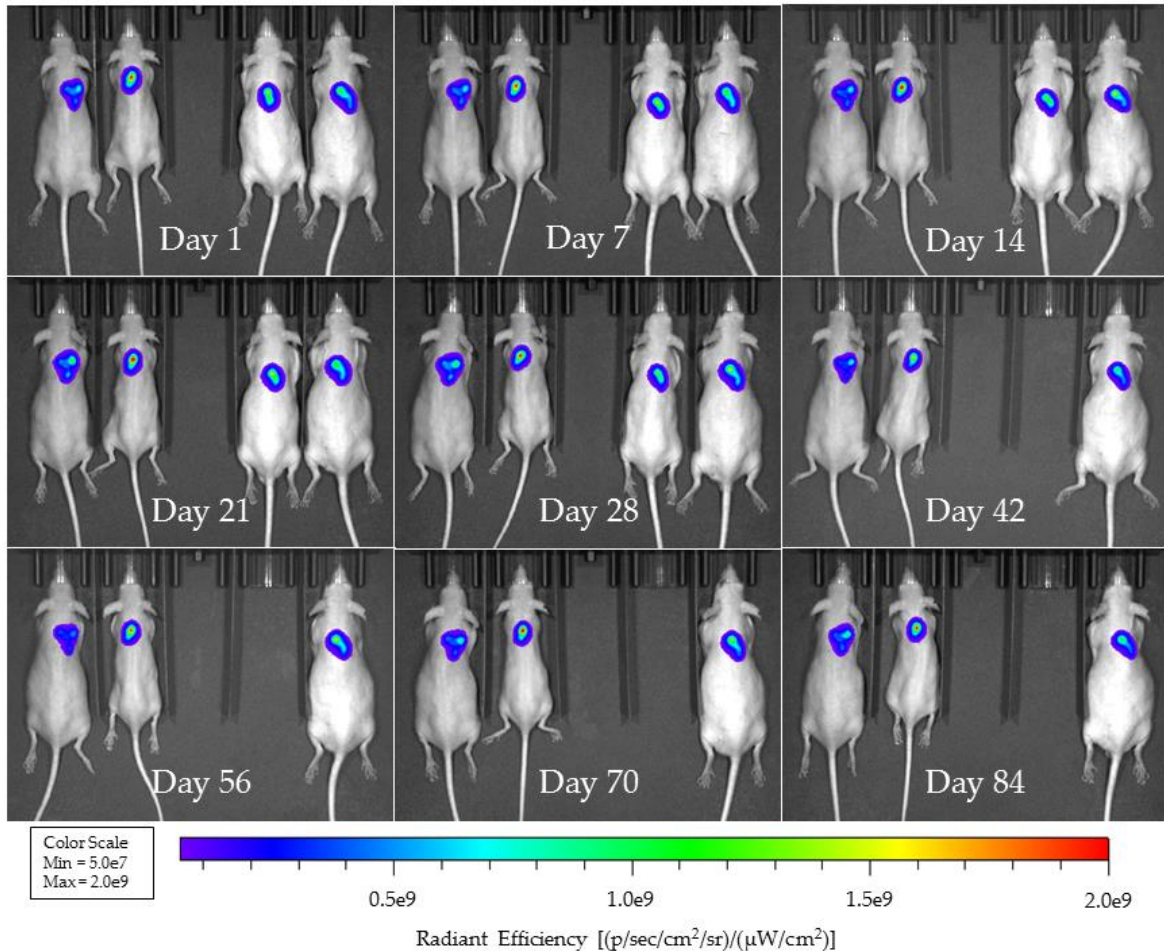


Figure 42: *In vivo* fluorescence imaging of PGA-B75-DY782 microparticles in SKH1-*Hr^{Hr}* mice over 84 days. The two female mice are shown on the left side of the images, the two male mice on the right.

An overview of the fluorescence images obtained for the PGA-B75-DY782 microparticles over 84 days is given in Figure 42. No considerable decrease in the radiant efficiency was observed. The microparticles were well tolerated by all mice and no signs of inflammation or edema were detected over the course of the experiment. On day 32 one male mouse had to be withdrawn from the study due to an ocular disease not related to the microparticle administration. Figure 43 displays the evaluation of the fluorescence intensities over time. Considering the standard deviations, no distinct trend was detected over the 84 days and the fluorescence signal remained almost constant. One of the challenges for *in vivo* imaging is the positioning of the mice in the same posture for each measurement. Small variations in the mouse position and changes in the mouse body itself affect the detected fluorescence signal unavoidably. Due to that, high standard deviations occurred in some cases. However, the fluorescence intensity did not decrease distinctly. Since the fluorescent dye is labeled covalently to the polymer via esterification, a signal decrease would imply a

degradation of the ester bond and subsequent diffusion of the dye out of the microparticle. Therefore, the constant fluorescence signal indicates that the polymer was still intact after 84 days and no distinct degradation occurred.

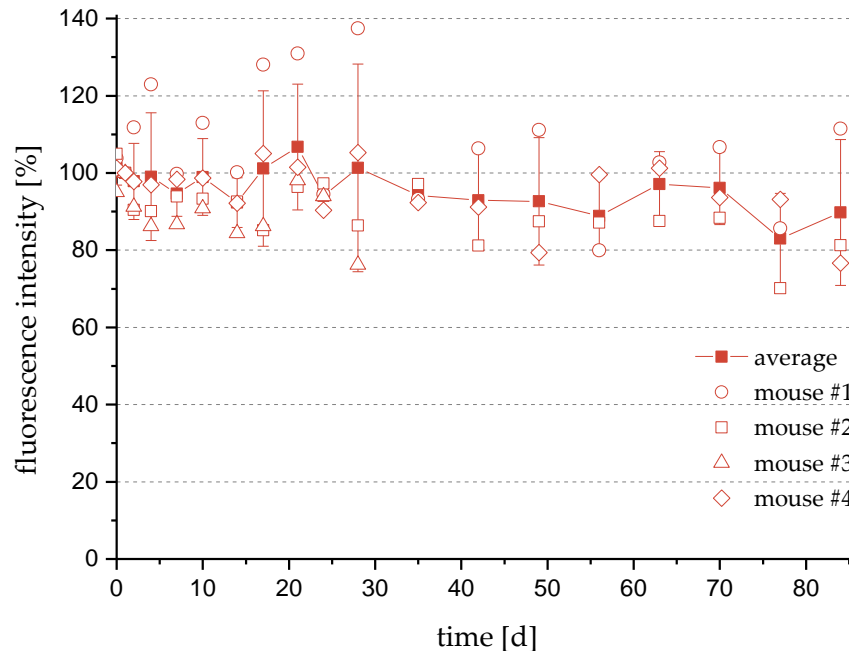


Figure 43: *In vivo* fluorescence intensity of PGA-B75-DY782 microparticles. Filled symbols represent the average fluorescence intensity, empty symbols indicate the measured intensity value of each respective mouse.

Figure 44 shows fluorescence images of mice after the application of PGA-B75 microparticles containing DiR as a lipophilic drug model at different time points. A decrease in fluorescence intensity is visible over 84 days. Again, no indication for irritation or inflammation of the skin around the injection site was visible, hence, the microspheres were well tolerated. One male mouse had to be removed from the experiment due to neoplasia at a bite wound located at the right flank away from the injection site. Therefore, the removal was incoherent with the administered microparticle formulation. The evaluation of the fluorescence intensity in Figure 45 displays the clear decline of the signal. After 84 days, the release of DiR was almost completed and residual fluorescence intensity of 4.3% was measured. Potential bleaching effects on the intensity decline can be excluded due to *in vitro* bleaching tests conducted as mentioned in 4.2.10. Compared to the *in vitro* release of DiR in the previous section, the release was considerably faster *in vivo*. While it took 47 days to release 50% of DiR *in vitro*, more than 50% of DiR were released after 14 days *in vivo*. The faster release can be attributed to various physiological processes. For example,

the pressure in the subcutaneous tissue and the animal movement, as well as immune responses and histological alterations, can influence the drug release [3,221]. Other potential factors influencing the release rate are enzymatic degradation and protein adsorption [31]. The general release pattern of the *in vivo* release of DiR was similar to the *in vitro* release of DBT (section 4.2.6.3) and showed a decrease in the release rate during the experiment. This decrease in the release rate was not visible for the *in vitro* release of DiR but would have most likely occurred with further progression of the release. Since diffusional mass transport plays a major role in the API/dye release out of the microspheres, the decrease in release rate is explainable by Fick's second law of diffusion [222,223].

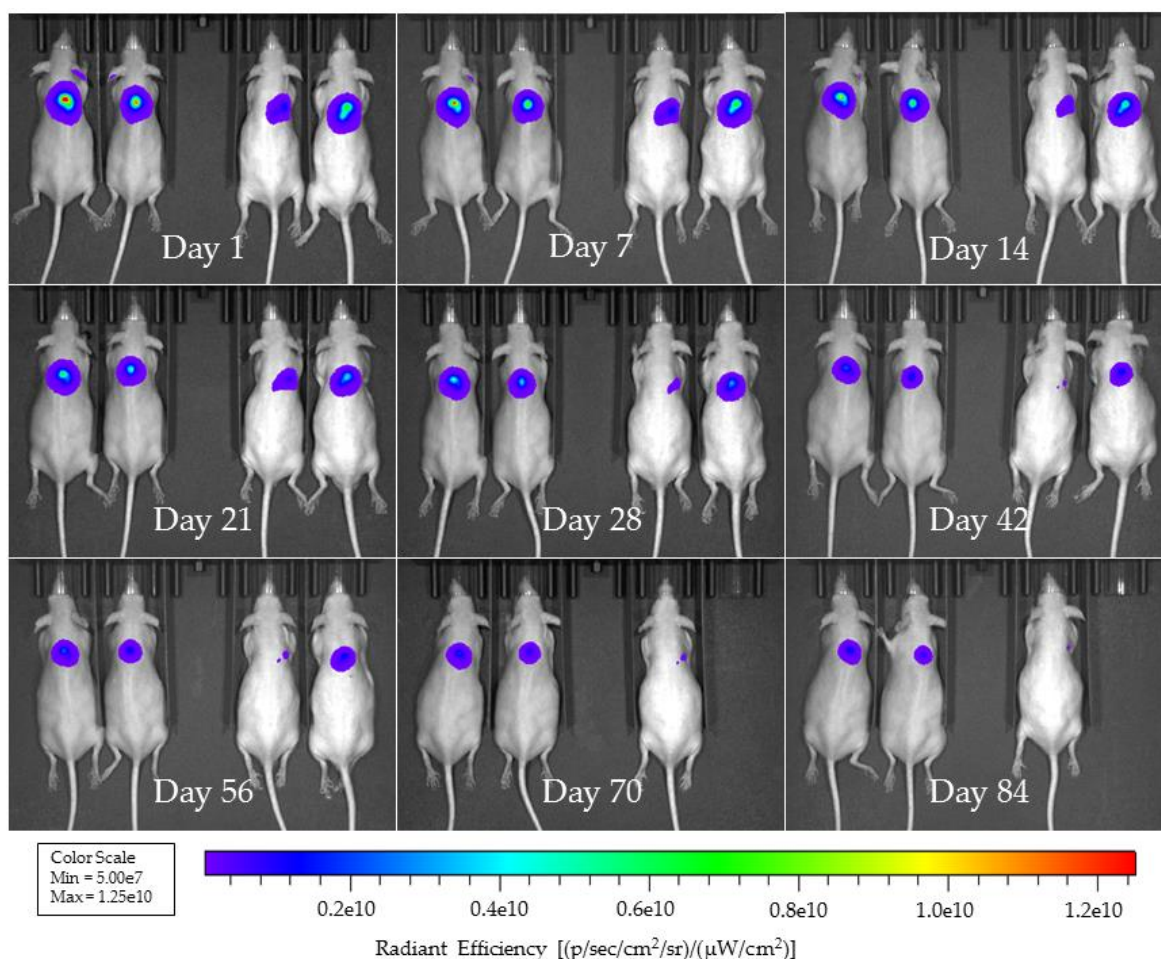


Figure 44: *In vivo* fluorescence imaging of PGA-B75 microparticles loaded with DiR in SKH1-*Hr^{tr}* mice over 84 days. The two female mice are shown on the left side of the images, the two male mice on the right.

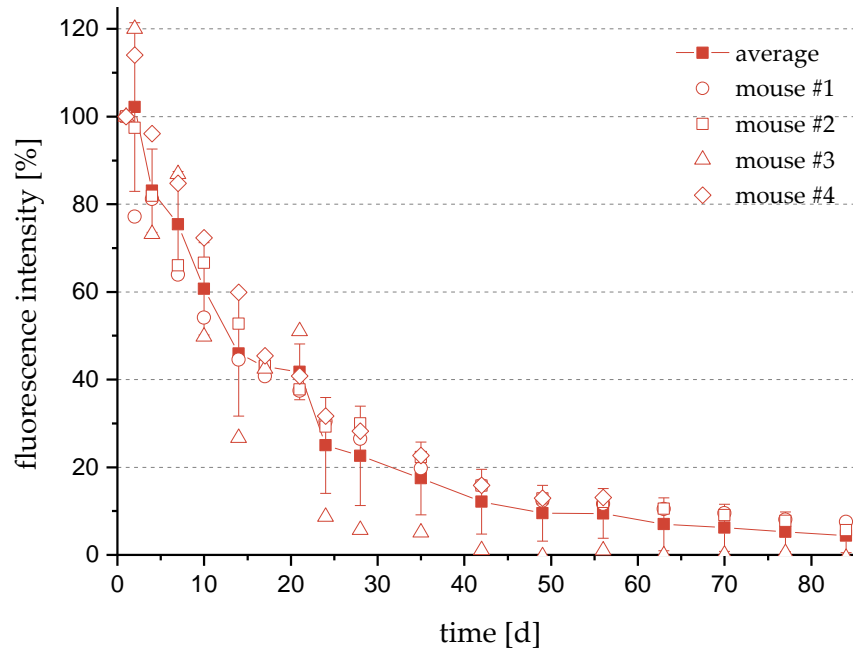


Figure 45: *In vivo* release of DiR from PGA-B75 microparticles. Filled symbols represent the average fluorescence intensity, empty symbols indicate the measured intensity value of each respective mouse.

After the termination of the experiment, the mice were dissected to exclude internal irritations caused by the formulation and to observe the particles visually at the site of injection. Although the dissections were within normal limits and no physiological changes were detected, it was discovered that the particles were encapsulated by connective tissue. An exemplary image of the injection site during dissection is shown in Figure 46. The encapsulation by a fibrous capsule can be attributed to the foreign body reaction and is a common response of the host following the implantation of biomaterials [29,224–226]. The extent of that response is influenced by several factors including the size, surface topography, shape, charge and stiffness of the material. It should be mentioned that this capsule could act as an additional barrier and could impact the release and degradation behaviour of the DDS [224].



Figure 46: Exemplary image of the microparticle injection site after termination of the experiment. The red circle indicates the tissue capsule surrounding the microparticles.

4.3 PREPARATION AND CHARACTERIZATION OF PREFORMED IMPLANTS

4.3.1 PREPARATION OF PREFORMED IMPLANTS AND TEXTURE ANALYSIS

Besides microparticles, implants gained commercial importance as parenteral controlled drug delivery systems [22,227]. Implants are categorized into preformed implants and *in situ* forming implants. *In situ* forming implants (ISFI) are administered as injectable fluids and are solidified at the injection site by cross-linking, gelation or phase separation [228]. While the administration of ISFIs is less painful and less invasive, the main obstacles of the formulation of biodegradable *in situ* forming implants are the control of the implant's shape and the toxicity of the solvents used. Preformed implants are commonly prepared via melt extrusion and are cylindrically shaped. Both implant types are mostly administered subcutaneously as a depot formulation. As apparent from the characterization of the microparticles, the size of the DDS affects the release of the API from the formulation. Moreover, the shape of the dosage form has an impact on the drug release as well [223,229]. To investigate the properties of an FA-PGA dosage form with a larger geometry compared to microparticles, implants were prepared and characterized. Due to their favourable physicochemical properties at 37 °C, PGA-B45, PGA-B75 and PGA-B45-S35 were selected as polymeric matrices. As mentioned earlier, one of the main concerns about ISFIs is the toxicity of the organic solvent used for the preparation of the injectable fluid. Organic solvents with acceptable biocompatibility profiles are NMP and dimethyl sulfoxide (DMSO) [228,230]. Nonetheless, high amounts of organic solvent can cause unwanted local irritations, thus, the solvent percentage in the formulation should be as low as possible. Since the solubilities of all behenoyl PGAs in DMSO were very low (< 0.2%) and only PGA-B45-S35 had an acceptable solubility in NMP (approx. 38%, supplementary data Figure S 3), the preparation of preformed implants was selected as the preferred approach. Due to the high polymer amounts necessary for melt extrusion, the preformed implants were prepared with the heating press (schematic illustration see Figure 9). The preformed implants are shown in Figure 47. Regularly shaped cylindrical implants with diameters of 5.5 mm and heights of 1.6 mm were obtained for all investigated FA-PGAs. The visual appearance of the implants did, however, slightly differ. While the highly substituted PGA-B75 and PGA-B45-S35 were white, the low substituted PGA-B45 was more transparent. Due to temperatures above the melting points of the side chains during

preparation, the powdered polymer is compressed to a dense matrix with even surfaces. The faint pattern on the surface can be attributed to the texture of the Teflon stamp which transferred to the implant.

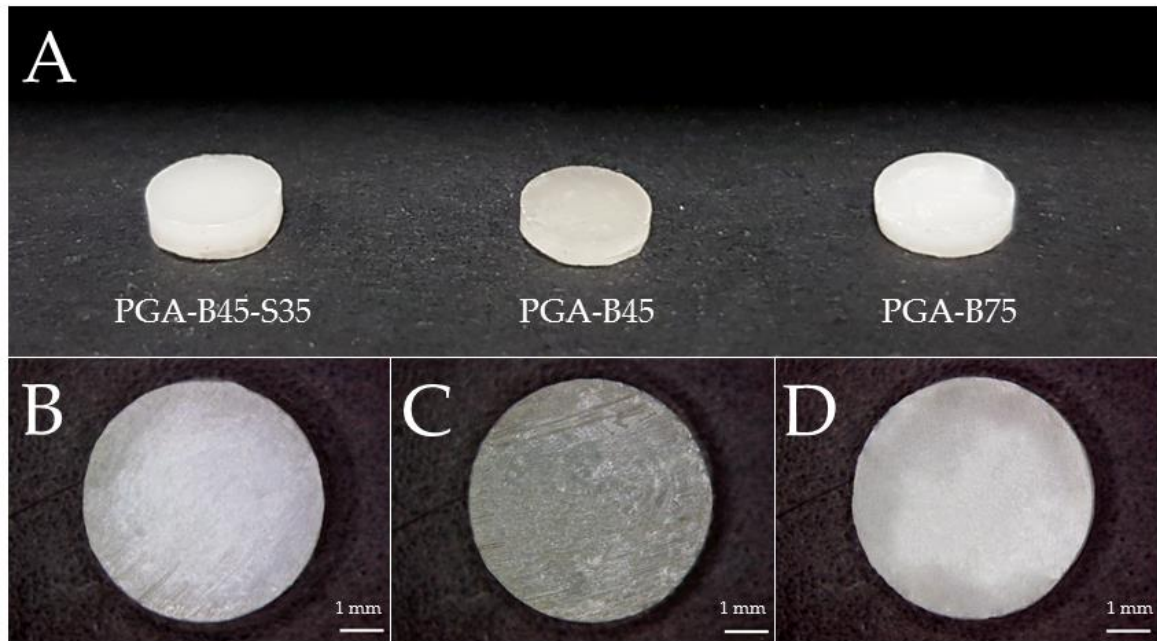


Figure 47: (A): Optical appearance of preformed implants prepared with different FA-PGAs. (B-C): Microscopic images of the surface of (B) PGA-B45-S35, (C) PGA-B45 and (D) PGA-B75 implants.

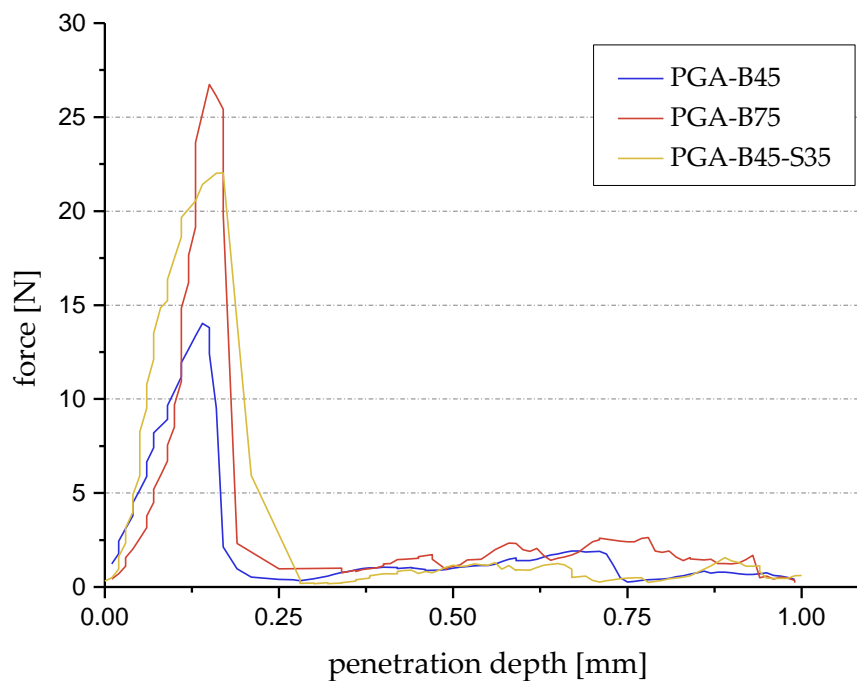


Figure 48: Exemplary penetration depth - force graphs of FA-PGA preformed implants obtained from texture analysis.

To obtain further information about the mechanical properties of the FA-PGA implants texture analysis was performed. Figure 48 displays characteristic compression curves of the investigated polymers. Evident from the individual curves, the force increased with advancing penetration until the peak maximum before rapidly decreasing. The sharp decline in force was caused by the breakdown of the implant's structure.

The peak force in the compression curves is indicative of the hardness of the sample [231,232]. Table 13 summarizes the obtained values for the maximal forces during compression. It is obvious that the maximum force, and therefore the hardness, is affected by the esterification degree of the backbone and the selection of the side chain. By increasing the portion of behenoyl side chains from 45% to 75% the peak force more than doubled. Despite the overall higher acylation degree, a slightly lower hardness was measured for the double substituted PGA-B45-S35 compared to PGA-B75. This indicates that stearic acid had less impact on the peak force than behenic acid which is explainable by the shorter carbon chain. Similar results were obtained by the rheological measurements in section 4.1.4.

Table 13: Peak forces of FA-PGA implants during compression test measured with the Texture Analyzer.

Polymer	Maximum Force [N]
PGA-B45	13.6 ± 1.7
PGA-B75	28.4 ± 3.9
PGA-B45-S35	23.6 ± 1.7

In summary, the modification of the PGA backbone influenced the mechanical properties of the implants. The hardness increased with increasing esterification degree. Thereby, the shorter C₁₈-side chain impacted the hardness to a lesser degree than the C₂₂-substituents.

4.3.2 DETERMINATION OF DRUG DISTRIBUTION

During the preparation process of the preformed implants, the powdered polymer and DBT were mixed before compression in the heating press. Therefore, the mixing process (6x/2.5 min/20 Hz) is determining the homogeneity of the drug distribution inside the DDS. The drug distribution inside the implant is an important parameter since the release properties are affected by it. The effect of the drug distribution on API release has been discussed in both traditional and advanced dosage forms [233–236]. Homogeneous drug

distribution in the respective dosage form is generally favourable to achieve a reproducible and uniform release. In order to assess the effectiveness of the mixing process, the drug distribution inside the implant was investigated. Therefore, the compressed implant was divided into four fractions as displayed in chapter 3.3.4 (Figure 10). For each fraction, the drug content was measured individually and the standard deviation was calculated. The values are presented in Table 14. Relative standard deviations below 5.0% were achieved for all polymeric implants. These values indicate a homogeneous distribution of DBT inside the dosage form. Therefore, the preparation of uniform implants with the aforementioned process parameters was successful.

Table 14: Relative standard deviation of the drug distribution inside the implants calculated from the DBT content of four different implant fractions.

Polymer	Relative Standard Deviation [%]
PGA-B45	4.7 ± 1.1
PGA-B75	4.0 ± 2.5
PGA-B45-S35	2.9 ± 2.4

4.3.3 IN VITRO RELEASE OF DIBENZOYL THIAMINE

The same issues as for the microparticle release (section 4.2.6) had to be resolved first in order to investigate the *in vitro* release behaviour of the FA-PGA implants. Based on these previous investigations, phosphate buffer pH 7.4 containing 0.2% SDS was selected as the release medium to assure sink conditions. Compared to microparticulate systems, the sampling technique for release studies on implants is straightforward. The larger geometry allows the complete exchange of the buffer medium during sampling without damaging the DDS. Due to the complete medium exchange, the contact time of API and buffer is reduced and the low stability of DBT in the medium is less problematic. Therefore, the duration of the experiment can be extended in comparison to the microparticles. To avoid API degradation in the buffer medium short sampling intervals were maintained for the duration of the experiment.

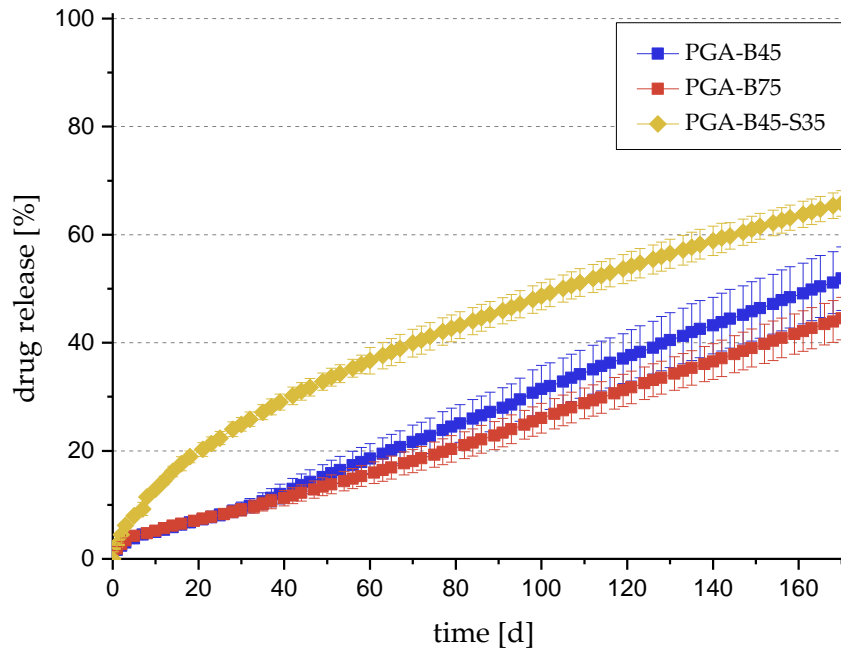


Figure 49: *In vitro* release of FA-PGA preformed implants loaded with 6% DBT in PBS pH 7.4 + 0.2% SDS over a period of 170 days at 37 °C.

As apparent from the release curves in Figure 49, the release patterns of PGA-B45 and PGA-B75 were almost identical during the first 30 days of the experiment. Thereafter, the release rate of PGA-B45 increased slightly. The lowest release rate was observed for PGA-B75 which released 44.5% DBT throughout the experiment. The slower release of PGA-B75 compared to PGA-B45 is explainable by the higher esterification degree and therefore higher lipophilicity of PGA-B75. PGA-B45 and PGA-B75 showed almost linear release profiles whereas a decrease in the release rate was detected for PGA-B45-S35 after approximately 20 days. The PGA-B45-S35 implants showed the highest release rate over the course of the experiment. After 170 days 65.8% of the incorporated amount of DBT were released. Interestingly, PGA-B45-S35 revealed the fastest release of the investigated FA-PGAs despite its high amount of acylated OH-groups. A possible explanation for this is the disparity in microviscosity of the FA-PGAs as discussed in 4.1.5. Due to the substituted stearic acid, PGA-B45-S35 revealed a higher internal fluidity at 37 °C. Therefore, diffusion out of the polymer matrix is increased and higher release rates were observed. No clear burst release was observed for the investigated FA-PGA implants. During the release, the preformed implants did not disintegrate, hence, diffusion and not erosion was the prevailing factor of the DBT release. Moreover, no visible swelling was observed. That indicates only small amounts of water penetrating the implant which was also observed

during the EPR investigation. Compared to microparticulate-based formulations the release of DBT was considerably prolonged for the preformed implants. One reason is the larger geometry which results in longer diffusion paths and a smaller specific surface area. Furthermore, the preparation method impacts the release duration as well. Due to the solvent evaporation method, microparticles tend to form more porous structures than expected for implants prepared via melt extrusion or melt compression [135,136,148]. Higher structural density hinders the penetration of water into the DDS and therefore prolongs the drug release by diffusion [41,237,238].

In summary, the release behaviour of the implants was affected by the esterification degree of the PGA backbone and the selection of the substituted fatty acid. Furthermore, the FA-PGA implants showed a considerably longer DBT release than the microparticles. The extension of the release period can be attributed to the larger geometry and the different preparation method. Therefore, it is possible to prolong the release period of DBT from weeks to months by adjusting the geometry of the DDS.

5 SUMMARY AND PERSPECTIVES

In recent years extensive research has been performed on the synthesis of new drug substances and the formulation of various drug delivery systems for controlled drug release. The increasing interest in these dosage forms and the variety of therapeutic applications led to the need for new biodegradable polymers as drug matrices. Furthermore, biorefinery and sustainable chemistry have currently become an increasing focus of attention. Poly(glycerol adipate) as a novel biodegradable polyester meets all these requirements. The free pendant hydroxyl groups of the PGA backbone allow the modification of the polymer and therefore the adjustment of its characteristics. Through the esterification of the backbone with different fatty acids, fatty acid-modified PGAs with varying properties were obtained.

Stearoyl-, behenoyl- and stearoyl-behenoyl-PGAs were characterized regarding their physicochemical characteristics. These modifications of the rather hydrophilic PGA backbone led to a clear increase in hydrophobicity resulting in lipophilic FA-PGAs. It has been shown that the lipophilicity of these polymers is substantially affected by the substitution degree and the selection of the fatty acid. DSC measurements revealed the semi-crystalline nature of the bulk polymers and the dependence of the thermal behaviour on the acylation of the polymer backbone. The stearoyl PGAs showed melting of the side chains below 37 °C body temperature, thus, their ability to form solid DDS in a physiological environment was questioned. Subsequently, these findings were supported by rheological measurements. The results obtained by oscillatory rheology confirmed that the stearoyl PGAs behave fluid-like at 37 °C. By comparison of the rheological properties at 23 °C and 37 °C, this fluid-like behaviour could be effectively attributed to the melting of the stearoyl side chains. Therefore, the form stability of stearoyl PGA systems after injection into the body cannot be guaranteed. By grafting the backbone with behenic acid the rheological properties could be adjusted and polyesters that were solid at body temperature could be obtained. Regarding the double substituted PGA-B45-S35, partial melting of the stearoyl side chains was ascertained. For that reason, the microviscosity of PGA-B45-S35 was impacted at 37 °C. EPR measurements detected a lower microviscosity for the double substituted PGA compared to the less acylated PGA-B45. Consequently, water penetration into PGA-B45-S35 was increased even though it has a higher lipophilicity than PGA-B45.

Based on the results obtained from the bulk polymer characterization, microparticles and preformed implants were prepared as DDS for controlled drug delivery of DBT. The lipophilic vitamin B₁ derivative DBT was selected as a promising API for the prophylactic treatment of cleft lip and palate in a cooperative research study with the University Hospital of the Martin Luther University of Halle-Wittenberg.

The main focus of this thesis was the preparation and comprehensive characterization of FA-PGA microparticles. Microspheres with monomodal size distributions were prepared with a solvent evaporation method. It was possible to obtain different particle sizes by adjusting the process parameters. Furthermore, the particle sizes were dependent on the substitution degree of the FA-PGA. Higher substitution degrees led to larger particles. The median particles sizes of the microspheres loaded with DBT ranged, depending on the respective polymer, from 81-128 μm . Thus, injectability by standard cannula sizes could be ensured. From a process technological point of view, it would be interesting to examine the local flow conditions in the stirring vessel for example by computational fluid dynamics simulations in the future. That, in combination with an in-process particle size analysis, could give deeper insights into the microparticle formation and the influence of the stirring velocities on the particle size. Subsequently, the particle morphology was investigated by SEM. All FA-PGAs formed spherical particles without pores or DBT crystals visible on the particle surface. Based on this, the examination of the internal particle structure and porosity by micro-CT or fractography would be valuable for future research. To determine the impact of the PGA modification on the encapsulation efficiency, in addition to DBT the slightly more hydrophilic vitamin B₁ derivative SBT was incorporated into the microparticles. The differences in hydrophobicity of the FA-PGAs detected via contact angle measurements translated to the encapsulation efficiency. In general, the more lipophilic DBT was more efficiently incorporated in the more lipophilic FA-PGAs while the incorporation of SBT revealed higher efficiencies for the less hydrophobic polymers. This highlights the possibility to tailor the polymer properties to the API by adjusting the acylation degree and the substituted side chain. Furthermore, the crystallization behaviour of the API inside the polymer matrix was dependent on the physicochemical properties of the FA-PGA used. As observed from XRD measurements, DBT was incorporated in its amorphous form up to drug loads of 16% to 25%. In that regard, the stability of the

amorphously embedded DBT was the highest in the PGA-B75 microparticles. The physical state of the API inside the dosage form is directly influencing the release behaviour. The evaluation of the *in vitro* release of DBT was conducted within sink conditions in PBS pH 7.4 containing 0.2% SDS at 37 °C. Due to the low stability of DBT in the release medium, both a conventional approach and a residual analysis were conducted to extend the duration of the release experiment. It became apparent that the melting of the stearyl side chains at 37 °C in PGA-S65 and PGA-S90 led to a quick DBT release within two hours. By esterification of behenic acid to the PGA backbone, the release rate could be decreased. The substitution degree had a crucial impact on the release duration from the microparticles. PGA-B75 microspheres revealed the most sustained DBT release of the investigated FA-PGAs with a release duration of 14 days. Further, it would be interesting to investigate the influence of higher drug loads on potential burst release from the particles and the release behaviour of more hydrophilic drugs such as SBT. Compared to PLGA the behenoyl PGA microparticles revealed a more continuous DBT release without lag phases. Especially PGA-B75 microspheres showed advantageous release behaviour over long periods. Nevertheless, more linear release profiles were detected for the PLGA microparticles. Therefore, the additional coupling of other substituents to the FA-PGA could be an interesting approach to modify the release kinetics in the future. Throughout this thesis, the behenoyl PGAs emerged as the most promising FA-PGAs regarding the transfer to *in vivo* administration. In the steps towards *in vivo* experiments, the focus was therefore laid on the behenoyl FA-PGAs, especially on PGA-B75. In preparation for the *in vivo* tests, the cytotoxicity of the microparticle formulations on NHDF and 3T3 cells was evaluated. Initially, an experimental approach with direct particle-cell contact was chosen. It became apparent that this setup was not suitable to obtain valid results since the physical pressure on the cells could be misinterpreted as a cytotoxic effect. Hence, an indirect approach with cell culture inlays was conducted. In that case, the FA-PGA microparticles were well tolerated by both cell lines and no distinct cytotoxic effects were detected. Product sterility is a precondition for the administration *in vivo*. Therefore, the impact of e-beam sterilization on PGA-B75 was assessed. Due to changes in the molecular weight distribution of the polymer, alterations in the release behaviour of DBT occurred after sterilization. Consequently, e-beam sterilization was assessed as unsuitable and the formulations were

prepared aseptically. *In vivo* studies on SKH1 mice were conducted with two different PGA-B75 microparticle formulations for 84 days. DiR was incorporated into the particles as a lipophilic drug model to assess the release from the dosage form. Additionally, the fluorescence dye Dy-782 was covalently bound to the PGA backbone to investigate the degradation behaviour. The fluorescence signal intensity of the PGA-B75-Dy782 microparticles did not considerably change throughout the experiment which indicates that no noticeable degradation happened during this period. For the PGA-B75 microspheres containing DiR a decrease in fluorescence intensity occurred. After 84 days about 4% of the initial signal was detected at the site of injection. Compared to the evaluation of the DiR release *in vitro* by fluorescence imaging and fluorospectroscopic measurements, an accelerated release was detected *in vivo*. These differences can be attributed to various physiological processes which influence the drug release *in vivo*. The investigated FA-PGA formulations were both well tolerated by all animals and no signs of irritation or inflammation were observed. Investigations regarding the *in vivo* release and bioavailability of DBT would be the next step towards the transfer into clinical administration.

Finally, preformed implants were prepared to assess the properties of the behenoyl PGAs in a DDS with a larger geometry. The implants were manufactured by melt compression with a heating press. The mechanical properties of the different FA-PGA implants were assessed by texture analysis. Regarding the *in vitro* release behaviour of the implants, considerably longer release durations were observed compared to the microparticles. After 170 days 45% to 65% of DBT were released depending on the substitution degree and the selection of the fatty acid. This can be attributed to the larger geometry of the dosage form and the varying method of preparation. Despite its high substitution degree, PGA-B45-S35 showed an increased release rate. The lower microviscosity and increased water penetration observed by EPR measurements could explain this phenomenon. The preparation of FA-PGA implants by melt extrusion and their investigation *in vivo* would be the next step towards the application of FA-PGA implants in the clinical praxis.

Overall, the modification of PGA with various fatty acids offers the flexibility to adjust the polymer to the requirements of the API or the application form. Within this work, the suitability of FA-PGAs as materials for the development of depot DDSs has been

demonstrated. It has been shown that it is possible to optimize the encapsulation efficiencies and release profiles through the alteration of the polymer's physicochemical properties. The *in vitro* and *in vivo* results of this study are very promising and show the wide range of applications for these polymers in drug delivery - from microparticles to implants. The here proposed research ideas and further improvement of the polymers could consolidate the position of FA-PGA as an equivalent alternative for PLGA.

REFERENCES

- [1] J. Folkman, D.M. Long, The use of silicone rubber as a carrier for prolonged drug therapy, *J. Surg. Res.* 4 (1964) 139–142. [https://doi.org/10.1016/S0022-4804\(64\)80040-8](https://doi.org/10.1016/S0022-4804(64)80040-8).
- [2] H. Wahid, S. Ahmad, M.A.M. Nor, M.A. Rashid, *Fundamentals and Applications of Controlled Release Drug Delivery*, Springer US, Boston, MA, 2012. <https://doi.org/10.1007/978-1-4614-0881-9>.
- [3] C.L. Stevenson, C.A. Rhodes, S.J. Prestrelski, *Long Acting Injections and Implants*, Springer US, Boston, MA, 2012. <https://doi.org/10.1007/978-1-4614-0554-2>.
- [4] D.J. Burgess, A.S. Hussain, T.S. Ingallinera, M.L. Chen, Assuring quality and performance of sustained and controlled release parenterals: AAPS workshop report, co-sponsored by FDA and USP, *Pharm. Res.* 19 (2002) 1761–1768. <https://doi.org/10.1023/A:1020730102176>.
- [5] K. Chaudhary, M.M. Patel, P.J. Mehta, Long-acting injectables: Current perspectives and future promise, *Crit. Rev. Ther. Drug Carrier Syst.* 36 (2019) 137–181. <https://doi.org/10.1615/CritRevTherDrugCarrierSyst.2018025649>.
- [6] C.A. Lipinski, Drug-like properties and the causes of poor solubility and poor permeability, *J. Pharmacol. Toxicol. Methods.* 44 (2000) 235–249. [https://doi.org/10.1016/S1056-8719\(00\)00107-6](https://doi.org/10.1016/S1056-8719(00)00107-6).
- [7] A.S. Hoffman, The origins and evolution of “controlled” drug delivery systems, *J. Control. Release.* 132 (2008) 153–163. <https://doi.org/10.1016/j.jconrel.2008.08.012>.
- [8] B.B. Pharriss, R. Erickson, J. Bashaw, S. Hoff, V.A. Place, A. Zaffaroni, Progestasert: A Uterine Therapeutic System for Long-term Contraception: I. Philosophy and Clinical Efficacy, *Fertil. Steril.* 25 (1974) 915–921. [https://doi.org/10.1016/s0015-0282\(16\)40748-x](https://doi.org/10.1016/s0015-0282(16)40748-x).
- [9] M. Polaneczky, G. Slap, C. Forke, A. Rappaport, S. Sondheimer, The Use of Levonorgestrel Implants (Norplant) for Contraception in Adolescent Mothers, *N. Engl. J. Med.* 331 (1994) 1201–1206. <https://doi.org/10.1056/NEJM199411033311806>.
- [10] H.. Croxatto, L. Mäkäräinen, The pharmacodynamics and efficacy of Implanon®, *Contraception.* 58 (1998) 91S-97S. [https://doi.org/10.1016/s0010-7824\(98\)00118-8](https://doi.org/10.1016/s0010-7824(98)00118-8).
- [11] K.A. Lewis, A.K. Goldyn, K.W. West, E.A. Eugster, A single histrelin implant is effective for 2 years for treatment of central precocious puberty, *J. Pediatr.* 163 (2013) 1214–1216. <https://doi.org/10.1016/j.jpeds.2013.05.033>.
- [12] N. Shore, Introducing Vantas: The First Once-Yearly Luteinising Hormone-Releasing Hormone Agonist, *Eur. Urol. Suppl.* 9 (2010) 701–705. <https://doi.org/10.1016/j.eursup.2010.08.004>.

- [13] A. Patel, T. Mehta, M. Patel, K. Patel, N. Patel, Recent Patent in Controlled Porosity Osmotic Pump, *Recent Pat. Drug Deliv. Formul.* 7 (2013) 66–72. <https://doi.org/10.2174/187221113804805810>.
- [14] E.E. Schmitt, R.A. Polistina, *Surgical sutures*, 1963.
- [15] F.G. Hutchinson, B.J.A. Furr, Biodegradable polymer systems for the sustained release of polypeptides, *J. Control. Release.* 13 (1990) 279–294. [https://doi.org/10.1016/0168-3659\(90\)90018-O](https://doi.org/10.1016/0168-3659(90)90018-O).
- [16] R.L. Dunn, J.P. English, D.R. Cowsar, D.P. Vanderbilt, *Biodegradable in situ forming implants and methods of producing the same*, 1999.
- [17] O. Sartor, Eligard: Leuprolide acetate in a novel sustained-release delivery system, *Urology.* 61 (2003) 25–31. [https://doi.org/10.1016/S0090-4295\(02\)02396-8](https://doi.org/10.1016/S0090-4295(02)02396-8).
- [18] J. Zech, M. Mader, D. Gündel, H. Metz, A. Odparlik, S. Agarwal, K. Mäder, A. Greiner, Noninvasive characterization (EPR, μ CT, NMR) of 3D PLA electrospun fiber sponges for controlled drug delivery, *Int. J. Pharm.* X. 2 (2020) 100055. <https://doi.org/10.1016/j.ijpx.2020.100055>.
- [19] J. Zech, S. Leisz, B. Göttel, F. Syrowatka, A. Greiner, C. Strauss, W. Knolle, C. Scheller, K. Mäder, Electrospun Nimodipine-loaded fibers for nerve regeneration: Development and in vitro performance, *Eur. J. Pharm. Biopharm.* 151 (2020) 116–126. <https://doi.org/10.1016/j.ejpb.2020.03.021>.
- [20] B. De la Riva, C. Nowak, E. Sánchez, A. Hernández, M. Schulz-Siegmund, M.K. Pec, A. Delgado, C. Évora, VEGF-controlled release within a bone defect from alginate/chitosan/PLA-H scaffolds, *Eur. J. Pharm. Biopharm.* 73 (2009) 50–58. <https://doi.org/10.1016/j.ejpb.2009.04.014>.
- [21] C. Kascholke, S. Hendrikx, T. Flath, D. Kuzmenka, H.M. Dörfler, D. Schumann, M. Gressenbuch, F.P. Schulze, M. Schulz-Siegmund, M.C. Hacker, Biodegradable and adjustable sol-gel glass based hybrid scaffolds from multi-armed oligomeric building blocks, *Acta Biomater.* 63 (2017) 336–349. <https://doi.org/10.1016/j.actbio.2017.09.024>.
- [22] Y.-S. Rhee, C.-W. Park, P.P. DeLuca, H.M. Monsour, Sustained-Release Injectable Drug Delivery, *Pharm. Tech.* Nov 1 (2010) 6–13.
- [23] C.I. Nkanga, A. Fisch, M. Rad-Malekshahi, M.D. Romic, B. Kittel, T. Ullrich, J. Wang, R.W.M. Krause, S. Adler, T. Lammers, W.E. Hennink, F. Ramazani, Clinically established biodegradable long acting injectables: An industry perspective, *Adv. Drug Deliv. Rev.* 167 (2020) 19–46. <https://doi.org/10.1016/j.addr.2020.11.008>.
- [24] M.S. Angst, D.R. Drover, Pharmacology of drugs formulated with DepoFoam™: A sustained release drug delivery system for parenteral administration using multivesicular liposome technology, *Clin. Pharmacokinet.* 45 (2006) 1153–1176. <https://doi.org/10.2165/00003088-200645120-00002>.

- [25] G.S. Kwon, D.Y. Furgeson, *Biodegradable polymers for drug delivery systems*, Woodhead Publishing Limited, 2007. <https://doi.org/10.1533/9781845693640.83>.
- [26] S.K. Prajapati, A. Jain, A. Jain, S. Jain, *Biodegradable polymers and constructs: A novel approach in drug delivery*, *Eur. Polym. J.* 120 (2019) 109191. <https://doi.org/10.1016/j.eurpolymj.2019.08.018>.
- [27] S. Doppalapudi, A. Jain, W. Khan, A.J. Domb, *Biodegradable polymers-an overview*, *Polym. Adv. Technol.* 25 (2014) 427–435. <https://doi.org/10.1002/pat.3305>.
- [28] K.E. Uhrich, S.M. Cannizzaro, R.S. Langer, K.M. Shakesheff, *Polymeric Systems for Controlled Drug Release*, *Chem. Rev.* 99 (1999) 3181–3198. <https://doi.org/10.1021/cr940351u>.
- [29] J.M. Anderson, M.S. Shive, *Biodegradation and biocompatibility of PLA and PLGA microspheres*, *Adv. Drug Deliv. Rev.* 64 (2012) 72–82. <https://doi.org/10.1016/j.addr.2012.09.004>.
- [30] M.A. Tracy, K.L. Ward, L. Firouzabadian, Y. Wang, N. Dong, R. Qian, Y. Zhang, *Factors affecting the degradation rate of poly(lactide-co-glycolide) microspheres in vivo and in vitro*, *Biomaterials.* 20 (1999) 1057–1062. [https://doi.org/10.1016/S0142-9612\(99\)00002-2](https://doi.org/10.1016/S0142-9612(99)00002-2).
- [31] B.S. Zolnik, D.J. Burgess, *Evaluation of in vivo-in vitro release of dexamethasone from PLGA microspheres*, *J. Control. Release.* 127 (2008) 137–145. <https://doi.org/10.1016/j.jconrel.2008.01.004>.
- [32] H.B. Ravivarapu, K. Burton, P.P. DeLuca, *Polymer and microsphere blending to alter the release of a peptide from PLGA microspheres*, *Eur. J. Pharm. Biopharm.* 50 (2000) 263–270. [https://doi.org/10.1016/S0939-6411\(00\)00099-0](https://doi.org/10.1016/S0939-6411(00)00099-0).
- [33] T.G. Park, *Degradation of poly(D,L-lactic acid) microspheres: effect of molecular weight*, *J. Control. Release.* 30 (1994) 161–173. [https://doi.org/10.1016/0168-3659\(94\)90263-1](https://doi.org/10.1016/0168-3659(94)90263-1).
- [34] S. Li, M. Vert, *Biodegradation of Aliphatic Polyesters*, in: *Degrad. Polym.*, Springer Netherlands, Dordrecht, 2002: pp. 71–131. https://doi.org/10.1007/978-94-017-1217-0_5.
- [35] K.A. Athanasiou, G.G. Niederauer, C.M. Agrawal, *Sterilization, toxicity, biocompatibility and clinical applications of polylactic acid/polyglycolic acid copolymers*, *Biomaterials.* 17 (1996) 93–102. [https://doi.org/10.1016/0142-9612\(96\)85754-1](https://doi.org/10.1016/0142-9612(96)85754-1).
- [36] F. von Burkersroda, L. Schedl, A. Göpferich, *Why degradable polymers undergo surface erosion or bulk erosion*, *Biomaterials.* 23 (2002) 4221–4231. [https://doi.org/10.1016/S0142-9612\(02\)00170-9](https://doi.org/10.1016/S0142-9612(02)00170-9).
- [37] M. Dunne, O.I. Corrigan, Z. Ramtoola, *Influence of particle size and dissolution conditions on the degradation properties of polylactide-co-glycolide particles*, *Biomaterials.* 21 (2000) 1659–1668. [https://doi.org/10.1016/S0142-9612\(00\)00040-5](https://doi.org/10.1016/S0142-9612(00)00040-5).

- [38] J. Siepmann, K. Elkharraz, F. Siepmann, D. Klose, How autocatalysis accelerates drug release from PLGA-based microparticles: A quantitative treatment, *Biomacromolecules*. 6 (2005) 2312–2319. <https://doi.org/10.1021/bm050228k>.
- [39] A.N. Ford Versypt, D.W. Pack, R.D. Braatz, Mathematical modeling of drug delivery from autocatalytically degradable PLGA microspheres - A review, *J. Control. Release*. 165 (2013) 29–37. <https://doi.org/10.1016/j.jconrel.2012.10.015>.
- [40] S. Li, S. McCarthy, Further investigations on the hydrolytic degradation of poly (DL-lactide), *Biomaterials*. 20 (1999) 35–44. [https://doi.org/10.1016/S0142-9612\(97\)00226-3](https://doi.org/10.1016/S0142-9612(97)00226-3).
- [41] S. Fredenberg, M. Wahlgren, M. Reslow, A. Axelsson, The mechanisms of drug release in poly(lactic-co-glycolic acid)-based drug delivery systems - A review, *Int. J. Pharm.* 415 (2011) 34–52. <https://doi.org/10.1016/j.ijpharm.2011.05.049>.
- [42] S.M. Li, H. Garreau, M. Vert, Structure-property relationships in the case of the degradation of massive poly(α -hydroxy acids) in aqueous media - Part 2 Degradation of lactide-glycolide copolymers: PLA37.5GA25 and PLA75GA25, *J. Mater. Sci. Mater. Med.* 1 (1990) 131–139. <https://doi.org/10.1007/BF00700872>.
- [43] A. Schädlich, S. Kempe, K. Mäder, Non-invasive in vivo characterization of microclimate pH inside in situ forming PLGA implants using multispectral fluorescence imaging, *J. Control. Release*. 179 (2014) 52–62. <https://doi.org/10.1016/j.jconrel.2014.01.024>.
- [44] A.G. Ding, S.P. Schwendeman, Acidic microclimate pH Distribution in PLGA microspheres monitored by confocal laser scanning microscopy, *Pharm. Res.* 25 (2008) 2041–2052. <https://doi.org/10.1007/s11095-008-9594-3>.
- [45] L. Li, S.P. Schwendeman, Mapping neutral microclimate pH in PLGA microspheres, *J. Control. Release*. 101 (2005) 163–173. <https://doi.org/10.1016/j.jconrel.2004.07.029>.
- [46] A. Brunner, K. Mäder, A. Göpferich, pH and osmotic pressure inside biodegradable microspheres during erosion, *Pharm. Res.* 16 (1999) 847–853. <https://doi.org/10.1023/A:1018822002353>.
- [47] K. Mäder, B. Gallez, K.J. Liu, H.M. Swartz, Non-invasive in vivo characterization of release processes in biodegradable polymers by low-frequency electron paramagnetic resonance spectroscopy, *Biomaterials*. 17 (1996) 457–461. [https://doi.org/10.1016/0142-9612\(96\)89664-5](https://doi.org/10.1016/0142-9612(96)89664-5).
- [48] D.K.-L. Xing, D.T. Crane, B. Bolgiano, M.J. Corbel, C. Jones, D. Sesardic, Physicochemical and immunological studies on the stability of free and microsphere-encapsulated tetanus toxoid in vitro, *Vaccine*. 14 (1996) 1205–1213. [https://doi.org/10.1016/S0264-410X\(96\)00032-1](https://doi.org/10.1016/S0264-410X(96)00032-1).
- [49] L. Chen, R.N. Apte, S. Cohen, Characterization of PLGA microspheres for the controlled delivery of IL-1 α for tumor immunotherapy, *J. Control. Release*. 43 (1997) 261–272. [https://doi.org/10.1016/S0168-3659\(96\)01496-4](https://doi.org/10.1016/S0168-3659(96)01496-4).

- [50] T. Uchida, A. Yagi, Y. Oda, Y. Nakada, S. Goto, Instability of Bovine Insulin in Poly(lactide-co-glycolide) (PLGA) Microspheres., *Chem. Pharm. Bull.* 44 (1996) 235–236. <https://doi.org/10.1248/cpb.44.235>.
- [51] Y.Y. Hsu, T. Hao, M.L. Hedley, Comparison of process parameters for microencapsulation of plasmid DNA in poly(D,L-lactic-co-glycolic) acid microspheres, *J. Drug Target.* 7 (1999) 313–323. <https://doi.org/10.3109/10611869909085514>.
- [52] E. Walter, K. Moelling, J. Pavlovic, H.P. Merkle, Microencapsulation of DNA using poly(DL-lactide-co-glycolide): Stability issues and release characteristics, *J. Control. Release.* 61 (1999) 361–374. [https://doi.org/10.1016/S0168-3659\(99\)00151-0](https://doi.org/10.1016/S0168-3659(99)00151-0).
- [53] T. Estey, J. Kang, S.P. Schwendeman, J.F. Carpenter, BSA Degradation Under Acidic Conditions: A Model For Protein Instability During Release From PLGA Delivery Systems, *J. Pharm. Sci.* 95 (2006) 1626–1639. <https://doi.org/10.1002/jps.20625>.
- [54] L. Lu, C.A. Garcia, A.G. Mikos, In vitro degradation of thin poly(DL-lactic-co-glycolic acid) films, *J. Biomed. Mater. Res.* 46 (1999) 236–244. [https://doi.org/10.1002/\(SICI\)1097-4636\(199908\)46:2<236::AID-JBM13>3.0.CO;2-F](https://doi.org/10.1002/(SICI)1097-4636(199908)46:2<236::AID-JBM13>3.0.CO;2-F).
- [55] S. Mao, Y. Shi, L. Li, J. Xu, A. Schaper, T. Kissel, Effects of process and formulation parameters on characteristics and internal morphology of poly(D,L-lactide-co-glycolide) microspheres formed by the solvent evaporation method, *Eur. J. Pharm. Biopharm.* 68 (2008) 214–223. <https://doi.org/10.1016/j.ejpb.2007.06.008>.
- [56] C. Berkland, E. Pollauf, C. Raman, R. Silverman, K. Kim, D.W. Pack, Macromolecule Release from Monodisperse PLG Microspheres: Control of Release Rates and Investigation of Release Mechanism, *J. Pharm. Sci.* 96 (2007) 1176–1191. <https://doi.org/10.1002/jps.20948>.
- [57] B.S. Zolnik, D.J. Burgess, Effect of acidic pH on PLGA microsphere degradation and release, *J. Control. Release.* 122 (2007) 338–344. <https://doi.org/10.1016/j.jconrel.2007.05.034>.
- [58] B.J. Kline, E.J. Beckman, A.J. Russell, One-step biocatalytic synthesis of linear polyesters with pendant hydroxyl groups, *J. Am. Chem. Soc.* 120 (1998) 9475–9480. <https://doi.org/10.1021/ja9808907>.
- [59] H. Uyama, K. Inada, S. Kobayashi, Regioselectivity Control in Lipase-Catalyzed Polymerization of Divinyl Sebacate and Triols, *Macromol. Biosci.* 1 (2001) 40–44. [https://doi.org/10.1002/1616-5195\(200101\)1:1<40::AID-MABI40>3.0.CO;2-T](https://doi.org/10.1002/1616-5195(200101)1:1<40::AID-MABI40>3.0.CO;2-T).
- [60] V. Taresco, R.G. Creasey, J. Kennon, G. Mantovani, C. Alexander, J.C. Burley, M.C. Garnett, Variation in structure and properties of poly(glycerol adipate) via control of chain branching during enzymatic synthesis, *Polymer (Guildf).* 89 (2016) 41–49. <https://doi.org/10.1016/j.polymer.2016.02.036>.
- [61] S.I. Shoda, H. Uyama, J.I. Kadokawa, S. Kimura, S. Kobayashi, Enzymes as green catalysts for precision macromolecular synthesis, *Chem. Rev.* 116 (2016) 2307–2413. <https://doi.org/10.1021/acs.chemrev.5b00472>.

- [62] S. Kobayashi, Lipase-catalyzed polyester synthesis - A green polymer chemistry, *Proc. Japan Acad. Ser. B Phys. Biol. Sci.* 86 (2010) 338–365. <https://doi.org/10.2183/pjab.86.338>.
- [63] I.K. Varma, A.C. Albertsson, R. Rajkhowa, R.K. Srivastava, Enzyme catalyzed synthesis of polyesters, *Prog. Polym. Sci.* 30 (2005) 949–981. <https://doi.org/10.1016/j.progpolymsci.2005.06.010>.
- [64] O. Valerio, M. Misra, A.K. Mohanty, Poly(glycerol- co -diacids) Polyesters: From Glycerol Biorefinery to Sustainable Engineering Applications, A Review, *ACS Sustain. Chem. Eng.* 6 (2018) 5681–5693. <https://doi.org/10.1021/acssuschemeng.7b04837>.
- [65] P. Kallinteri, S. Higgins, G.A. Hutcheon, S. Pourcain, C. B., M.C. Garnett, Novel functionalized biodegradable polymers for nanoparticle drug delivery systems, *Biomacromolecules.* 6 (2005) 1885–1894. <https://doi.org/10.1021/bm049200j>.
- [66] M.H. Bilal, R. Alaneed, J. Steiner, K. Mäder, M. Pietzsch, J. Kressler, Multiple grafting to enzymatically synthesized polyesters, in: *Methods Enzymol.*, Academic Press Inc., 2019: pp. 57–97. <https://doi.org/10.1016/bs.mie.2019.04.031>.
- [67] V.M. Weiss, T. Naolou, T. Groth, J. Kressler, K. Mäder, In vitro toxicity of stearyl-poly(glycerol adipate) nanoparticles, *J. Appl. Biomater. Funct. Mater.* 10 (2012) 163–169. <https://doi.org/10.5301/jabfm.2012.10294>.
- [68] S.M.E. Swainson, V. Taresco, A.K. Pearce, L.H. Clapp, B. Ager, M. McAllister, C. Bosquillon, M.C. Garnett, Exploring the enzymatic degradation of poly(glycerol adipate), *Eur. J. Pharm. Biopharm.* 142 (2019) 377–386. <https://doi.org/10.1016/j.ejpb.2019.07.015>.
- [69] W. Meng, T.L. Parker, P. Kallinteri, D.A. Walker, S. Higgins, G.A. Hutcheon, M.C. Garnett, Uptake and metabolism of novel biodegradable poly (glycerol-adipate) nanoparticles in DAOY monolayer, *J. Control. Release.* 116 (2006) 314–321. <https://doi.org/10.1016/j.jconrel.2006.09.014>.
- [70] S. Puri, P. Kallinteri, S. Higgins, G.A. Hutcheon, M.C. Garnett, Drug incorporation and release of water soluble drugs from novel functionalised poly(glycerol adipate) nanoparticles, *J. Control. Release.* 125 (2008) 59–67. <https://doi.org/10.1016/j.jconrel.2007.09.009>.
- [71] V.M. Weiss, T. Naolou, G. Hause, J. Kuntsche, J. Kressler, K. Mäder, Poly(glycerol adipate)-fatty acid esters as versatile nanocarriers: From nanocubes over ellipsoids to nanospheres, *J. Control. Release.* 158 (2012) 156–164. <https://doi.org/10.1016/j.jconrel.2011.09.077>.
- [72] V.M. Weiss, T. Naolou, E. Amado, K. Busse, K. Mäder, J. Kressler, Formation of Structured Polygonal Nanoparticles by Phase-Separated Comb-Like Polymers, *Macromol. Rapid Commun.* 33 (2012) 35–40. <https://doi.org/10.1002/marc.201100565>.

- [73] T. Naolou, H. Hussain, S. Baleed, K. Busse, B.D. Lechner, J. Kressler, The behaviour of fatty acid modified poly(glycerol adipate) at the air/water interface, *Colloids Surfaces A Physicochem. Eng. Asp.* 468 (2015) 22–30. <https://doi.org/10.1016/j.colsurfa.2014.12.003>.
- [74] T. Naolou, V.M. Weiss, D. Conrad, K. Busse, K. Mäder, J. Kressler, Fatty Acid Modified Poly(glycerol adipate) - Polymeric Analogues of Glycerides, in: *ACS Symp.*, 2013: pp. 39–52. <https://doi.org/10.1021/bk-2013-1135.ch004>.
- [75] V.M. Weiss, H. Lucas, T. Mueller, P. Chytil, T. Etrych, T. Naolou, J. Kressler, K. Mäder, Intended and Unintended Targeting of Polymeric Nanocarriers: The Case of Modified Poly(glycerol adipate) Nanoparticles, *Macromol. Biosci.* 18 (2018). <https://doi.org/10.1002/mabi.201700240>.
- [76] A. Wahab, M.E. Favretto, N.D. Onyeagor, G.M. Khan, D. Douroumis, M.A. Casely-Hayford, P. Kallinteri, Development of poly(glycerol adipate) nanoparticles loaded with non-steroidal anti-inflammatory drugs, *J. Microencapsul.* 29 (2012) 497–504. <https://doi.org/10.3109/02652048.2012.665087>.
- [77] R.K. Animasawun, V. Taresco, S.M.E. Swainson, J. Suksiriworapong, J. Suksiriworapong, D.A. Walker, M.C. Garnett, Screening and Matching Polymers with Drugs to Improve Drug Incorporation and Retention in Nanoparticles, *Mol. Pharm.* 17 (2020) 2083–2098. <https://doi.org/10.1021/acs.molpharmaceut.0c00236>.
- [78] M. Jbeily, T. Naolou, M. Bilal, E. Amado, J. Kressler, Enzymatically synthesized polyesters with pendent OH groups as macroinitiators for the preparation of well-defined graft copolymers by atom transfer radical polymerization, *Polym. Int.* 63 (2014) 894–901. <https://doi.org/10.1002/pi.4676>.
- [79] D. Pfefferkorn, M. Pulst, T. Naolou, K. Busse, J. Balko, J. Kressler, Crystallization and melting of poly(glycerol adipate)-based graft copolymers with single and double crystallizable side chains, *J. Polym. Sci. Part B Polym. Phys.* 51 (2013) 1581–1591. <https://doi.org/10.1002/polb.23373>.
- [80] T. Naolou, A. Meister, R. Schöps, M. Pietzsch, J. Kressler, Synthesis and characterization of graft copolymers able to form polymersomes and worm-like aggregates, *Soft Matter.* 9 (2013) 10364–10372. <https://doi.org/10.1039/c3sm51716k>.
- [81] H. Tawfeek, S. Khidr, E. Samy, S. Ahmed, M. Murphy, A. Mohammed, A. Shabir, G. Hutcheon, I. Saleem, Poly(glycerol adipate-co- Ω -pentadecalactone) Spray-dried microparticles as sustained release carriers for pulmonary delivery, *Pharm. Res.* 28 (2011) 2086–2097. <https://doi.org/10.1007/s11095-011-0433-6>.
- [82] H.M. Tawfeek, A.R. Evans, A. Iftikhar, A.R. Mohammed, A. Shabir, S. Somavarapu, G.A. Hutcheon, I.Y. Saleem, Dry powder inhalation of macromolecules using novel PEG-co-polyester microparticle carriers, *Int. J. Pharm.* 441 (2013) 611–619. <https://doi.org/10.1016/j.ijpharm.2012.10.036>.

- [83] N.K. Kunda, I.M. Alfagih, S.R. Dennison, S. Somavarapu, Z. Merchant, G.A. Hutcheon, I.Y. Saleem, Dry powder pulmonary delivery of cationic PGA-co-PDL nanoparticles with surface adsorbed model protein, *Int. J. Pharm.* 492 (2015) 213–222. <https://doi.org/10.1016/j.ijpharm.2015.07.015>.
- [84] P.L. Jacob, L.A. Ruiz Cantu, A.K. Pearce, Y. He, J.C. Lentz, J.C. Moore, F. Machado, G. Rivers, E. Apebende, M.R. Fernandez, I. Francolini, R. Wildman, S.M. Howdle, V. Taresco, Poly (glycerol adipate) (PGA) backbone modifications with a library of functional diols: Chemical and physical effects, *Polymer (Guildf)*. 228 (2021) 123912. <https://doi.org/10.1016/j.polymer.2021.123912>.
- [85] T. Wersig, M.C. Hacker, J. Kressler, K. Mäder, Poly(glycerol adipate) – indomethacin drug conjugates – synthesis and in vitro characterization, *Int. J. Pharm.* 531 (2017) 225–234. <https://doi.org/10.1016/j.ijpharm.2017.08.093>.
- [86] T. Wersig, R. Krombholz, C. Janich, A. Meister, J. Kressler, K. Mäder, Indomethacin functionalised poly(glycerol adipate) nanospheres as promising candidates for modified drug release, *Eur. J. Pharm. Sci.* 123 (2018) 350–361. <https://doi.org/10.1016/j.ejps.2018.07.053>.
- [87] J. Suksiriworapong, V. Taresco, D.P. Ivanov, I.D. Styliari, K. Sakchaisri, V.B. Junyaprasert, M.C. Garnett, Synthesis and properties of a biodegradable polymer-drug conjugate: Methotrexate-poly(glycerol adipate), *Colloids Surfaces B Biointerfaces*. 167 (2018) 115–125. <https://doi.org/10.1016/j.colsurfb.2018.03.048>.
- [88] D. Gordhan, S.M.E. Swainson, A.K. Pearce, I.D. Styliari, T. Lovato, J.C. Burley, M.C. Garnett, V. Taresco, Poly (Glycerol Adipate): From a Functionalized Nanocarrier to a Polymeric-Prodrug Matrix to Create Amorphous Solid Dispersions, *J. Pharm. Sci.* 109 (2020) 1347–1355. <https://doi.org/10.1016/j.xphs.2019.12.004>.
- [89] R. Alaneed, Y. Golitsyn, T. Hauenschild, M. Pietzsch, D. Reichert, J. Kressler, Network formation by aza-Michael addition of primary amines to vinyl end groups of enzymatically synthesized poly(glycerol adipate), *Polym. Int.* 70 (2021) 135–144. <https://doi.org/10.1002/pi.6102>.
- [90] M.H. Bilal, H. Hussain, M. Prehm, U. Baumeister, A. Meister, G. Hause, K. Busse, K. Mäder, J. Kressler, Synthesis of poly(glycerol adipate)-g-oleate and its ternary phase diagram with glycerol monooleate and water, *Eur. Polym. J.* 91 (2017) 162–175. <https://doi.org/10.1016/j.eurpolymj.2017.03.057>.
- [91] D. Lonsdale, A review of the biochemistry, metabolism and clinical benefits of thiamin(e) and its derivatives, *Evidence-Based Complement. Altern. Med.* 3 (2006) 49–59. <https://doi.org/10.1093/ecam/nek009>.
- [92] P.R. Martin, C.K. Singleton, S. Hiller-Sturmhöfel, The role of thiamine deficiency in alcoholic brain disease, *Alcohol Res. Heal.* 27 (2003) 134–142.
- [93] A. Bâ, Metabolic and structural role of thiamine in nervous tissues, *Cell. Mol. Neurobiol.* 28 (2008) 923–931. <https://doi.org/10.1007/s10571-008-9297-7>.

- [94] G. Mkrtchyan, V. Aleshin, Y. Parkhomenko, T. Kaehne, M. Luigi Di Salvo, A. Parroni, R. Contestabile, A. Vovk, L. Bettendorff, V. Bunik, Molecular mechanisms of the non-coenzyme action of thiamin in brain: Biochemical, structural and pathway analysis, *Sci. Rep.* 5 (2015) 1–26. <https://doi.org/10.1038/srep12583>.
- [95] K.C. Whitfield, M.W. Bourassa, B. Adamolekun, G. Bergeron, L. Bettendorff, K.H. Brown, L. Cox, A. Fattal-Valevski, P.R. Fischer, E.L. Frank, L. Hiffler, L.M. Hlaing, M.E. Jefferds, H. Kapner, S. Kounnavong, M.P.S. Mousavi, D.E. Roth, M.N. Tsaloglou, F. Wieringa, G.F. Combs, Thiamine deficiency disorders: diagnosis, prevalence, and a roadmap for global control programs, *Ann. N. Y. Acad. Sci.* 1430 (2018) 3–43. <https://doi.org/10.1111/nyas.13919>.
- [96] J. Lavoie, R.F. Butterworth, Reduced Activities of Thiamine-Dependent Enzymes in Brains of Alcoholics in the Absence of Wernicke's Encephalopathy, *Alcohol. Clin. Exp. Res.* 19 (1995) 1073–1077. <https://doi.org/10.1111/j.1530-0277.1995.tb00991.x>.
- [97] R.F. Butterworth, C. Gaudreau, J. Vincelette, A.-M. Bourgault, F. Lamothe, A.-M. Nutini, Thiamine deficiency and wernicke's encephalopathy in AIDS, *Metab. Brain Dis.* 6 (1991) 207–212. <https://doi.org/10.1007/BF00996920>.
- [98] L. Bettendorff, P. Wins, Mechanism of thiamine transport in neuroblastoma cells. Inhibition of a high affinity carrier by sodium channel activators and dependence of thiamine uptake on membrane potential and intracellular ATP, *J. Biol. Chem.* 269 (1994) 14379–14385. [https://doi.org/10.1016/s0021-9258\(17\)36633-4](https://doi.org/10.1016/s0021-9258(17)36633-4).
- [99] M. Sambon, P. Wins, L. Bettendorff, Neuroprotective effects of thiamine and precursors with higher bioavailability: Focus on benfotiamine and dibenzoylthiamine, *Int. J. Mol. Sci.* 22 (2021). <https://doi.org/10.3390/ijms22115418>.
- [100] F. Xie, Z. Cheng, S. Li, X. Liu, X. Guo, P. Yu, Z. Gu, Pharmacokinetic study of benfotiamine and the bioavailability assessment compared to thiamine hydrochloride, *J. Clin. Pharmacol.* 54 (2014) 688–695. <https://doi.org/10.1002/jcph.261>.
- [101] R. Bitsch, M. Wolf, J. Moeller, L. Heuzeroth, D. Grueneklee, Bioavailability Assessment of the Lipophilic Benfotiamine as Compared to a Water-Soluble Thiamin Derivative, *Ann. Nutr. Metab.* 35 (1991) 292–296. <https://doi.org/10.1159/000177659>.
- [102] W.S. Park, J. Lee, T. Hong, G. Park, S. Youn, Y. Seo, S. Lee, S. Han, Comparative Pharmacokinetic Analysis of Thiamine and Its Phosphorylated Metabolites Administered as Multivitamin Preparations, *Clin. Ther.* 38 (2016) 2277–2285. <https://doi.org/10.1016/j.clinthera.2016.08.009>.
- [103] D. Loew, Pharmacokinetics of thiamine derivatives especially of benfotiamine., *Int. J. Clin. Pharmacol. Ther.* 34 (1996) 47–50. <http://www.ncbi.nlm.nih.gov/pubmed/8929745>.
- [104] R. Babaei-Jadidi, N. Karachalias, N. Ahmed, S. Battah, P.J. Thornalley, Prevention of incipient diabetic nephropathy by high-dose thiamine and benfotiamine, *Diabetes.* 52 (2003) 2110–2120. <https://doi.org/10.2337/diabetes.52.8.2110>.

- [105] E. Beltramo, E. Berrone, S. Buttiglieri, M. Porta, Thiamine and benfotiamine prevent increased apoptosis in endothelial cells and pericytes cultured in high glucose, *Diabetes. Metab. Res. Rev.* 20 (2004) 330–336. <https://doi.org/10.1002/dmrr.470>.
- [106] J. Vignisse, M. Sambon, A. Gorlova, D. Pavlov, N. Caron, B. Malgrange, E. Shevtsova, A. Svistunov, D.C. Anthony, N. Markova, N. Bazhenova, B. Coumans, B. Lakaye, P. Wins, T. Strekalova, L. Bettendorff, Thiamine and benfotiamine prevent stress-induced suppression of hippocampal neurogenesis in mice exposed to predation without affecting brain thiamine diphosphate levels, *Mol. Cell. Neurosci.* 82 (2017) 126–136. <https://doi.org/10.1016/j.mcn.2017.05.005>.
- [107] M. Sambon, A. Gorlova, A. Demellenne, J. Alhama-Riba, B. Coumans, B. Lakaye, P. Wins, M. Fillet, D.C. Anthony, T. Strekalova, L. Bettendorff, Dibenzoylthiamine has powerful antioxidant and anti-inflammatory properties in cultured cells and in mouse models of stress and neurodegeneration, *Biomedicines.* 8 (2020). <https://doi.org/10.3390/BIOMEDICINES8090361>.
- [108] A. Gorlova, D. Pavlov, D.C. Anthony, E.D. Ponomarev, M. Sambon, A. Proshin, I. Shafarevich, D. Babaevskaya, K.P. Lesch, L. Bettendorff, T. Strekalova, Thiamine and benfotiamine counteract ultrasound-induced aggression, normalize AMPA receptor expression and plasticity markers, and reduce oxidative stress in mice, *Neuropharmacology.* 156 (2019). <https://doi.org/10.1016/j.neuropharm.2019.02.025>.
- [109] H.C. Jonus, C.C. Byrnes, J. Kim, M.L. Valle, M.G. Bartlett, H.M. Said, J.A. Zastre, Thiamine mimetics sulbutiamine and benfotiamine as a nutraceutical approach to anticancer therapy, *Biomed. Pharmacother.* 121 (2020) 109648. <https://doi.org/10.1016/j.biopha.2019.109648>.
- [110] J. Schubert, R. Schmidt, E. Syska, B group vitamins and cleft lip and cleft palate, *Int. J. Oral Maxillofac. Surg.* 31 (2002) 410–413. <https://doi.org/10.1054/ijom.2001.0212>.
- [111] K. Scheller, T. Röckl, C. Scheller, J. Schubert, Lower concentrations of B-vitamin subgroups in the serum and amniotic fluid correlate to cleft lip and palate appearance in the offspring of A/WySn mice, *J. Oral Maxillofac. Surg.* 71 (2013) 1601.e1-1601.e7. <https://doi.org/10.1016/j.joms.2013.02.020>.
- [112] K. Scheller, F. Kalmring, J. Schubert, Sex distribution is a factor in teratogenically induced clefts and in the anti-teratogenic effect of thiamine in mice, but not in genetically determined cleft appearance, *J. Cranio-Maxillofacial Surg.* 44 (2016) 104–109. <https://doi.org/10.1016/j.jcms.2015.10.025>.
- [113] Molinspiration Cheminformatics free web services, <https://www.molinspiration.com>, (n.d.). <https://www.molinspiration.com>.
- [114] I. V. Tetko, J. Gasteiger, R. Todeschini, A. Mauri, D. Livingstone, P. Ertl, V.A. Palyulin, E. V. Radchenko, N.S. Zefirov, A.S. Makarenko, V.Y. Tanchuk, V. V. Prokopenko, Virtual computational chemistry laboratory - Design and description, *J. Comput. Aided. Mol. Des.* 19 (2005) 453–463. <https://doi.org/10.1007/s10822-005-8694-y>.

- [115] T. Cheng, Y. Zhao, X. Li, F. Lin, Y. Xu, X. Zhang, Y. Li, R. Wang, L. Lai, Computation of octanol-water partition coefficients by guiding an additive model with knowledge, *J. Chem. Inf. Model.* 47 (2007) 2140–2148. <https://doi.org/10.1021/ci700257y>.
- [116] S.K. Niazi, Stability Testing of New Drug Substances and Products, *Handb. Pharm. Manuf. Formul.* (2020) 31–40. <https://doi.org/10.1201/9781420048452-7>.
- [117] J. Štrancar, M. Šentjurc, M. Schara, Fast and Accurate Characterization of Biological Membranes by EPR Spectral Simulations of Nitroxides, *J. Magn. Reson.* 142 (2000) 254–265. <https://doi.org/10.1006/jmre.1999.1919>.
- [118] L.R. Beck, D.R. Cowsar, D.H. Lewis, R.J. Cosgrove, C.T. Riddle, S.L. Lowry, T. Epperly, A new long-acting injectable microcapsule system for the administration of progesterone, *Fertil. Steril.* 31 (1979) 545–551. [https://doi.org/10.1016/S0015-0282\(16\)44002-1](https://doi.org/10.1016/S0015-0282(16)44002-1).
- [119] P.B. O'Donnell, J.W. McGinity, Preparation of microspheres by the solvent evaporation technique, *Adv. Drug Deliv. Rev.* 28 (1997) 25–42. [https://doi.org/10.1016/S0169-409X\(97\)00049-5](https://doi.org/10.1016/S0169-409X(97)00049-5).
- [120] N.A. Platé, V.P. Shibaev, Comb-like polymers. Structure and properties, *J. Polym. Sci. Macromol. Rev.* 8 (1974) 117–253. <https://doi.org/10.1002/pol.1974.230080103>.
- [121] K. Inomata, E. Nakanishi, Y. Sakane, M. Koike, T. Nose, Side-chain crystallization behaviour of graft copolymers consisting of amorphous main chain and crystalline side chains: Poly(methyl methacrylate)-graft-poly(ethylene glycol) and poly(methyl acrylate)-graft-poly(ethylene glycol), *J. Polym. Sci. Part B Polym. Phys.* 43 (2005) 79–86. <https://doi.org/10.1002/polb.20311>.
- [122] K. Inomata, Y. Sakamaki, T. Nose, S. Sasaki, Solid-state structure of comb-like polymers having n-octadecyl side chains II. Crystalline-amorphous layered structure, *Polym. J.* 28 (1996) 992–999. <https://doi.org/10.1295/polymj.28.992>.
- [123] H. Shi, Y. Zhao, X. Zhang, Y. Zhou, Y. Xu, S. Zhou, D. Wang, C.C. Han, D. Xu, Packing mode and conformational transition of alkyl side chains in N-alkylated poly(p-benzamide) comb-like polymer, *Polymer (Guildf).* 45 (2004) 6299–6307. <https://doi.org/10.1016/j.polymer.2004.07.005>.
- [124] V. Taresco, J. Suksiriworapong, R. Creasey, J.C. Burley, G. Mantovani, C. Alexander, K. Treacher, J. Booth, M.C. Garnett, Properties of acyl modified poly(glycerol-adipate) comb-like polymers and their self-assembly into nanoparticles, *J. Polym. Sci. Part A Polym. Chem.* 54 (2016) 3267–3278. <https://doi.org/10.1002/pola.28215>.
- [125] K.Y. Law, Definitions for hydrophilicity, hydrophobicity, and superhydrophobicity: Getting the basics right, *J. Phys. Chem. Lett.* 5 (2014) 686–688. <https://doi.org/10.1021/jz402762h>.
- [126] J. Aho, J.P. Boetker, S. Baldursdottir, J. Rantanen, Rheology as a tool for evaluation of melt processability of innovative dosage forms, *Int. J. Pharm.* 494 (2015) 623–642. <https://doi.org/10.1016/j.ijpharm.2015.02.009>.

- [127] J.M. Dealy, K.F. Wissbrun, *Melt Rheology and Its Role in Plastics Processing*, Springer Netherlands, Dordrecht, 1990. <https://doi.org/10.1007/978-94-009-2163-4>.
- [128] H.A. Barnes, *A Handbook of Elementary Rheology*, University of Wales, Institute of Non-Newtonian Fluid Mechanics, Aberystwyth, 2000.
- [129] J.D. Ferry, *Viscoelastic properties of polymers*, *Viscoelastic Prop. Polym.* (1980). <https://doi.org/10.1149/1.2428174>.
- [130] N.M. Atherton, *Principles of Electron Spin Resonance*, Ellis Horwood PTR Prentice Hall. (1993) 585. <https://doi.org/10.1007/bf00997253>.
- [131] J.A. Weil, J.R. Bolton, *Electron paramagnetic resonance: elementary theory and practical applications*, John Wiley Sons. (2007).
- [132] S. Kempe, H. Metz, K. Mäder, *Application of Electron Paramagnetic Resonance (EPR) spectroscopy and imaging in drug delivery research - Chances and challenges*, *Eur. J. Pharm. Biopharm.* 74 (2010) 55–66. <https://doi.org/10.1016/j.ejpb.2009.08.007>.
- [133] D.J. Lurie, K. Mäder, *Monitoring drug delivery processes by EPR and related techniques - Principles and applications*, *Adv. Drug Deliv. Rev.* 57 (2005) 1171–1190. <https://doi.org/10.1016/j.addr.2005.01.023>.
- [134] M.F. Ottaviani, G. Martini, L. Nuti, *Nitrogen hyperfine splitting of nitroxide solutions: Differently structured and charged nitroxides as probes of environmental properties*, *Magn. Reson. Chem.* 25 (1987) 897–904. <https://doi.org/10.1002/mrc.1260251014>.
- [135] Z. Dong, A. Chatterji, H. Sandhu, D.S. Choi, H. Chokshi, N. Shah, *Evaluation of solid state properties of solid dispersions prepared by hot-melt extrusion and solvent co-precipitation*, *Int. J. Pharm.* 355 (2008) 141–149. <https://doi.org/10.1016/j.ijpharm.2007.12.017>.
- [136] N. Kiss, G. Brenn, D. Suzzi, S. Scheler, H. Jennewein, J. Wieser, J. Khinast, *The Influence of Process Parameters on the Properties of PLGA-Microparticles Produced by the Emulsion Extraction Method*, *AIChE J.* 59 (2013) 1868–1881. <https://doi.org/10.1002/aic.13968>.
- [137] L. Mainali, J.B. Feix, J.S. Hyde, W.K. Subczynski, *Membrane fluidity profiles as deduced by saturation-recovery EPR measurements of spin-lattice relaxation times of spin labels*, *J. Magn. Reson.* 212 (2011) 418–425. <https://doi.org/10.1016/j.jmr.2011.07.022>.
- [138] K. Nakagawa, J. Mizushima, Y. Takino, K. Sakamoto, H.I. Maibach, *Chain ordering of Stratum corneum lipids investigated by EPR slow-tumbling simulation*, *Spectrochim. Acta - Part A Mol. Biomol. Spectrosc.* 63 (2006) 816–820. <https://doi.org/10.1016/j.saa.2005.10.008>.
- [139] R.E. Glover, R.R. Smith, M. V. Jones, S.K. Jackson, C.C. Rowlands, *An EPR investigation of surfactant action on bacterial membranes*, *FEMS Microbiol. Lett.* 177 (1999) 57–62. [https://doi.org/10.1016/S0378-1097\(99\)00289-X](https://doi.org/10.1016/S0378-1097(99)00289-X).

- [140] R. Xu, *Particle Characterization: Light Scattering Methods*, Kluwer Academic Publishers, Dordrecht, 2002. <https://doi.org/10.1007/0-306-47124-8>.
- [141] J. Kuntsche, K. Klaus, F. Steiniger, Size determinations of colloidal fat emulsions: A comparative study, *J. Biomed. Nanotechnol.* 5 (2009) 384–395. <https://doi.org/10.1166/jbn.2009.1047>.
- [142] L. Dougherty, S. Lister, A. West-Oram, eds., *The Royal Marsden Manual of Clinical Nursing Procedures*, 9th ed., John Wiley & Sons, 2015.
- [143] C. Washington, Drug release from microdisperse systems: a critical review, *Int. J. Pharm.* 58 (1990) 1–12. [https://doi.org/10.1016/0378-5173\(90\)90280-H](https://doi.org/10.1016/0378-5173(90)90280-H).
- [144] C. Busatto, J. Pesoa, I. Helbling, J. Luna, D. Estenoz, Effect of particle size, polydispersity and polymer degradation on progesterone release from PLGA microparticles: Experimental and mathematical modeling, *Int. J. Pharm.* 536 (2018) 360–369. <https://doi.org/10.1016/j.ijpharm.2017.12.006>.
- [145] I.D. Rosca, F. Watari, M. Uo, Microparticle formation and its mechanism in single and double emulsion solvent evaporation, *J. Control. Release.* 99 (2004) 271–280. <https://doi.org/10.1016/j.jconrel.2004.07.007>.
- [146] P. Walstra, Principles of emulsion formation, *Chem. Eng. Sci.* 48 (1993) 333–349. [https://doi.org/10.1016/0009-2509\(93\)80021-H](https://doi.org/10.1016/0009-2509(93)80021-H).
- [147] S.M. Jafari, E. Assadpoor, Y. He, B. Bhandari, Re-coalescence of emulsion droplets during high-energy emulsification, *Food Hydrocoll.* 22 (2008) 1191–1202. <https://doi.org/10.1016/j.foodhyd.2007.09.006>.
- [148] S. Freiberg, X.X. Zhu, Polymer microspheres for controlled drug release, *Int. J. Pharm.* 282 (2004) 1–18. <https://doi.org/10.1016/j.ijpharm.2004.04.013>.
- [149] P. Sansdrap, A.J. Moës, Influence of manufacturing parameters on the size characteristics and the release profiles of nifedipine from poly(DL-lactide-co-glycolide) microspheres, *Int. J. Pharm.* 98 (1993) 157–164. [https://doi.org/10.1016/0378-5173\(93\)90052-H](https://doi.org/10.1016/0378-5173(93)90052-H).
- [150] S. Benita, J.P. Benoit, F. Puisieux, C. Thies, Characterization of Drug-Loaded Poly(D,L-lactide) Microspheres, *J. Pharm. Sci.* 73 (1984) 1721–1724. <https://doi.org/10.1002/jps.2600731215>.
- [151] E.A. Simone, T.D. Dziubla, V.R. Muzykantov, Polymeric carriers: Role of geometry in drug delivery, *Expert Opin. Drug Deliv.* 5 (2008) 1283–1300. <https://doi.org/10.1517/17425240802567846>.
- [152] J.A. Champion, Y.K. Katare, S. Mitragotri, Particle shape: A new design parameter for micro- and nanoscale drug delivery carriers, *J. Control. Release.* 121 (2007) 3–9. <https://doi.org/10.1016/j.jconrel.2007.03.022>.

- [153] D.S.T. Hsieh, W.D. Rhine, R. Langer, Zero-order controlled-release polymer matrices for micro- and macromolecules, *J. Pharm. Sci.* 72 (1983) 17–22. <https://doi.org/10.1002/jps.2600720105>.
- [154] M.N. Pons, H. Vivier, K. Belaroui, B. Bernard-Michel, F. Cordier, D. Oulhana, J.A. Dodds, Particle morphology: From visualisation to measurement, *Powder Technol.* 103 (1999) 44–57. [https://doi.org/10.1016/S0032-5910\(99\)00023-6](https://doi.org/10.1016/S0032-5910(99)00023-6).
- [155] W.I. Li, K.W. Anderson, R.C. Mehta, P.P. Deluca, Prediction of solvent removal profile and effect on properties for peptide-loaded PLGA microspheres prepared by solvent extraction/ evaporation method, *J. Control. Release.* 37 (1995) 199–214. [https://doi.org/10.1016/0168-3659\(95\)00076-3](https://doi.org/10.1016/0168-3659(95)00076-3).
- [156] S. Izumikawa, S. Yoshioka, Y. Aso, Y. Takeda, Preparation of poly(l-lactide) microspheres of different crystalline morphology and effect of crystalline morphology on drug release rate, *J. Control. Release.* 15 (1991) 133–140. [https://doi.org/10.1016/0168-3659\(91\)90071-K](https://doi.org/10.1016/0168-3659(91)90071-K).
- [157] S.K. Ghosh, ed., *Functional Coatings: by Polymer Microencapsulation*, Wiley-VCH Verlag GmbH & KGaA, Weinheim, 2006. <https://doi.org/10.1002/3527608478>.
- [158] Y. Yeo, K. Park, Control of encapsulation efficiency and initial burst in polymeric microparticle systems, *Arch. Pharm. Res.* 27 (2004) 1–12. <https://doi.org/10.1007/BF02980037>.
- [159] N.V.N. Jyothi, P.M. Prasanna, S.N. Sakarkar, K.S. Prabha, P.S. Ramaiah, G.Y. Srawan, Microencapsulation techniques, factors influencing encapsulation efficiency, *J. Microencapsul.* 27 (2010) 187–197. <https://doi.org/10.3109/02652040903131301>.
- [160] M. Sairam, V.R. Babu, B.V.K. Naidu, T.M. Aminabhavi, Encapsulation efficiency and controlled release characteristics of crosslinked polyacrylamide particles, *Int. J. Pharm.* 320 (2006) 131–136. <https://doi.org/10.1016/j.ijpharm.2006.05.001>.
- [161] R.O. Williams III, A.B. Watts, D.A. Miller, eds., *Formulating Poorly Water Soluble Drugs*, Springer International Publishing, Cham, 2016. <https://doi.org/10.1007/978-3-319-42609-9>.
- [162] S. Thakral, M.W. Terban, N.K. Thakral, R. Suryanarayanan, Recent advances in the characterization of amorphous pharmaceuticals by X-ray diffractometry, *Adv. Drug Deliv. Rev.* 100 (2016) 183–193. <https://doi.org/10.1016/j.addr.2015.12.013>.
- [163] H. Sandhu, N. Shah, H. Chokshi, A.W. Malick, *Amorphous Solid Dispersions*, Springer New York, New York, NY, 2014. <https://doi.org/10.1007/978-1-4939-1598-9>.
- [164] B.C. Hancock, M. Parks, What is the true solubility advantage for amorphous pharmaceuticals?, *Pharm. Res.* 17 (2000) 397–404. <https://doi.org/10.1023/A:1007516718048>.
- [165] S.B. Murdande, M.J. Pikal, R.M. Shanker, R.H. Bogner, Solubility advantage of amorphous pharmaceuticals: I. A thermodynamic analysis, *J. Pharm. Sci.* 99 (2010) 1254–1264. <https://doi.org/10.1002/jps.21903>.

- [166] Council of Europe, Monographs, Solubility, 1.4., European Pharmacopoeia 8.0, Strasbourg, 2010.
- [167] M. Vasanthavada, W.Q. Tong, Y. Joshi, M.S. Kislalioglu, Phase behaviour of amorphous molecular dispersions II: Role of hydrogen bonding in solid solubility and phase separation kinetics, *Pharm. Res.* 22 (2005) 440–448. <https://doi.org/10.1007/s11095-004-1882-y>.
- [168] S. Baghel, H. Cathcart, N.J. O'Reilly, Polymeric Amorphous Solid Dispersions: A Review of Amorphization, Crystallization, Stabilization, Solid-State Characterization, and Aqueous Solubilization of Biopharmaceutical Classification System Class II Drugs, *J. Pharm. Sci.* 105 (2016) 2527–2544. <https://doi.org/10.1016/j.xphs.2015.10.008>.
- [169] Council of Europe, Recommendations on dissolution testing, 5.12.1., European Pharmacopoeia 8.0, Strasbourg, 2010.
- [170] V.P. Shah, L.J. Lesko, J. Fan, N. Fleischer, J. Handerson, H. Malinowski, M. Makary, L. Ouderkirk, S. Bay, P. Sathe, G.J.P. Singh, L. Iillman, Y. Tsong, R.I. Williams, FDA guidance for industry 1 dissolution testing of immediate release solid oral dosage forms, *Dissolution Technol.* 4 (1997) 15–22. <https://doi.org/10.14227/DT040497P15>.
- [171] European Medicines Agency Committee for Medicinal Products for Human use (CHMP) Committee for Medicinal Products for Veterinary use (CVMP) Quality Working Party (QWP), Reflection paper on the dissolution specification for generic solid oral immediate release products with systemic action, 44 (2017).
- [172] A.A. Noyes, W.R. Whitney, The Rate of Solution of Solid Substances In Their Own Solutions, *J. Am. Chem. Soc.* 19 (1897) 930–934. <https://doi.org/10.1021/ja02086a003>.
- [173] B.M. Gibaldi, S. Feldman, Establishment of Sink Conditions in Dissolution Rate Determinations, *J. Pharmaceutical Sci.* 56 (1967) 1238–1242.
- [174] D.J. Phillips, S.R. Pygall, V.B. Cooper, J.C. Mann, Overcoming sink limitations in dissolution testing: A review of traditional methods and the potential utility of biphasic systems, *J. Pharm. Pharmacol.* 64 (2012) 1549–1559. <https://doi.org/10.1111/j.2042-7158.2012.01523.x>.
- [175] W.D. Walkling, R.K. Nayak, J. Plostnieks, W.A. Cressman, A partially organic dissolution medium for griseofulvin dosage forms, *Drug Dev. Ind. Pharm.* 5 (1979) 17–27. <https://doi.org/10.3109/03639047909055659>.
- [176] B. Gander, K. Ventouras, R. Gurny, E. Doelker, In vitro dissolution medium with supramicellar surfactant concentration and its relevance for in vivo absorption, *Int. J. Pharm.* 27 (1985) 117–124. [https://doi.org/10.1016/0378-5173\(85\)90190-5](https://doi.org/10.1016/0378-5173(85)90190-5).
- [177] N. Fotaki, W. Brown, J. Kochling, H. Chokshi, H. Miao, K. Tang, V. Gray, Rationale for selection of dissolution media: Three case studies, *Dissolution Technol.* 20 (2013) 6–13. <https://doi.org/10.14227/DT200313P6>.

- [178] V.P. Shah, J.J. Konecny, R.L. Everett, B. McCullough, A.C. Noorizadeh, J.P. Skelly, In Vitro Dissolution Profile of Water-Insoluble Drug Dosage Forms in the Presence of Surfactants, *Pharm. Res. An Off. J. Am. Assoc. Pharm. Sci.* 6 (1989) 612–618. <https://doi.org/10.1023/A:1015909716312>.
- [179] L. Maggi, M.L. Torre, P. Giunchedi, U. Conte, Supramicellar solutions of sodium dodecyl sulphate as dissolution media to study the in vitro release characteristics of sustained-release formulations containing an insoluble drug: Nifedipine, *Int. J. Pharm.* 135 (1996) 73–79. [https://doi.org/10.1016/0378-5173\(95\)04352-7](https://doi.org/10.1016/0378-5173(95)04352-7).
- [180] S. Amatya, E.J. Park, J.H. Park, J.S. Kim, E. Seol, H. Lee, H. Choi, Y.H. Shin, D.H. Na, Drug release testing methods of polymeric particulate drug formulations, *J. Pharm. Investig.* 43 (2013) 259–266. <https://doi.org/10.1007/s40005-013-0072-5>.
- [181] S.S. D'Souza, P.P. DeLuca, Methods to assess in Vitro drug release from injectable polymeric particulate systems, *Pharm. Res.* 23 (2006) 460–474. <https://doi.org/10.1007/s11095-005-9397-8>.
- [182] A. Göpferich, Mechanisms of polymer degradation and erosion, *Biomater. Silver Jubil. Compend.* 17 (1996) 117–128. <https://doi.org/10.1016/B978-008045154-1.50016-2>.
- [183] J.M. Bezemer, R. Radersma, D.W. Grijpma, P.J. Dijkstra, C.A. Van Blitterswijk, J. Feijen, Microspheres for protein delivery prepared from amphiphilic multiblock copolymers 2. Modulation of release rate, *J. Control. Release.* 67 (2000) 249–260. [https://doi.org/10.1016/S0168-3659\(00\)00212-1](https://doi.org/10.1016/S0168-3659(00)00212-1).
- [184] J.H. Park, M. Ye, K. Park, Biodegradable polymers for microencapsulation of drugs, *Molecules.* 10 (2005) 146–161. <https://doi.org/10.3390/10010146>.
- [185] I. Grizzi, H. Garreau, S. Li, M. Vert, Hydrolytic degradation of devices based on poly(DL-lactic acid) size-dependence, *Biomaterials.* 16 (1995) 305–311. [https://doi.org/10.1016/0142-9612\(95\)93258-F](https://doi.org/10.1016/0142-9612(95)93258-F).
- [186] I. Mylonaki, E. Allémann, F. Delie, O. Jordan, Imaging the porous structure in the core of degrading PLGA microparticles: The effect of molecular weight, *J. Control. Release.* 286 (2018) 231–239. <https://doi.org/10.1016/j.jconrel.2018.07.044>.
- [187] S. Duvvuri, K.G. Janoria, A.K. Mitra, Development of a novel formulation containing poly(D,L-lactide-co-glycolide) microspheres dispersed in PLGA-PEG-PLGA gel for sustained delivery of ganciclovir, *J. Control. Release.* 108 (2005) 282–293. <https://doi.org/10.1016/j.jconrel.2005.09.002>.
- [188] X. Huang, C.S. Brazel, On the importance and mechanisms of burst release in matrix-controlled drug delivery systems, *J. Control. Release.* 73 (2001) 121–136. [https://doi.org/10.1016/S0168-3659\(01\)00248-6](https://doi.org/10.1016/S0168-3659(01)00248-6).

- [189] N. Kumskova, Y. Ermolenko, N. Osipova, A. Semyonkin, N. Kildeeva, M. Gorshkova, A. Kovalskii, T. Kovshova, V. Tarasov, J. Kreuter, O. Maksimenko, S. Gelperina, How subtle differences in polymer molecular weight affect doxorubicin-loaded PLGA nanoparticles degradation and drug release, *J. Microencapsul.* 37 (2020) 283–295. <https://doi.org/10.1080/02652048.2020.1729885>.
- [190] K. Makino, T. Mogi, N. Ohtake, M. Yoshida, S. Ando, T. Nakajima, H. Ohshima, Pulsatile drug release from poly (lactide-co-glycolide) microspheres: How does the composition of the polymer matrices affect the time interval between the initial burst and the pulsatile release of drugs?, *Colloids Surfaces B Biointerfaces.* 19 (2000) 173–179. [https://doi.org/10.1016/S0927-7765\(00\)00148-X](https://doi.org/10.1016/S0927-7765(00)00148-X).
- [191] K. Makino, T. Nakajima, M. Shikamura, F. Ito, S. Ando, C. Kochi, H. Inagawa, G.I. Soma, H. Terada, Efficient intracellular delivery of rifampicin to alveolar macrophages using rifampicin-loaded PLGA microspheres: Effects of molecular weight and composition of PLGA on release of rifampicin, *Colloids Surfaces B Biointerfaces.* 36 (2004) 35–42. <https://doi.org/10.1016/j.colsurfb.2004.03.018>.
- [192] G. Mittal, D.K. Sahana, V. Bhardwaj, M.N.V. Ravi Kumar, Estradiol loaded PLGA nanoparticles for oral administration: Effect of polymer molecular weight and copolymer composition on release behaviour in vitro and in vivo, *J. Control. Release.* 119 (2007) 77–85. <https://doi.org/10.1016/j.jconrel.2007.01.016>.
- [193] M.J. Stoddart, *Mammalian Cell Viability*, Humana Press, Totowa, NJ, 2011. <https://doi.org/10.1007/978-1-61779-108-6>.
- [194] R.S. Twigg, Oxidation-Reduction Aspects of Resazurin, *Nature.* 155 (1945) 401–402. <https://doi.org/10.1038/155401a0>.
- [195] T. Groth, P. Falck, R.R. Miethke, Cytotoxicity of biomaterials - Basic mechanisms and in vitro test methods: A review, *ATLA Altern. to Lab. Anim.* 23 (1995) 790–799. <https://doi.org/10.1177/026119299502300609>.
- [196] ISO-10993: biological evaluation of medical devices- Part 5: tests for cytotoxicity: in vitro methods, International Organization for Standardisation, London, 1992.
- [197] M. Fallahi-Sichani, S. Honarnejad, L.M. Heiser, J.W. Gray, P.K. Sorger, Metrics other than potency reveal systematic variation in responses to cancer drugs, *Nat. Chem. Biol.* 9 (2013) 708–714. <https://doi.org/10.1038/nchembio.1337>.
- [198] J.L. Sebaugh, Guidelines for accurate EC50/IC50 estimation, *Pharm. Stat.* 10 (2011) 128–134. <https://doi.org/10.1002/pst.426>.
- [199] A. Wennberg, G. Hasselgren, L. Tronstad, A method for toxicity screening of biomaterials using cells cultured on millipore filters, *J. Biomed. Mater. Res.* 13 (1979) 109–120. <https://doi.org/10.1002/jbm.820130112>.
- [200] M. Nakamura, J.C. Thonard, Apparatus for Applying Compressive Forces to Cells in Vitro, *J. Dent. Res.* 52 (1973) 1341. <https://doi.org/10.1177/00220345730520063301>.

- [201] European Medicines Agency Committee for Medicinal Products for Human use (CHMP) Committee for Medicinal Products for Veterinary use (CVMP) Quality Working Party (QWP), Guideline on the sterilisation of the medicinal product, active substance, excipient and primary container, *Eur. Med. Agency*. 31 (2019) 1–25.
- [202] U.S. Department of Health and Human Services - Food and Drug Administration, Submission and Review of Sterility Information in Premarket Notification (510(k)) Submissions for Devices Labeled as Sterile - Guidance for Industry and Food and Drug Administration Staff, 2016.
- [203] G.C.C. Mendes, T.R.S. Brandão, C.L.M. Silva, Ethylene oxide sterilization of medical devices: A review, *Am. J. Infect. Control*. 35 (2007) 574–581. <https://doi.org/10.1016/j.ajic.2006.10.014>.
- [204] W. Friess, M. Schlapp, Sterilization of gentamicin containing collagen/PLGA microparticle composites, *Eur. J. Pharm. Biopharm.* 63 (2006) 176–187. <https://doi.org/10.1016/j.ejpb.2005.11.007>.
- [205] D. Mohr, M. Wolff, T. Kissel, Gamma irradiation for terminal sterilization of 17 β -estradiol loaded poly-(D,L-lactide-co-glycolide) microparticles, *J. Control. Release*. 61 (1999) 203–217. [https://doi.org/10.1016/S0168-3659\(99\)00118-2](https://doi.org/10.1016/S0168-3659(99)00118-2).
- [206] A.G. Hausberger, R.A. Kenley, P.P. DeLuca, Gamma Irradiation Effects on Molecular Weight and in Vitro Degradation of Poly(D,L-Lactide- CO-Glycolide) Microparticles, *Pharm. Res. An Off. J. Am. Assoc. Pharm. Sci.* 12 (1995) 851–856. <https://doi.org/10.1023/A:1016256903322>.
- [207] M.B. Sintzel, K. Schwach-Abdellaoui, K. Mäder, R. Stösser, J. Heller, C. Tabatabay, R. Gurny, Influence of irradiation sterilization on a semi-solid poly(ortho ester), *Int. J. Pharm.* 175 (1998) 165–176. [https://doi.org/10.1016/S0378-5173\(98\)00274-9](https://doi.org/10.1016/S0378-5173(98)00274-9).
- [208] M. Silindir, A.Y. Özer, Sterilization methods and the comparison of E-beam sterilization with gamma radiation sterilization, *Fabad J. Pharm. Sci.* 34 (2009) 43–53.
- [209] R. Navarro, G. Burillo, E. Adem, A. Marcos-Fernández, Effect of ionizing radiation on the chemical structure and the physical properties of polycaprolactones of different molecular weight, *Polymers (Basel)*. 10 (2018). <https://doi.org/10.3390/polym10040397>.
- [210] A.J. Satti, N.A. Andreucetti, J.A. Ressia, M.F. Vallat, C. Sarmoria, E.M. Vallés, Modelling molecular weight changes induced in polydimethylsiloxane by gamma and electron beam irradiation, *Eur. Polym. J.* 44 (2008) 1548–1555. <https://doi.org/10.1016/j.eurpolymj.2008.02.017>.
- [211] R. Dorati, C. Colonna, M. Serra, I. Genta, T. Modena, F. Pavanetto, P. Perugini, B. Conti, γ -Irradiation of PEGd , IPLA and PEG-PLGA Multiblock Copolymers : I . Effect of Irradiation Doses, 9 (2008) 718–725. <https://doi.org/10.1208/s12249-008-9103-3>.

- [212] O. Sedlacek, J. Kucka, B.D. Monnery, M. Slouf, M. Vetric, R. Hoogenboom, M. Hruby, The effect of ionizing radiation on biocompatible polymers: From sterilization to radiolysis and hydrogel formation, *Polym. Degrad. Stab.* 137 (2017) 1–10. <https://doi.org/10.1016/j.polymdegradstab.2017.01.005>.
- [213] S. Dänmark, A. Finne-Wistrand, K. Schander, M. Hakkarainen, K. Arvidson, K. Mustafa, A.C. Albertsson, In vitro and in vivo degradation profile of aliphatic polyesters subjected to electron beam sterilization, *Acta Biomater.* 7 (2011) 2035–2046. <https://doi.org/10.1016/j.actbio.2011.02.011>.
- [214] S. Çalş, S. Bozda, H.S. Kaş, M. Tunçay, A.A. Hncal, Influence of irradiation sterilization on poly(lactide-co-glycolide) microspheres containing anti-inflammatory drugs, *Farmaco.* 57 (2002) 55–62. [https://doi.org/10.1016/S0014-827X\(01\)01171-5](https://doi.org/10.1016/S0014-827X(01)01171-5).
- [215] G. Spenlehauer, M. Vert, J.P. Benoît, F. Chabot, M. Veillard, Biodegradable cisplatin microspheres prepared by the solvent evaporation method: Morphology and release characteristics, *J. Control. Release.* 7 (1988) 217–229. [https://doi.org/10.1016/0168-3659\(88\)90054-5](https://doi.org/10.1016/0168-3659(88)90054-5).
- [216] J.R. Lakowicz, *Principles of Fluorescence Spectroscopy*, Springer US, Boston, MA, 2006. <https://doi.org/10.1007/978-0-387-46312-4>.
- [217] J. Mérian, J. Gravier, F. Navarro, I. Texier, Fluorescent nanoprobe dedicated to in vivo imaging: From preclinical validations to clinical translation, *Molecules.* 17 (2012) 5564–5591. <https://doi.org/10.3390/molecules17055564>.
- [218] F. Benavides, T.M. Oberyszyn, A.M. VanBuskirk, V.E. Reeve, D.F. Kusewitt, The hairless mouse in skin research, *J. Dermatol. Sci.* 53 (2009) 10–18. <https://doi.org/10.1016/j.jdermsci.2008.08.012>.
- [219] S.A. Hilderbrand, R. Weissleder, Near-infrared fluorescence: application to in vivo molecular imaging, *Curr. Opin. Chem. Biol.* 14 (2010) 71–79. <https://doi.org/10.1016/j.cbpa.2009.09.029>.
- [220] J. V. Frangioni, In vivo near-infrared fluorescence imaging, *Curr. Opin. Chem. Biol.* 7 (2003) 626–634. <https://doi.org/10.1016/j.cbpa.2003.08.007>.
- [221] A. Rawat, U. Bhardwaj, D.J. Burgess, Comparison of in vitro-in vivo release of Risperdal® Consta® microspheres, *Int. J. Pharm.* 434 (2012) 115–121. <https://doi.org/10.1016/j.ijpharm.2012.05.006>.
- [222] J. Siepmann, F. Siepmann, Modeling of diffusion controlled drug delivery, *J. Control. Release.* 161 (2012) 351–362. <https://doi.org/10.1016/j.jconrel.2011.10.006>.
- [223] P.L. Ritger, N.A. Peppas, A simple equation for description of solute release I. Fickian and non-fickian release from non-swellable devices in the form of slabs, spheres, cylinders or discs, *J. Control. Release.* 5 (1987) 23–36. [https://doi.org/10.1016/0168-3659\(87\)90034-4](https://doi.org/10.1016/0168-3659(87)90034-4).

- [224] J. Zandstra, C. Hiemstra, A. Petersen, J. Zuidema, M. van Beuge, S. Rodriguez, A. Lathuile, G. Veldhuis, R. Steendam, R. Bank, E. Popa, Microsphere size influences the foreign body reaction, *Eur. Cells Mater.* 28 (2014) 335–347. <https://doi.org/10.22203/eCM.v028a23>.
- [225] D.P. Link, J. Van Den Dolder, J.J.J.P. Van Den Beucken, V.M. Cuijpers, J.G.C. Wolke, A.G. Mikos, J.A. Jansen, Evaluation of the biocompatibility of calcium phosphate cement/PLGA microparticle composites, *J. Biomed. Mater. Res. - Part A.* 87 (2008) 760–769. <https://doi.org/10.1002/jbm.a.31831>.
- [226] J.M. Anderson, A. Rodriguez, D.T. Chang, Foreign body reaction to biomaterials, *Semin. Immunol.* 20 (2008) 86–100. <https://doi.org/10.1016/j.smim.2007.11.004>.
- [227] T. Kissel, Z. Brich, S. Bantle, I. Lancranjan, F. Nimmerfall, P. Vit, Parenteral depot-systems on the basis of biodegradable polyesters, *J. Control. Release.* 16 (1991) 27–41. [https://doi.org/10.1016/0168-3659\(91\)90028-C](https://doi.org/10.1016/0168-3659(91)90028-C).
- [228] S. Kempe, K. Mäder, In situ forming implants - An attractive formulation principle for parenteral depot formulations, *J. Control. Release.* 161 (2012) 668–679. <https://doi.org/10.1016/j.jconrel.2012.04.016>.
- [229] J. Siepmann, N.A. Peppas, Modeling of drug release from delivery systems based on hydroxypropyl methylcellulose (HPMC), *Adv. Drug Deliv. Rev.* 48 (2001) 139–157. [https://doi.org/10.1016/S0169-409X\(01\)00112-0](https://doi.org/10.1016/S0169-409X(01)00112-0).
- [230] M.A. Royals, S.M. Fujita, G.L. Yewey, J. Rodriguez, P.C. Schultheiss, R.L. Dunn, Biocompatibility of a biodegradable in situ forming implant system in rhesus monkeys, *J. Biomed. Mater. Res.* 45 (1999) 231–239. [https://doi.org/10.1002/\(SICI\)1097-4636\(19990605\)45:3<231::AID-JBM11>3.0.CO;2-H](https://doi.org/10.1002/(SICI)1097-4636(19990605)45:3<231::AID-JBM11>3.0.CO;2-H).
- [231] H.H. Friedman, J.E. Whitney, A.S. Szczesniak, The Texturometer—A New Instrument for Objective Texture Measurement, *J. Food Sci.* 28 (1963) 390–396. <https://doi.org/10.1111/j.1365-2621.1963.tb00216.x>.
- [232] I. Brookfield Engineering Laboratories, Brookfield CT3 Texture Analyzer Operating Instructions-Manual No. M08-372-E0315, 2016.
- [233] M. Windbergs, M. Haaser, C.M. McGoverin, K.C. Gordon, P. Kleinebudde, C.J. Strachan, Investigating the relationship between drug distribution in solid lipid matrices and dissolution behaviour using raman spectroscopy and mapping**Maïke Windbergs and Miriam Haaser contributed equally to this work., *J. Pharm. Sci.* 99 (2010) 1464–1475. <https://doi.org/10.1002/jps.21894>.
- [234] J. Pajander, A.-M. Soikkeli, O. Korhonen, R.T. Forbes, J. Ketolainen, Drug Release Phenomena Within a Hydrophobic Starch Acetate Matrix: FTIR Mapping of Tablets After In Vitro Dissolution Testing, *J. Pharm. Sci.* 97 (2008) 3367–3378. <https://doi.org/10.1002/jps.21236>.

- [235] S. Schrank, B. Kann, E. Saurugger, M. Hainschitz, M. Windbergs, B.J. Glasser, J. Khinast, E. Roblegg, The effect of the drying temperature on the properties of wet-extruded calcium stearate pellets: Pellet microstructure, drug distribution, solid state and drug dissolution, *Int. J. Pharm.* 478 (2015) 779–787. <https://doi.org/10.1016/j.ijpharm.2014.12.030>.
- [236] Y. Xu, J.J. Li, D.G. Yu, G.R. Williams, J.H. Yang, X. Wang, Influence of the drug distribution in electrospun gliadin fibers on drug-release behaviour, *Eur. J. Pharm. Sci.* 106 (2017) 422–430. <https://doi.org/10.1016/j.ejps.2017.06.017>.
- [237] J. Schnieders, U. Gbureck, E. Vorndran, M. Schossig, T. Kissel, The effect of porosity on drug release kinetics from vancomycin microsphere/calcium phosphate cement composites, *J. Biomed. Mater. Res. - Part B Appl. Biomater.* 99 B (2011) 391–398. <https://doi.org/10.1002/jbm.b.31910>.
- [238] J. Braunecker, M. Baba, G.E. Milroy, R.E. Cameron, The effects of molecular weight and porosity on the degradation and drug release from polyglycolide, *Int. J. Pharm.* 282 (2004) 19–34. <https://doi.org/10.1016/j.ijpharm.2003.08.020>.

SUPPLEMENTARY DATA

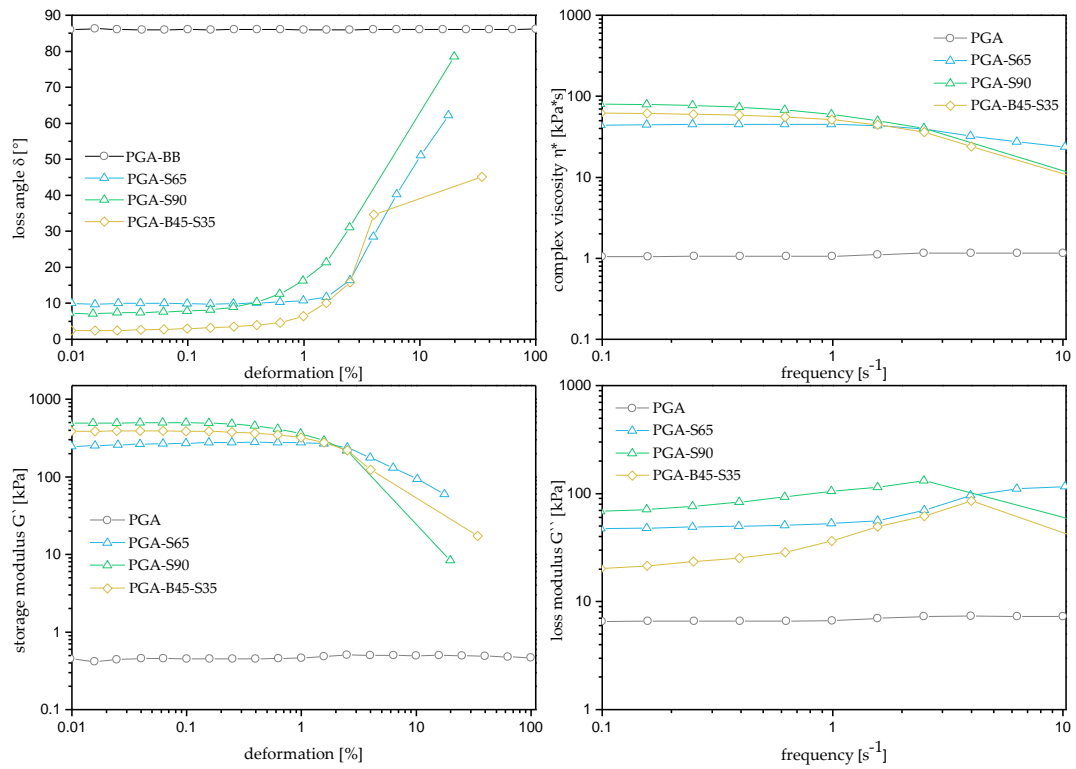


Figure S1: Amplitude sweep test for PGA-S65, PGAS-90 and PGA-B45-S35 at a set frequency of 1 s⁻¹. Deformation dependence of loss angle δ , complex viscosity η^* , storage modulus G' and loss modulus G'' at a temperature of 23 °C.

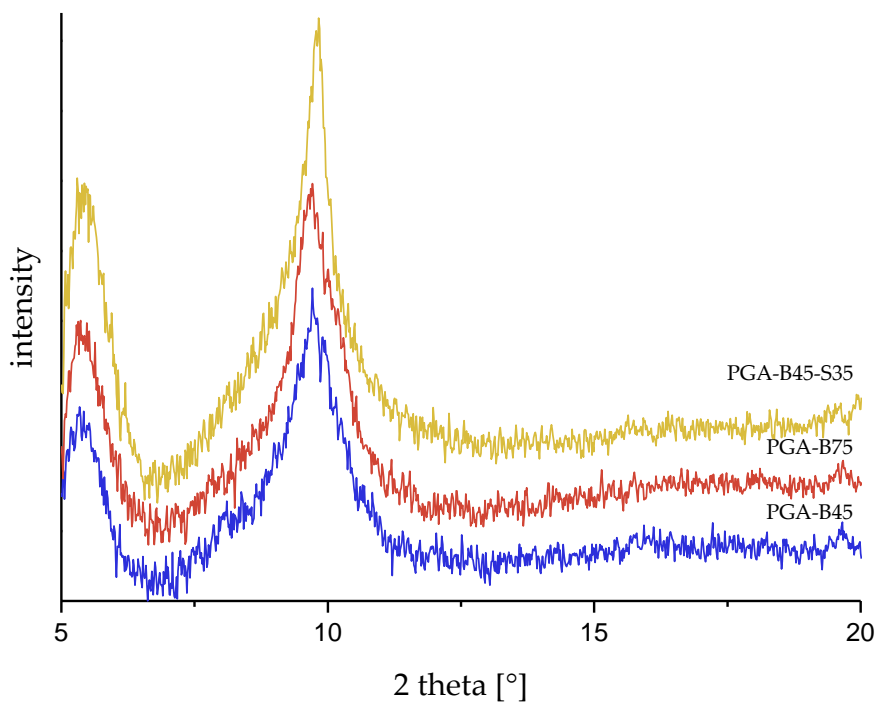


Figure S 2: XRD traces of powdered PGA-B45, PGA-B75 and PGA-B45-S35.

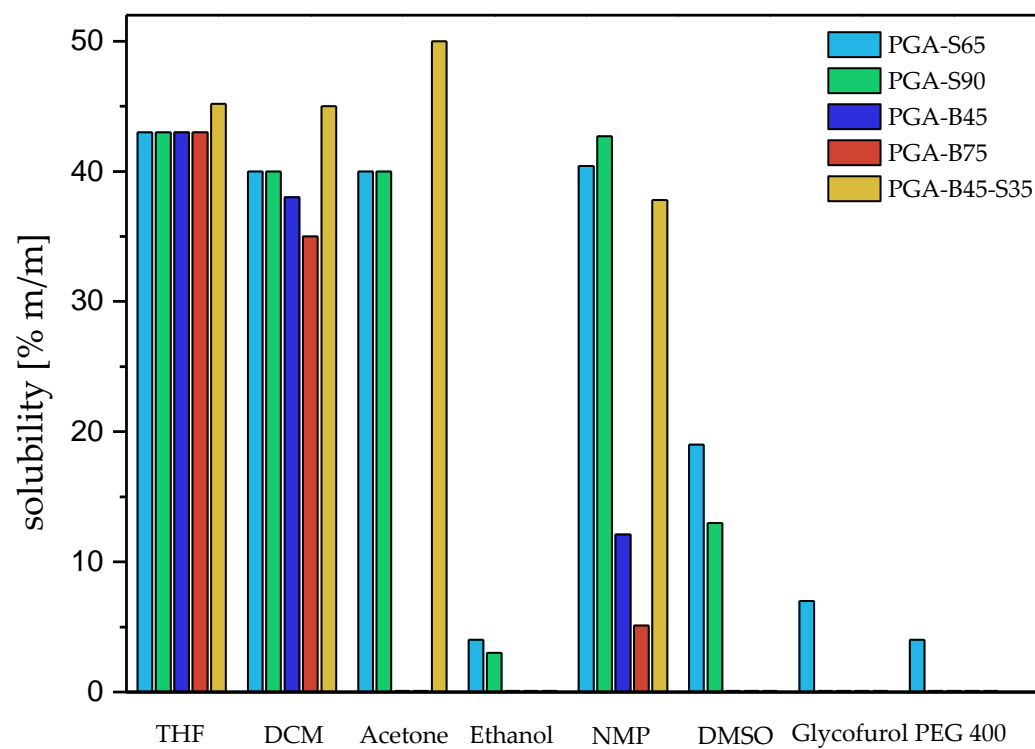


Figure S 3: Solubilities of FA-PGAs in various solvents.

DEUTSCHE ZUSAMMENFASSUNG

In den letzten Jahren wurde intensiv an der Synthese neuer Wirkstoffe und der Formulierung verschiedener Darreichungsformen zur kontrollierten Wirkstofffreisetzung geforscht. Das zunehmende Interesse an diesen Darreichungsformen und die Vielfalt der therapeutischen Anwendungen führten zu einer gesteigerten Nachfrage nach neuen biologisch abbaubaren Polymeren als Wirkstoffmatrices. Darüber hinaus rücken die Bioaffinerie und nachhaltige Chemie derzeit zunehmend in den Fokus der Forschung. Poly(glyceroladipat) (PGA) als neuartiger biologisch abbaubarer Polyester erfüllt all diese Anforderungen. Die freien Hydroxylgruppen des PGA-Grundgerüsts ermöglichen die Modifizierung des Polymers und damit die Anpassung seiner Eigenschaften. Durch die Veresterung der Polymerkette mit verschiedenen Fettsäuren wurden fettsäuremodifizierte PGAs (FA-PGAs) mit unterschiedlichen Eigenschaften erhalten.

Stearoyl-, Behenoyl- und Stearoyl-Behenoyl-PGAs wurden hinsichtlich ihrer physikalisch-chemischen Eigenschaften charakterisiert. Die Modifikationen des eher hydrophilen PGA-Grundgerüsts führten zu einer deutlichen Erhöhung der Hydrophobie und damit zu lipophilen FA-PGAs. Es zeigte sich, dass die Lipophilie dieser Polymere wesentlich durch den Substitutionsgrad und die Auswahl der Fettsäure beeinflusst wird. DSC-Messungen gaben Aufschluss über die teilkristalline Natur der Bulk-Polymere und die Abhängigkeit des thermischen Verhaltens von der Acylierung des Polymerrückgrats. Die Schmelzpunkte der Seitenketten der Stearoyl-PGAs lagen unterhalb von 37 °C Körpertemperatur, was ihre Fähigkeit zur Bildung von festen Darreichungsformen in einer physiologischen Umgebung in Frage stellte. Diese Annahme wurde durch rheologische Messungen bekräftigt. Die Ergebnisse der Oszillationsrheologie bestätigten, dass sich die Stearoyl-PGAs bei 37 °C flüssigkeitsartig verhalten. Durch Vergleich der rheologischen Eigenschaften bei 23 °C und 37 °C konnte dieses Verhalten tatsächlich auf das Schmelzen der Stearoylseitenketten zurückgeführt werden. Daher kann die Formstabilität von Stearoyl-PGA-Systemen nach Injektion in den Körper nicht garantiert werden. Die Modifizierung des Rückgrats mit Behensäure führte zu einer Veränderung der rheologischen Eigenschaften. Die erhaltenen Polymere waren bei Körpertemperatur fest. Bezüglich des doppelt substituierten PGA-B45-S35 wurde ein teilweises Schmelzen der Stearoylseitenketten bei 37 °C festgestellt. Dies beeinflusste die Mikroviskosität des Polymers. EPR-Messungen ergaben

eine niedrigere Mikroviskosität für das doppelt substituierte PGA im Vergleich zum weniger acylierten PGA-B45. Aus diesem Grund wurde, trotz der höheren Lipophilie verglichen mit PGA-B45, eine verstärkte Penetration von Wasser in PGA-B45-S35 beobachtet.

Basierend auf den Ergebnissen der Polymercharakterisierung erfolgte die Herstellung von Mikropartikeln und vorgeformte Implantaten als Drug-Delivery-Systeme (DDS) für die kontrollierte Wirkstofffreisetzung von Dibenzoyl Thiamin (DBT). Das lipophile Vitamin B1-Derivat DBT wurde in einer kooperativen Forschungsstudie mit dem Universitätsklinikum der Martin-Luther-Universität Halle-Wittenberg als vielversprechender Wirkstoff zur prophylaktischen Behandlung von Lippen-Kiefer-Gaumenspalten ausgewählt.

Der Schwerpunkt dieser Arbeit lag auf der Herstellung und umfassenden Charakterisierung von FA-PGA-Mikropartikeln. Sphärische Mikropartikel mit monomodalen Größenverteilungen wurden mit einem Lösungsmittelverdampfungsverfahren hergestellt. Durch Anpassung der Prozessparameter konnten unterschiedliche Partikelgrößen erzielt werden. Außerdem waren die Partikelgrößen vom Substitutionsgrad des FA-PGA abhängig. Höhere Substitutionsgrade führten zu größeren Partikeln. Die mittleren Partikelgrößen der mit DBT beladenen Mikropartikeln lagen je nach Polymer zwischen 81 μm und 128 μm . Somit konnte die Injizierbarkeit durch Standardkanülengrößen sichergestellt werden. Die Partikelmorphologie wurde mittels SEM untersucht. Alle FA-PGAs bildeten kugelförmige Partikel ohne sichtbare Poren oder Wirkstoffkristalle auf der Partikeloberfläche. Diesbezüglich wäre die Untersuchung der inneren Partikelstruktur und Porosität mittels Mikro-CT oder Fraktographie interessant für zukünftige Forschungen. Um den Einfluss der PGA-Modifikation auf die Verkapselungseffizienz zu bestimmen, wurde zusätzlich zu DBT das etwas hydrophilere Vitamin B1-Derivat Sulbutiamin (SBT) in die Mikropartikel eingeschlossen. Die Unterschiede in der Hydrophobie der FA-PGAs, die über Kontaktwinkelmessungen nachgewiesen wurden, übertrugen sich auf die Einkapselungseffizienz. Im Allgemeinen wurde das lipophilere DBT effizienter in die lipophileren FA-PGAs eingeschlossen, während der Einschluss von SBT höhere Einschlusseffizienzen für die weniger hydrophoben Polymere ergab. Dies unterstreicht die Möglichkeit, die

Polymereigenschaften durch Modifikation des Acylierungsgrades sowie der Seitenkette an den Wirkstoff anzupassen. Weiterhin wurde anhand von röntgendiffraktometrischen Untersuchungen beobachtet, dass DBT bis zu einer Arzneistoffbeladung von 16% bis 25% in seiner amorphen Form eingeschlossen wurde. Das Kristallisationsverhalten des Wirkstoffes innerhalb der Polymermatrix war abhängig von den physikalisch-chemischen Eigenschaften des verwendeten FA-PGAs. Die Stabilität des amorph eingebetteten DBT war diesbezüglich bei den PGA-B75-Mikropartikeln am höchsten. Anschließend, erfolgte die *in vitro*-Freisetzung von DBT unter Sinkbedingungen in PBS pH 7,4 mit 0,2 % SDS bei 37 °C. Aufgrund der geringen Stabilität von DBT im Freisetzungsmedium wurden sowohl ein konventioneller Ansatz als auch eine Rückstandsanalyse durchgeführt. Dadurch konnte die Dauer des Freisetzungsexperiments verlängert werden. Es zeigte sich, dass das Schmelzen der Stearoylseitenketten bei 37 °C in PGA-S65 und PGA-S90 zu einer schnellen DBT-Freisetzung innerhalb von zwei Stunden führte. Durch Veresterung von Behensäure an das PGA-Rückgrat konnte die Freisetzungsrates verringert werden. Des Weiteren hatte der Substitutionsgrad einen entscheidenden Einfluss auf die Freisetzungsdauer aus den Mikropartikeln. PGA-B75-Mikrosphären zeigten, mit einer Freisetzungsdauer von 14 Tagen, die am längsten anhaltende DBT-Freisetzung der untersuchten FA-PGAs. Verglichen mit PLGA kam es bei den Behenoyl-PGA-Mikropartikeln zu einer kontinuierlicheren DBT-Freisetzung ohne Lag-Phasen. Somit zeigten insbesondere die PGA-B75-Mikrosphären über lange Zeiträume ein vorteilhaftes Freisetzungsverhalten. Dennoch wurden für PLGA-Mikropartikel linearere Freisetzungsprofile festgestellt. Daher könnte die zusätzliche Koppelung anderer Substituenten an das FA-PGA ein interessanter Ansatz sein, um die Freisetzungskinetik zukünftig zu modifizieren. Während dieser Arbeit haben sich die Behenoyl-PGAs als die vielversprechendsten FA-PGAs im Hinblick auf die Übertragung auf eine *in vivo*-Verabreichung herausgestellt. Bei den Vorbereitungen auf die *in vivo*-Experimente lag der Fokus daher auf den diesen Polymeren, insbesondere auf PGA-B75. Zur Vorbereitung des *in-vivo* Tests wurde die Zytotoxizität der Mikropartikel-Formulierungen auf NHDF- und 3T3-Zellen bewertet. Zunächst wurde ein experimenteller Ansatz mit direktem Partikel-Zell-Kontakt gewählt. Es zeigte sich, dass dieser Aufbau nicht geeignet war valide Ergebnisse zu generieren, da der physikalische Druck auf die Zellen als zytotoxischer Effekt fehlinterpretiert werden konnte. Aus diesem Grund wurde

nachfolgend ein indirekter Ansatz mit Zellkultureinsätzen gewählt. In diesem Fall wurden die FA-PGA-Mikropartikel von beiden Zelllinien gut vertragen und es konnten keine ausgeprägten zytotoxischen Effekte festgestellt werden. Da die Sterilität der Mikropartikel eine Voraussetzung für die Verabreichung *in vivo* ist, erfolgte anschließend eine Bewertung der Auswirkungen von einer Elektronenstrahlsterilisation auf PGA-B75. Aufgrund von Veränderungen der Molekulargewichtsverteilung des Polymers kam es nach der Sterilisation zu Veränderungen im Freisetzungsverhalten von DBT. Folglich wurde die Elektronenstrahlsterilisation als nicht geeignet bewertet. Die Formulierungen wurden daraufhin aseptisch hergestellt. Die *In vivo*-Studien an SKH1-Mäusen erfolgten mit zwei verschiedenen PGA-B75-Mikropartikelformulierungen. DiR wurde als lipophiles Wirkstoffmodell in die Partikel eingeschlossen. Die Beurteilung der Freisetzung aus der Darreichungsform erfolgte anschließend über 84 Tage. Zusätzlich wurde der Fluoreszenzfarbstoff Dy-782 kovalent an das PGA-Rückgrat gebunden, um das Abbauverhalten des Polymers zu untersuchen. Die Fluoreszenzsignalintensität der PGA-B75-Dy782-Mikropartikel blieb während des gesamten Experiments nahezu konstant, was darauf hinweist, dass während dieses Zeitraums kein merklicher Abbau stattfand. Bei den PGA-B75-Mikrosphären die DiR enthielten trat eine Abnahme der Fluoreszenzintensität auf. Nach 84 Tagen wurden etwa 4% des anfänglichen Signals an der Injektionsstelle festgestellt. Im Vergleich zur Auswertung der DiR-Freisetzung *in vitro*, welche durch Fluoreszenzbildgebung und fluorospektroskopische Messungen erfolgte, wurde *in vivo* eine beschleunigte Freisetzung nachgewiesen. Diese Unterschiede können auf verschiedene physiologische Prozesse zurückgeführt werden, welche die Wirkstofffreisetzung *in vivo* beeinflussen. Die untersuchten FA-PGA-Formulierungen wurden von allen Tieren gut vertragen und es konnten keine Anzeichen von Reizung oder Entzündung beobachtet werden. Eine Untersuchung der *in vivo* Freisetzung und Bioverfügbarkeit von DBT wäre der nächste Schritt zur Überführung der FA-PGAs in die klinische Anwendung.

Zuletzt erfolgte die Herstellung von Implantaten mittels Schmelzkompression, um die Eigenschaften der Behenoyl-PGAs in einem DDS mit größerer Geometrie zu bewerten. Die mechanischen Eigenschaften der verschiedenen FA-PGA-Implantate wurden anschließend mittels Texturanalyse bewertet. Im Vergleich zum *in vitro* Freisetzungsverhalten der

Mikropartikel konnten bei den Implantaten deutlich längere Freisetzungsdauern beobachtet werden. Je nach Substitutionsgrad und Auswahl der Fettsäure betrug das freigesetzte DBT nach 170 Tagen 45% bis 65% der Ausgangsbeladung. Dies ist auf die größere Geometrie der Darreichungsform und die unterschiedliche Herstellungsweise zurückzuführen. Trotz seines hohen Substitutionsgrades zeigte PGA-B45-S35 eine erhöhte Freisetzungsrate. Die bei EPR-Messungen beobachtete niedrigere Mikroviskosität und erhöhte Wasserpenetration könnten dieses Phänomen erklären. Die Herstellung von FA-PGA-Implantaten durch Schmelzextrusion und deren Untersuchung *in vivo* wären die nächsten Schritte hin zur Anwendung in der klinischen Praxis.

Insgesamt bietet die Modifizierung von PGA mit verschiedenen Fettsäuren die Möglichkeit, das Polymer an die Anforderungen des Wirkstoffs oder der Darreichungsform anzupassen. Im Rahmen dieser Arbeit wurde die Eignung von FA-PGAs als Materialien für die Entwicklung von Depotsystemen nachgewiesen. Es hat sich gezeigt, dass es möglich ist, die Verkapselungseffizienzen und Freisetzungsprofile durch die Veränderung der physikalisch-chemischen Eigenschaften des Polymers zu optimieren. Die *in vitro*- und *in vivo*-Ergebnisse dieser Studie sind sehr vielversprechend und zeigen das breite Anwendungsspektrum dieser Polymere als Darreichungsform – von Mikropartikeln bis hin zu Implantaten. Die hier vorgeschlagenen Forschungsideen und die weitere Verbesserung der Polymere könnten die Position von FA-PGAs als gleichwertige Alternative zu PLGA festigen.

ACKNOWLEDGEMENTS

Mein Dank gilt jedem, der mich bei der Entstehung dieser Arbeit unterstützt hat und mir mit Rat und Tat zur Seite stand.

Allen voran danke ich meinem Doktorvater und Betreuer Prof. Dr. Karsten Mäder für die Möglichkeit, diese Forschungsarbeit in seiner Arbeitsgruppe anfertigen zu dürfen und für das mir entgegengebrachte Vertrauen. Weiterhin bedanke ich mich für die Unterstützung bei der Bearbeitung dieses Themas sowie seine menschliche und unkomplizierte Art, welche eine angenehme Zusammenarbeit ermöglichte.

Zudem danke ich der gesamten Arbeitsgruppe Pharmazeutische Technologie für die schöne gemeinsame Zeit.

Besonderer Dank gilt außerdem:

- Prof. Jörg Kreßler für die wertvollen Ratschläge bei der Bearbeitung dieses Themas und der hervorgegangenen Publikationen sowie für die Co-Betreuung im Rahmen meines Stipendiums.
- Razan AlAneed für die Synthese der Polymere und die hervorragende Zusammenarbeit an wissenschaftlichen Fragestellungen.
- Frank Syrowatka für die elektronenmikroskopischen Aufnahmen.
- Prof. Dr. Kurt Merzweiler und Dr. Christoph Wagner für die Arbeit am Röntgendiffraktometer.
- Dr. Wolfgang Knolle für die Elektronenstrahlsterilisation der Proben.
- Dr. Hendrik Metz für die Unterstützung bei den EPR-Messungen.
- Dr. Tom Wersig für die Einführung in das Thema und die Unterstützung bei allen weiteren wissenschaftlichen oder privaten Fragestellungen.
- Dr. Christopher Janich für die Unterstützung zu Beginn der Promotion.
- Dr. Marie-Luise Trutschel für die Unterstützung bei den EPR- und Rheologie-Messungen sowie für die regelmäßigen Aufmunterung der AG durch das Bereitstellen von Süßigkeiten.
- Dr. Henrike Lucas für ihren täglichen Einsatz für die AG, für die Organisation des Praktikums und allem was damit zusammenhängt. Außerdem für die Unterstützung bei den Fluoreszenzmessungen, den Cytotoxizitätstests und den *in*

vivo Experimenten. Und zu guter Letzt für die wissenschaftlichen und privaten Diskussionen und die angenehme Zusammenarbeit.

- Manuela Woigk für ihre beispielhaften HPLC-Kenntnisse und ihren Arbeitseinsatz, der den Laboralltag erleichterte.
- Kerstin Schwarz für die Unterstützung bei den DSC-Messungen.
- Eric Lehner für die gemeinsame Betreuung der Modernen AF im Praktikum, das Probelesen der Arbeit, die wissenschaftlichen Diskussionen und die zahlreichen Fußballabende.
- Benedikt Göttel für die wissenschaftliche Zusammenarbeit während der gesamten Promotion, die gemeinsame Betreuung der Praktikumsstation Flüssigen AF, sowie für die schöne gemeinsame Zeit im Labor und darüber hinaus.
- Anastasios Nalbadis und Johannes Albrecht für das Probelesen der Arbeit und für die zahlreichen wissenschaftlichen und privaten Diskussionen beim Kaffeetrinken. Außerdem für die schöne Zeit in Halle und ihre Freundschaft.
- Eike Busmann für die Hilfestellungen beim Thema Origin und allen weiteren wissenschaftlichen Problemen sowie die schönen gemeinsamen Jahre innerhalb und außerhalb des Büros.
- Dr. Janet Dehmer für das Korrekturlesen und die sprachliche Aufwertung der Arbeit.

Abschließend möchte ich meiner Familie danken. Meinen Eltern für die bedingungslose und andauernde Unterstützung und die Ermöglichung meines Studiums. Besonderer Dank gilt meiner Verlobten Felicia und meinem Sohn Aaron für ihre Liebe und Geduld. Vielen Dank, dass ihr mich immer unterstützt und motiviert habt und mir in anstrengenden Zeiten den Rücken freigehalten habt. Ohne euch wäre das nicht möglich gewesen!

CURRICULUM VITAE**PERSONAL DETAILS**

Name: Jonas Steiner
Date of birth: 06.03.1991
Place of birth: Würzburg

EDUCATION AND WORK EXPERIENCE

Since 08/2021 **QC Manager**
Novartis Deutschland GmbH, Rudolstadt, Germany

08/2017 - 07/2021 **Ph.D. student**
Department of Pharmaceutical Technology and
Biopharmaceutics (Prof. Dr. K. Mäder),
Martin Luther University of Halle-Wittenberg, Germany

06/2017 **Approbation as pharmacist**

12/2016 - 02/2017 **Pharmacist in training**
Aspen Pharmacare, Port Elizabeth, South Africa

05/2016 - 11/2016 **Pharmacist in training**
Glocken-Apotheke, Würzburg, Germany

11/2015 - 04/2016 **Pharmacist in training**
Aspen Germany, Bad Oldesloe, Germany

10/2011 - 04/2017 **Pharmacy student**
Leipzig University, Leipzig, Germany

09/2001 – 07/2010 **A-levels (Abitur)**
Riemenschneider-Gymnasium, Würzburg, Germany

Arnstadt, den 20.12.2021

Jonas Steiner

PUBLICATIONS**RESEARCH PAPERS**

J. Steiner, R. Alaneed, J. Kressler, and K. Mäder, "Fatty acid-modified poly(glycerol adipate) microparticles for controlled drug delivery," *J. Drug Deliv. Sci. Technol.*, vol. 61, no. August, p. 102206, Feb. 2021.

BOOK CHAPTERS

M. H. Bilal, R. Alaneed, J. Steiner, K. Mäder, M. Pietzsch, and J. Kressler, "Multiple grafting to enzymatically synthesized polyesters," in *Methods in Enzymology*, vol. 627, Academic Press Inc., 2019, pp. 57–97.

ABSTRACTS AND POSTERS

J. Steiner, V. Weiss, M. Bilal, R. Alaneed, J. Kressler, K. Mäder; "Nanoscale drug delivery systems based on novel fatty acid-modified poly(glycerol adipate)", 22nd annual meeting, Controlled Release Society Local Chapter 2018, Halle (Saale), Germany

J. Steiner, V. Weiss, M. Bilal, R. Alaneed, J. Kressler, K. Mäder; "Fatty acid-modified poly(glycerol adipate) as a versatile matrix for biodegradable drug delivery systems", 11th World Meeting on Pharmaceutics, Biopharmaceutics and Pharmaceutical Technology 2018; Granada, Spain

J. Steiner, V. Weiss, M. Bilal, R. Alaneed, J. Kressler, K. Mäder; "The preparation and characterization of biodegradable FA-PGA nanoparticles for parenteral drug delivery", 23rd annual meeting, Controlled Release Society Local Chapter 2019, Leipzig, Germany

J. Steiner, V. Weiss, R. Alaneed, J. Kressler, K. Mäder; "Fatty acid-modified poly(glycerol adipate) as a new biodegradable polymer for parenteral drug delivery", 46th annual meeting, Controlled Release Society 2019, Valencia, Spain

J. Steiner, T. Wersig, V. Weiss, R. Alaneed, J. Kressler, K. Mäder; "Modified poly(glycerol adipate) as a versatile platform for parenteral drug delivery", 1st Doktoranden- und PostDoc-Konferenz, ProMatLeben Polymere, Berlin, Germany

SELBSTSTÄNDIGKEITSERKLÄRUNG

Hiermit erkläre ich an Eides statt, dass ich die vorliegende Arbeit selbstständig und ohne fremde Hilfe angefertigt und keine anderen als die angegebenen Quellen und Hilfsmittel benutzt sowie die den verwendeten Werken wörtlich oder inhaltlich entnommenen Stellen als solche kenntlich gemacht habe.

Ferner erkläre ich, dass ich mich mit dieser Dissertation erstmals um die Erlangung eines Doktorgrads bewerbe. Die vorliegende Arbeit ist weder im Inland noch im Ausland in gleicher oder ähnlicher Form einer anderen Prüfungsbehörde zum Zweck einer Promotion oder eines anderen Prüfungsverfahrens vorgelegt worden.

Arnstadt, den 20.12.2021

Jonas Steiner